UNIVERSIDAD DE GUANAJUATO

CAMPUS GUANAJUATO

DIVISIÓN DE CIENCIAS NATURALES Y EXACTAS

POSGRADO EN QUÍMICA

Attaching Ionic Liquids to Surfaces: From Repellent Surfaces to Catalysis

TESIS

QUE PARA OBTENER EL GRADO DE:

DOCTOR EN CIENCIAS QUÍMICAS

PRESENTA

M.C. YARASET ALEJANDRA GALVÁN DOMÍNGUEZ

OCTUBRE 2021

UNIVERSIDAD DE GUANAJUATO

CAMPUS GUANAJUATO
DIVISIÓN DE CIENCIAS NATURALES Y EXACTAS

Attaching Ionic Liquids to Surfaces: From Repellent Surfaces to Catalysis

TESIS

QUE PARA OBTENER EL GRADO DE:
DOCTOR EN CIENCIAS QUÍMICAS

PRESENTA

YARASET ALEJANDRA GALVÁN DOMÍNGUEZ

ASESORES DE TESIS

Dr. RAMÓN ANTONIO ZÁRRAGA NÚÑEZ

Dr. JORGE ARMANDO CERVANTES JÁUREGUI

Dr. NICOLAS VOGEL

SINODALES

Dr. MARCO HAUMANN

Dr. HÉCTOR HERNÁNDEZ ESCOTO

Dr. JOSÉ ANTONIO GUERRA CONTRERAS

DECLARATORIA

Por medio de la presente me responsabilizo de la autenticidad y originalidad del presente trabajo titulado:

"Attaching Ionic Liquids to Surfaces: From Repellent Surfaces to Catalysis"

_____

YARASET ALEJANDRA GALVÁN DOMÍNGUEZ

_____	_____
Dr. RAMÓN ANTONIO ZÁRRAGA NÚÑEZ	**Dr. JORGE ARMANDO CERVANTES JÁUREGUI**
ASESOR	CO-ASESOR

AGRADEZCO EL APOYO OTORGADO POR:

BECA NACIONAL 2016 DEL CONSEJO NACIONAL DE CIENCIA Y TECNOLOGÍA

Attaching Ionic Liquids to Surfaces: From Repellent Surfaces to Catalysis

---

Anbringen von Ionischen Flüssigkeiten auf Oberflächen: von Abweisenden Oberflächen zur Katalyse

Der Technischen Fakultät der

Friedrich-Alexander-Universität Erlangen-Nürnberg

zur Erlangung des Doktorgrades

DOKTOR – INGENIEUR

vorgelegt von

Yaraset Alejandra Galván Domínguez

aus León

Als Dissertation genehmigt

von der Technischen Fakultät

der Friedrich-Alexander-Universität Erlangen-Nürnberg

Tag der müdndlichen Prüfung:

Vorsitzender des Promotionsorgans: Prof. Dr.-Ing Knut Graichen

Gutachter: Prof. Dr. Nicolas Vogel

Prof. Dr. Ramón Antonio Zárraga Núñez

Publications in Scientific Journals

1 **Yaraset Galvan**, Katherine R. Phillips, Marco Haumann, Peter Wasserscheid, Ramon Zarraga and N. Vogel*
Ionic liquid-infused nanostructures as repellent surfaces
Langmuir 2018*,* 34 (23), 6894-6902

DOI: 10.1021/acs.langmuir.7b03993

2 Cédric Giraudet, Matthias S. G. Knoll, **Yaraset Galvan**, Sebastian Süß, Doris Segets, Nicolas Vogel, Michael H. Rausch, Andreas P. Fröba*
Difusion of Gold Nanoparticles in Inverse Opals Probed by Heterodyne Dynamic Light Scattering
Transport in Porous Media. 2020, 131:723–737

DOI: 10.1007/s11242-019-01364-1

3 Tobias Salbaum[+], **Yaraset Galvan**[+], Marco Haumann, Peter Wasserscheid, Ramon Zarraga, Nicolas Vogel*
Enduring liquid repellency through slippery ionic liquid-infused organogels
Journal of Materials Chemistry A*, 2021, 9, 2357 – 2366*

DOI: 10.1039/D0TA10237G

4 **Yaraset Galvan**, Johannes Bauernfeind, Patrick Wolf, Ramon Zarraga, Marco Haumann, Nicolas Vogel*
Materials with hierarchical porosity enhance the stability of infused ionic liquid films
ACS Omega, 2021*, 6, 20956−20965*

DOI: https://doi.org/10.1021/acsomega.1c02405

[+] Authors contributed equally

*Corresponding authors.

Covers for Scientific Journals

1 Cover highlighting the paper “Ionic liquid-infused nanostructures as repellent surfaces”

Yaraset Galvan, Katherine R. Phillips, Marco Haumann, Peter Wasserscheid, Ramon Zarraga and N. Vogel
Langmuir, June 12, 2018 Volume 34, Issue 23 Pages 6645-6982

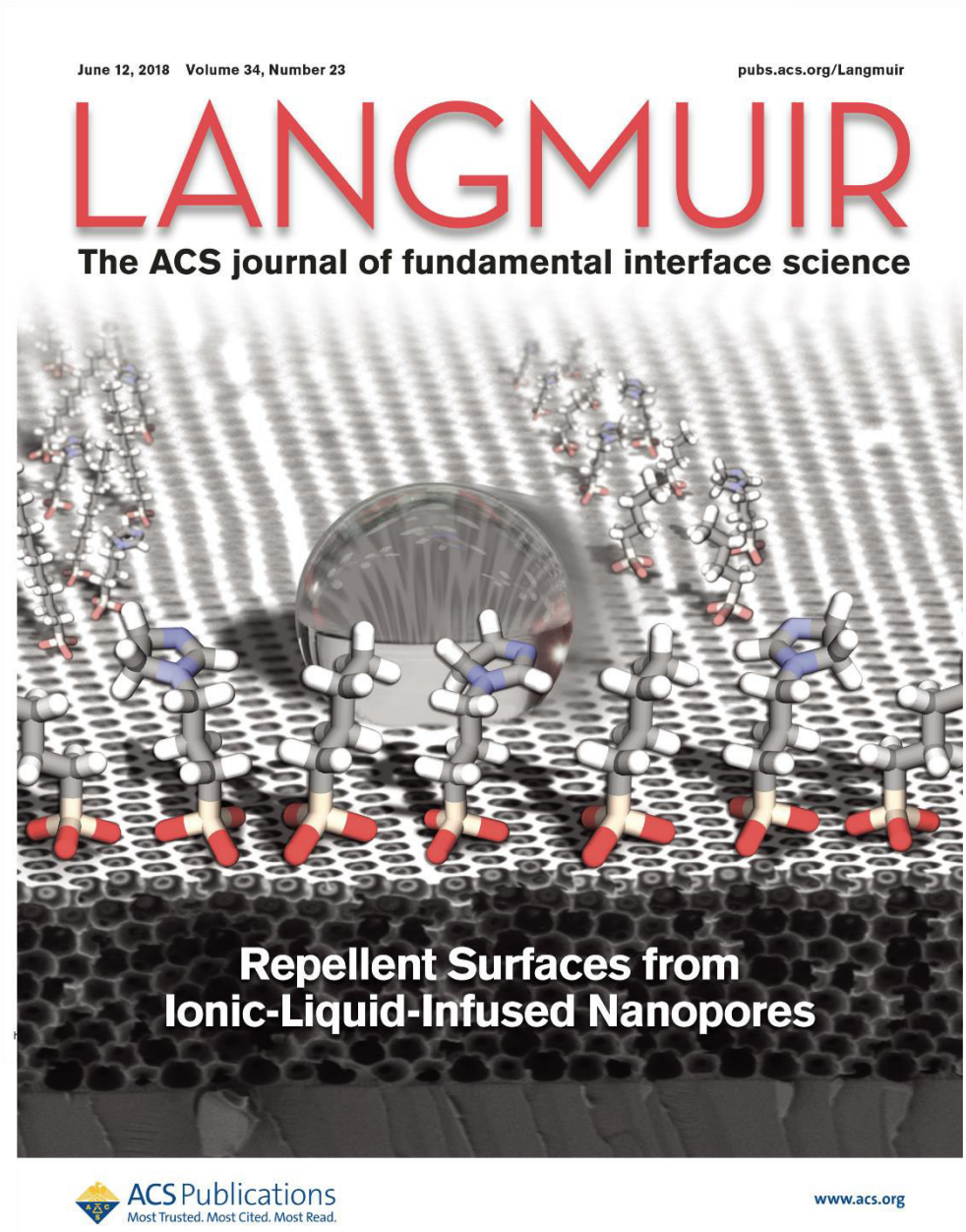

Supervised Student Theses

1. Tobias Salbaum “Liquid-repellent Surface coating”

   Mater thesis, 2018

2. Johannes Bauernfeind “Surface coating of porous materials for SILP catalysis”

   Master thesis, 2019

Conference Contributions

14th Zsigmondy Colloquium

2018, Mainz, Germany

Poster

Particle Based Materials Symposium

2018, Erlangen, Germany

Poster

2nd ITN-LubISS school (Innovative Training Network-Lubricant impregnated slippery surfaces)

2018, Mainz, Germany

Poster

Abstract

Liquid films that are strongly confined to a solid substrate are a concept that is exploited in many technological applications. It demands a detailed engineering design entirely based on the nature of the elements involved, which in turn are selected based on the final application. The control over the interfacial interactions between the liquid to be confined and the solid support is pivotal for the design and successful performance of such complex systems.

Ionic liquids are an unusual kind of compound formed of ions, so they inherently have ionic properties, yet they are in liquid form at room temperature or have melting points below 100°C. As a result, ionic liquids offer the advantages obtained from liquids in general with remarkable characteristics including extremely low vapor pressures, high thermal stability, and nonflammability.

The confinement of ionic liquids to solid surfaces while retaining their special properties requires control over the interfacial interactions between an ionic liquid, without neglecting its structural complexity, and the solid substrate to which it will be confined.

In this PhD thesis, we explore different approaches to confine ionic liquids to solid surfaces. These approaches are guided fundamentally for the same principle: the manipulation of the interfacial interactions of the ionic liquid and the support, in a way that a minimum energy state is obtained. Taking as a reference the chemical structure of an ionic liquid, we fabricate surface chemistries resembling the chemical structure of the ionic liquids to ensure low energy interfacial interactions.

First, we confine ionic liquids to the support through the solid surface modification, implementing both suitable surface chemistry and capillary forces. We make used of silane chemistry to modify the surface of SiO_2-based materials adding functionality resembling the ionic liquid functional groups. We add topography at the nano and micro-scale to increase capillary effects.

In a second approach, we form organogels with the functionality of the ionic liquid. We benefit from the active ester chemistry to design polymeric chains with the precise functionality encompassing the

different functionals groups present in an ionic liquid. We use benzophenone units to crosslink the polymeric chains and thus form surface-anchored organogels.

We implement independently the two routes for the confinement of ionic liquids in two relevant fields: repellent surfaces and catalysis. First, we studied the wetting behaviour of imidazole-based ionic liquids and identified a suitable surface chemistry to minimize the interfacial interactions with the solid surface. Then, we added topography to create lubricant-infused repellent surfaces, using the ionic liquids as lubricants. In a different approach, we developed an organogel with ionic liquid functionalities to create a robust long-lasting repellent surface.

In catalysis, we coated porous SiC monoliths with Al_2O_3 to create hierarchical porosity and increase the capillary effects for the retention of ionic liquids. In a different application, we coated SiO_2 with a synthesized organogel to create customized polymer supports to be used in the Supported Ionic Liquid Phase (SILP) catalysis.

Zusammenfassung

Flüssigkeitsfilme, die auf einer festen Oberfläche adhärieren oder in sie infiltriert sind, sind ein Konzept, das in vielen technologischen Anwendungen genutzt wird. Solche hybriden flüssigen/festen Oberflächen erfordern eine detailliertes Design von Oberflächenstruktur und chemischer Modifizierung, um die Grenzflächenenergien zu minimieren. Diese Kontrolle über die Grenzflächenenergien ist entscheidend für das Design und die erfolgreiche Anwendbarkeit solcher komplexen Systeme.

Ionische Flüssigkeiten sind eine ungewöhnliche Art chemischer Verbindungen. Sie werden aus Ionen gebildet und haben sie von Natur aus ionische Eigenschaften. Gleichzeitig sind sie aber per definition bei Raumtemperatur flüssig und haben Schmelzpunkte unter 100 °C. Infolgedessen bieten ionischen Flüssigkeiten die generelle Manipulierbarkeit einer Flüssigkeit bei gleichzeitiger Präsenz ihrer bemerkenswerten molekularen Eigenschaften wie extrem niedrigem Dampfdruck, hoher thermischer Stabilität und Nichtentflammbarkeit.

Das Anbinden ionischer Flüssigkeiten auf festen Oberflächen unter vollständiger Beibehaltung ihrer Eigenschaften erfordert eine präzise Kontrolle über die Grenzflächenwechselwirkungen zwischen einer ionischen Flüssigkeit, und dem festen Substrat, auf dem sie gebunden sein soll.

In dieser Dissertation erforschen wir verschiedene Ansätze, um flüssige Filme ionischer Flüssigkeiten auf festen Oberflächen anzubinden. Diese Ansätze werden grundsätzlich nach dem gleichen Prinzip geführt: die Kontrolle der Grenzflächenenergien der ionischen Flüssigkeit und des Trägers, so dass ein Zustand mit minimaler Energie erreicht wird. Ausgehend von der chemischen Struktur einer ionischen Flüssigkeit stellen wir chemische Oberflächenfunktionalität ein, die der Struktur der ionischen Flüssigkeiten ähneln, um eine Grenzfläche mit möglichst geringer Energie zu erhalten.

Zunächst binden wir ionische Flüssigkeiten durch die Modifikation der Festkörperoberfläche an den Träger, indem wir sowohl geeignete Oberflächenchemie als auch Kapillarkräfte einsetzen. Wir nutzen die Silanchemie, um die Oberfläche von SiO_2-basierten Materialien zu modifizieren, indem wir chemische Funktionalitäten hinzufügen, die den funktionellen Gruppen der ionischen Flüssigkeiten ähneln. Wir fügen Topographie auf der Nano- und Mikroskala hinzu, um die Kapillarwirkung zu erhöhen.

In einem zweiten Ansatz bilden wir Organogele mit der Funktionalität der ionischen Flüssigkeit. Wir nutzen die Aktivesterchemie, um polymere Ketten mit einer auf die verwendete ionische Flüssigkeit angepassten

Funktionalität zu synthetisieren.. Wir verwenden Benzophenon-Einheiten, um die Polymerketten zu vernetzen und die enstehenden Organogele auf der Oberfläche zu verankern.

Wir untersuchen diese beiden Routen zum Anbringen eines Flüssigkeitsfilms auf eine feste Oberfläche in zwei relevanten Bereichen: abweisende Oberflächen und Katalyse. Zunächst untersuchten wir das Benetzungsverhalten von ionischen Flüssigkeiten auf Imidazolbasis und identifizierten eine geeignete Oberflächenchemie, um die Grenzflächenenergien mit der festen Oberfläche zu minimieren. Dann fügten wir die Topographie hinzu, um mit flüssigkeitsinfiltrierte, abweisende Oberflächen auf Basis von ionischen Flüssigkeiten zu schaffen. In einem anderen Ansatz entwickelten wir ein Organogel mit ionischen Flüssigkeitsfunktionalitäten, um eine robuste, langlebige abweisende Oberfläche zu schaffen.

In der Katalyse beschichten wir poröse SiC-Monolithen mit Al_2O_3, um hierarchische Porosität zu erzeugen und die Kapillareffekte für die Retention ionischer Flüssigkeiten zu erhöhen. In einer anderen Anwendung beschichten wir SiO_2 Trägermaterialien mit den synthetisierten Organogelen, um maßgeschneiderte Polymerträger zu schaffen, die in der Supported Ionic Liquid Phase (SILP)-Katalyse verwendet werden können.

Resumen

Películas líquidas confinadas a una superficie sólida es un concepto que ofrece ventajas relevantes a muchas aplicaciones tecnológicas. Dicho concepto requiere un diseño de ingeniería detallado, basado completamente en la naturaleza del líquido y la superficie sólida, que a su vez se seleccionan en función de la aplicación final. El control de las interacciones interfaciales entre el líquido a confinar y el soporte sólido es fundamental para el diseño y el buen funcionamiento de estos complejos sistemas.

Los líquidos iónicos son un tipo inusual de compuestos formados enteramente por iones, por lo que tienen intrínsecamente propiedades iónicas, sin embargo, se encuentran en forma líquida a temperatura ambiente o tienen puntos de fusión por debajo de los 100°C. Como resultado, los líquidos iónicos ofrecen las características típicas de un fluido líquido con características no convencionales, como presiones de vapor extremadamente bajas, alta estabilidad térmica y no son inflamables.

Un confinamiento de líquidos iónicos en superficies sólidas que mantenga íntegramente las propiedades del líquido iónico requiere controlar las interacciones interfaciales entre un líquido iónico y el sustrato sólido donde será confinado, sin perder de vista la complejidad estructural inherente de los líquidos iónicos.

En esta tesis doctoral, exploramos diferentes enfoques para confinar líquidos iónicos en superficies sólidas, dichos enfoques están guiados fundamentalmente por el mismo principio: el manejo de las interacciones interfaciales del líquido iónico y el soporte o superficie sólida, de manera que se obtenga un estado de mínima energía. Tomando como referencia la estructura química de un líquido iónico, fabricamos superficies químicas que se asemejan a la estructura química de los líquidos iónicos para asegurar interacciones interfaciales de baja energía.

En primer lugar, confinamos los líquidos iónicos al soporte a través de la modificación de la superficie sólida, implementando la química superficial adecuada y fuerzas capilares. Hicimos uso de la química de silanos para modificar la superficie de los materiales basados en el SiO_2, añadiendo una funcionalidad que asemeja a los grupos funcionales de los líquidos iónicos. Además, añadimos topografía en la nano y microescala para aumentar los efectos capilares.

En un segundo enfoque, formamos órgano-geles que poseen funcionalidad semejante a la estructura química del líquido iónico. Nos beneficiamos de la química de los ésteres activos para diseñar cadenas

poliméricas con una funcionalidad precisa y específica que abarca los diferentes grupos funcionales presentes en un líquido iónico. Adicionalmente, utilizamos unidades de benzofenona para reticular las cadenas poliméricas y formar los órgano-geles.

Implementamos de forma independiente las dos vías para el confinamiento de líquidos iónicos en dos aplicaciones de relevancia: las superficies repelentes y la catálisis. En primer lugar, estudiamos el comportamiento de humectación de los líquidos iónicos basados en imidazoles e identificamos una química superficial adecuada para minimizar las interacciones interfaciales con la superficie sólida. Después, añadimos topografía para crear superficies repelentes con lubricante, haciendo uso d elíquidos iónicos como lubricantes. En un enfoque diferente, desarrollamos órgano-geles con funcionalidades de líquidos iónicos para crear una superficie repelente robusta y de larga duración.

En catálisis, recubrimos monolitos porosos de SiC con Al_2O_3 para crear una porosidad jerárquica y aumentar los efectos capilares para la retención de líquidos iónicos. En otra aplicación, recubrimos SiO_2 con un órgano-gel sintetizado para crear soportes poliméricos diseñados especialmente para su potencial aplicación en la catálisis de líquidos iónicos soportados (SILP) en fase líquida.

Table of Contents

1. Introduction

The accelerated evolution of science over the past 500 years, which began with the first contact with a fascinating world at the micro-scale thanks to the microscope of Antonie van Leeuwenhoek, has allowed us to explore beyond our senses, to imagine and realize the technological progress we can witness today.

Through the observation of the daily life phenomena around us and their interpretation, we have shaped our own development. The scientific tools available today have allowed us to scrutinise and replicate the most sophisticated technologies that have ever existed, those of nature: from the 'eternal', unbleachable structural colours of insects to the complex mechanisms involved in keeping bird feathers dry after a dive underwater in search of food.

Emerging technologies inspired by nature demand the integration of different fields of research. Such is the case of functional surfaces that are nowadays widely investigated and employed. The growing field of nanotechnology now offers ever closer sights and understanding of the physics and chemistry of surfaces, assisting the exploration of such functional interfaces. The community of interfacial scientists is experiencing exponential growth as nano and micronscale materials are very much dominated by interfacial effects.

Lubricant-infused surfaces have gained a lot of attention since their emergence 10 years ago due to their remarkable repellent properties. Inspired by the pitcher plant, a lubricant is firmly confined in a solid surface, causing all potential contaminants slide off the surface. The design of lubricant-infused surfaces has required detailed interfacial engineering, with the centrepiece being the understanding of the wetting phenomenon.

Wetting has been thoroughly investigated since the early 19th century, when Pierre Simon de Laplace and Thomas Young created the field of capillarity for the study of interfaces between two immiscible liquids, or between a liquid and air. Since then, we know that the interfaces are deformable i.e. they are free to change their shape to minimize their surface energy. Such knowledge has made possible the design of surfaces to tailor their wetting behaviour.

The most fundamental parameter in surface science is the surface tension, a parameter defined at the macroscopic scale, yet interpreted at the molecular level as follows: intermolecular attractions play an

important role in condensed matter, so it is energetically favourable for a molecule to be surrounded by other molecules. Molecules at the boundaries are surrounded by 1/2 of the molecules or less compared with the bulk, which is arranged asymmetrically around the interfacial molecule and is energetically unfavourable. The surface tension is the work needed to bring a molecule from the bulk to the surface.[1,2]

With the surface tension in mind, designing a solid surface to control its wetting behaviour becomes intuitive. To repel a liquid, one can modify the solid surface functionality to cause the molecules in the liquid boundaries to prefer the intermolecular interactions with its bulk rather than the interfacial interaction with the solid surface. Conversely, to make a liquid wet a solid surface, the solid surface functionality must cause the molecules of the liquid boundaries to like the interfacial interaction with the solid surface as much as possible, ideally at the same degree as the intermolecular attractions with its bulk. The solid surface functionality preferred by the liquid is a functionality resembling its chemical structure.

Repellent lubricant-infused surfaces are not the only application that requires a liquid to completely wet a surface and remain firmly confined. Supported ionic liquid phase (SILP) catalysis uses a thin layer of ionic liquid in solid surfaces in hybrid catalytic systems. The SILP catalysis can be benefited from the knowledge on the wetting phenomenon to stably retain the ionic liquid, avoiding the costs of losing ionic liquid during the catalytic process.

The peculiarity of the ionic liquids is their structural complexity. The molecular interactions governing the ionic liquids are difficult to identify for the interfacial engineering design, making confinement of ionic liquids a challenging task. To find the right components for an appropriate interfacial design able to achieve the confinement of ionic liquids and which challenges need to be overcome will be discussed in this thesis.

2. Theoretical Background

2.1 Ionic Liquids

Ionic liquids (ILs) are a class of compounds that are formed entirely of ions, yet have the peculiarity of being liquids at room temperature, or they have melting points below 100°C.[3–5] ILs are usually formed by the combination of a substituted organic cation, which can be large and/or asymmetric, and an inorganic anion of delocalized charge. This combination results in salts of relatively weak interactions, which decreases the ionic tendency to form crystals and, therefore, to form solids (Figure 1).[3,6]

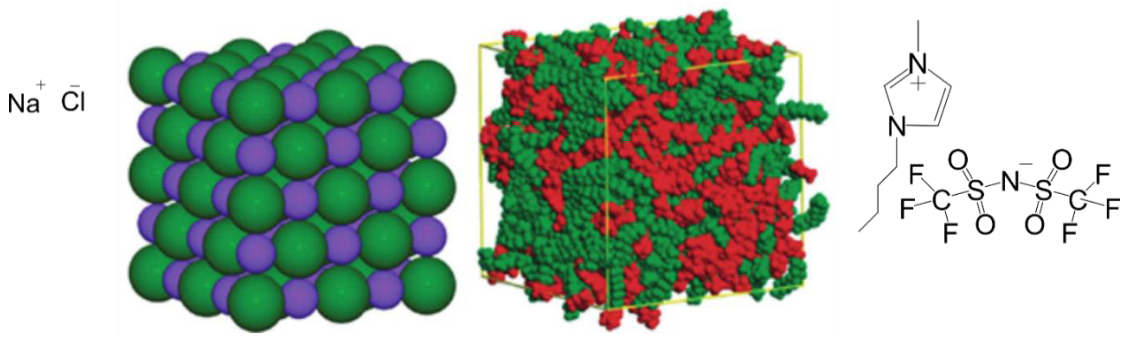

Figure 1. Schematic comparison of the structural arrangements of an ionic crystal with classical charge ordering structure (left) and an ionic liquid of 1-alkyl-3-methylimidazolium (right), that presents polar (red) and nonpolar (green) nano domains. Adapted from reference [7]

The ionic nature of the ILs, hydrogen bonds and van der Waals forces provide the ILs with extraordinarily interesting properties, including extremely low vapor pressures, high thermal stability and non-flammability.[3,4,8,9] In addition, the structural composition of the cation and anion determine properties such as melting point, viscosity, refractive index, density and solubility. Therefore, these properties can be tailored to specific applications by the combination of a suitable anion and cation.[8]

The design of an IL can be exploited in different directions, for instance in processes requiring solvent extraction or product separation, the relative solubility of the IL can be adjusted. Such is the case of 1-butyl-3-methylimidazolium hexafluorophosphate [BMIM][PF_6] that forms a triphasic solution with water

and alkanes, resulting in a so-called clean synthesis since the separation processes are simplified i.e. the required purification of products are processes with a low energy demand.[8]

Imidazole-based ILs (Figure 2), which are one of the most studied and used ILs,[8] can be tailored by modifying the side-chains, the substitution at 1- and 3- position on the imidazolium ring. In this way, functional carbon chains can be added to the imidazolium ring to perform specific tasks for the final application or as a tool in the design of functional materials.[10,11]

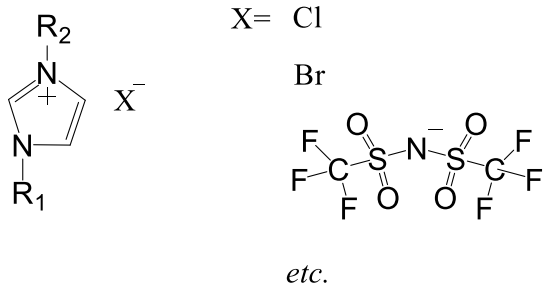

Figure 2. General chemical structure of imidazolium-based ionic liquids

There have been 10^{18} anion-cation combinations that can form ILs reported.[12] The vast variety of possible ILs allows their development for a large number of applications. When ILs first gained popularity, they were thought as green solvents based on the premise that their negligible vapor pressures avoid environmental contamination by evaporation and have a useful life time far superior to that of conventional solvents,[8] however, nowadays their environmental character is still up for debate due to their potential toxicity and long term soil contamination.[13,14]

In catalysis, the ILs have been widely studied due to their ability to dissolve many transition metals without the need for additional use of special ligands, which simplifies the catalytic process in general and allow tailoring activity and selectivity.[8,15–17] Additionally, some ILs exhibit catalytic activity on their own, so ILs have been used as reaction media and catalysts, such is the case of acidic chloroaluminates containing ILs for Friedel-Crafts and cyclization reactions.[16,18] Some of the most relevant reactions that have been optimized using ILs as solvents for catalysts include Diels-Alder reactions, Friedel-Crafts reactions, nitrations and halogenations.[5]

2.2 Confining Liquids to Surfaces

Confining a liquid to a surface is a concept explored in different fields since many applications involve a 2-phase system as the functional material. A liquid partially immobilized and strongly confined in a solid surface offers the availability of the liquid properties while either provide structural and mechanical advantages of the solid support or protection to the solid support.[13,19,20]

Liquids confined to solid surfaces have been extensively analysed in the last years, and the available literature currently encompasses their fabrication,[21,22] the physical phenomena surrounding them,[23,24] and their multiple applications developed until today.[25]

A liquid is confined to a solid surface and kept as a stable mobile interface by means of interfacial engineering.[1] The liquid and the solid are selected and/or modified so they have a mutually high affinity. The liquid can form a thin film on the solid surface if there is a favourable energetic state.[26] In terms of thermodynamics, this energetic state is described by a low interfacial energy of the liquid and the solid surface. The retention of the liquid can be further increased by capillary forces on a rough surface or by polymeric networks.[1,2,26]

In this thesis, we explore two different approaches for the confinement of liquids. The two approaches are governed by interfacial engineering and are describe in detail in this chapter. The first approach consists of two components: 1. Addition of surface topography to retain the liquid via capillary forces and, 2. Modification of the solid surface chemistry to tune the interfacial energy of the liquid and solid. Figure 3a, shows a schematic representation of a surface topography depicted by square pillars, and the presence of a surface compound (red line) to modify the surface chemistry and, in turn, the affinity between the liquid (yellow) and solid surface (black).

The second approach consists of using polymeric networks that are functionalized to provide a high affinity to the liquid to be confined. The functionalized polymeric chains are crosslinked forming three-dimensional covalently bonded networks, known as organogels. The organogels are able to be swollen by the desired liquid and therefore immobilize it by preferred chain-liquid interactions within the network. Before being swollen, the organogels can be attached covalently to surfaces to form a stable coating. Figure 3b shows a schematic representation of an organogel with a confined liquid in a solid surface.

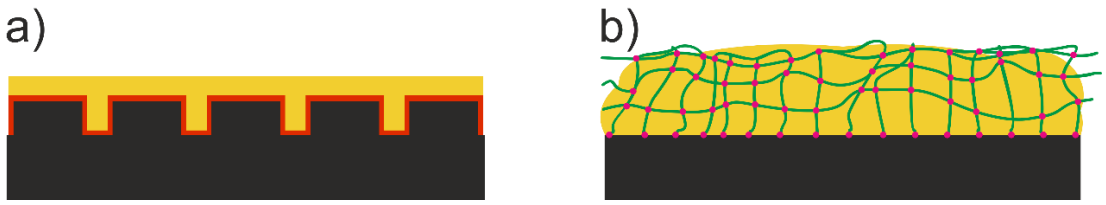

Figure 3. Schematic representation of the two approaches employed during the thesis. a) confinement of a liquid (yellow) through the combination of an appropiate interfacial energy by the modification of the surface chemisty (red line) and capillary forces generated by surface topography (black pillars). b) confinement of a liquid (yellow) through the use of a tailored organogel (polymer green with crosslinks in pink dots).

Approach A: Interfacial Energy and Capillary Forces

The pioneering works on lubricated surfaces described the conditions to form a thermodynamically stable system that uses topography and surface chemistry to keep in place a liquid, denominated lubricant, and takes the form of Figure 3a.[19,23,27] Several conditions need to be fulfilled to form a stable coating. First, the lubricating liquid must be immiscible with other liquids that potentially will be in contact with it. Second, the lubricant must wet completely and stably adhere to the solid surface, and in presence of another liquid the lubricant must remain wetting the surface without being replaced by the lubricant.[19,23,27]

2.2.1.1 Wetting and Contact Angle

The complete wetting of the solid surface is only possible if the lubricant has a high affinity to the surface i.e. there is a low interfacial energy between the solid surface and the liquid. The affinity can be increased by enlarging the surface area of the solid surface and by the chemical modification of the surface considering the structure of the given lubricant.[21] Furthermore, to ensure that the lubricant will adhere and remain on the solid surface in the presence of another liquid, the interfacial energy between the lubricant and the solid surface must be minimized.[21,27]

The affinity between a liquid and a solid surface is described by means of the contact angle, which is the angle formed by a drop of the liquid placed in the solid surface, in the intersection of the liquid-gas

interface and the liquid-solid interface.[2] The Young equation describes the interactions between a drop of liquid and a solid surface using the contact angle ant the tangent lines in the interfaces of the droplet profile, [28] as shown in Figure 4. It involves the surface tension of the liquid (γ_{gl}), the surface free energy of the solid (γ_{sg}) and the interfacial tension between the liquid and the solid (γ_{sl}). Young equation is a balance of the cohesive forces of the molecules at the boundaries of the liquid and the adhesive forces between the solid and the liquid. It represents a facile approximation of the affinity between the liquid and solid. The smaller the contact angle the higher is the affinity.[2,28]

$$\gamma_{sg} = \gamma_{sl} + \gamma_{lg} \cdot \cos\theta$$

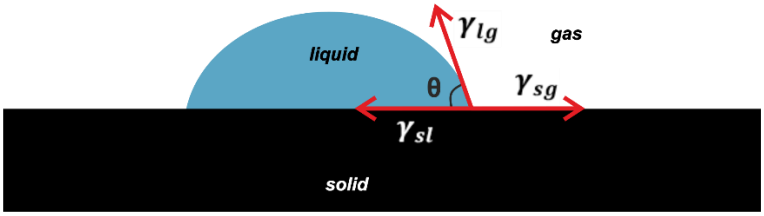

Figure 4. Schematic representation of the Young equation. A drop of a liquid forms a contact angle θ in the interface of the solid where is deposited and the gas phase. The Young equation describes the balance of surface energy of the solid γgl, the surface tension of the liquid γgl and the interfacial energy γsl

2.2.1.2 Surface Functionalization

The interfacial energy between a lubricant and the solid surface can be designed and adjusted through the modification of the surface chemistry of the solid.[21,22,27] The addition of a functional group to the surface that maximize the affinity between the lubricant and the solid will in turn minimize the interfacial energy.[2]

There are several techniques to modify a surface depending on the nature or composition of the surface. Among the possible different chemical processes, the formation of self-assembled monolayers (SAMs) offers the choice to adhere any functional group to a specific surface by using molecules that hold in their structure the desired functional group together with an anchor group. Some examples of anchor groups are thiols, silanes, phosphonates, and catechols.[2]

The concept of SAMs is attributed to the chemisorption of a molecule to specific solid surfaces.[2] Although the adsorption of a molecule that forms a covalent bond with the surface follows different reaction mechanisms based on the nature of the components, it occurs spontaneously, which is why it is described as self-assembled.[2]

The most studied SAMs are organic molecules containing a thiol group to bind to gold, and molecules containing a silane group to bind to silicon-based substrates. In general, the thiol or silane groups forming the covalent bond with the substrate, are denominated the anchor or reactive group. The rest of the molecule that decorates the surface and determines the surface chemistry of the substrate is called the rest or tail group (Figure 5).[2]

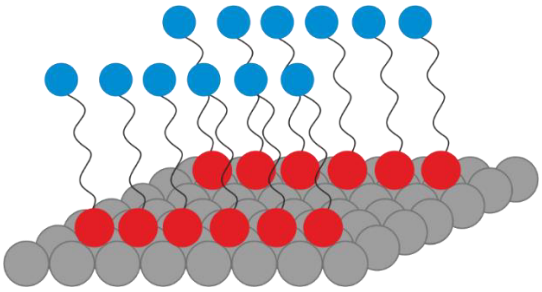

Figure 5. Schematic representation of self-assembled monolayers on surfaces. The grey circles represent the surface, the red circles represent the reactive or anchor group of the anchoring molecule and the blue circles represent the rest or tail group.

Molecules that contain a thiol group, have as general chemical structure R-SH or $R(CH_2)_nSH$ if they have an alkyl chain (Figure 6). The reaction mechanism of the formation of thiol-based SAMs has not been fully elucidated, but generally it is agreed to be a mechanism by which the thiol loses its hydrogen atom and binds as a thiolate.[2] The reactive group can also be disulfides. Addionally, thiols and disulfides are able to bind to other metallic surfaces like Ag, Cu, Pd, Pt, Ni and Fe. In any case the thiol requires a oxide-free surface.[29] In practical terms, the thiol-based SAMs are created by simple vapor deposition or in solution with an appropriate solvent, like ethanol or dichloromethane.[2,29]

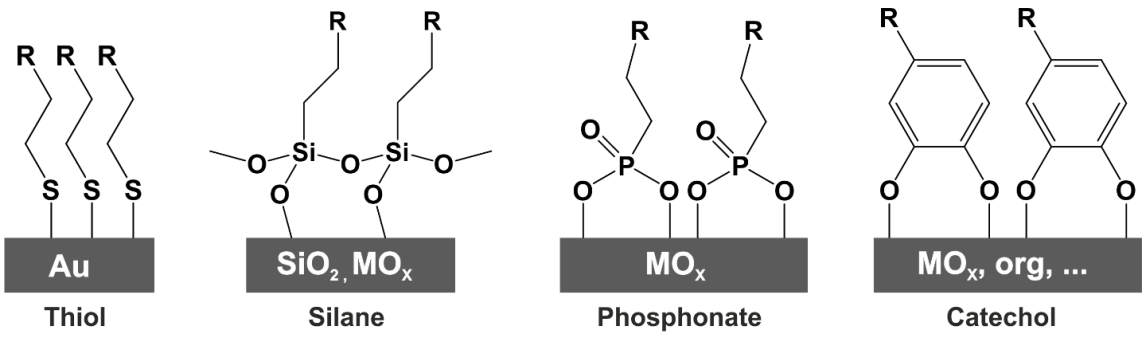

Figure 6. Chemical structure of some commonly used anchor groups in SAMs molecules in some of the surfaces they can adhere to. (MO_X = metal oxides, org= organic substrates).

Analogously, silanes are molecules that contains a silicon atom that holds up to three reactive groups, additional to the rest or tail group (Figure 6).[2] The reactive parts are usually hydroxy (-OH), chlorine (-Cl), methoxy (-OCH_3), or ethoxy (-OCH_2CH_3) groups. The tail group can be in many forms, from an alkyl chain to most of the functional groups available in organic chemistry[30,31]

The silanes react with silanol groups (SiOH) on silicon-based surfaces in a reaction denominated silanization.[30] The accepted reaction mechanism of the silanization encompasses a hydrolysis step, by which the silane, when it is approaching the surface, reacts with water molecules to form silanol groups. The hydrolysis determines the speed of reaction and depends on the reactive groups, with -Cl being the most reactive and -OCH_2CH_3 the least reactive. A second step of the silanization is the condensation of the silanol groups whereby a siloxane bond is formed.[2,30,32] Although silicon-based surfaces are the most effective substrate to modify by silanization, other metal oxide substrates are also effective, including Al_2O_3, TiO_2, Cr_2O_3, SnO_2 and indium tin oxide.[33] Silananizations can be carried out by vapor deposition in the case of volatile and reactive silanes, or in liquid phase with an appropriate solvent.[33]

Other anchoring groups are the phosphonates (Figure 6), that include molecules containing phosphoric acid, dimethyl phosphonate, diethyl phosphonate and 1,1,-bisphosphonic acid among the commonly used.[33] The phosphonates-based SAMs are typically assembled in liquid phase over hydroxylated oxidic substrates.[34]

It has been reported that the mechanisms of chemisorption of phosphoric acids is dictated by the reaction conditions including concentration, temperature, type of oxide and pH.[33,34] Generally, the phosphoryl oxygen coordinates, to an extent, with the surface depending on how Lewis acidic the surface is, to then

undergo a heterocondensation with a hydroxy group of the surface to form a strong covalent phosphorus-oxygen-metal. The phosphonates are less susceptible to self-condensation in presence of water than the silanes, the phosphonates-based SAMs can assembly even using water as solvent. [33]

Biomimetic SAMs have been extensively explored as well. Ortho-hydroxyaryl compounds or catechol-containing compounds constitute up to 30% of the amino acids in mussel adhesive proteins, for this reason these compounds represent a promising approach to form robust, strongly bonded monolayers.[33] Catechol derivates (Figure 6) can form SAMs in a wide variety of surfaces of both organic and inorganic materials, including noble metals, metal oxides, silica, ceramics and polymers.[35,36] The mechanism of adhesion is still not fully understood,[37] nevertheless there are proposed theories that suggest coordination bonding of the oxygen atoms of the catechol to centres in the surface. In the case of metallic surfaces, it has been suggested that bidentate chelating bonding where the two oxygen atoms in catechol bind to a single metallic centre could occur. But also bridged bidentate bonding involving two metallic centres, as well as hydrogen bonding.[33,35] With organic materials, the catechol can form covalent or strong noncovalent interactions like hydrogen bonding and π-electron interactions.[35,37]

Additional to the mentioned anchoring groups, other molecules have been reported to be able to bind to solid surfaces. Such is the case of alkyl amines that can coat hydroxylated surfaces, however the attachment is reported to be weak and in the form of random islands over the surface.[33] Alkenes and alkynes can also be attached onto hydroxylated surfaces with the help of UV irradiation.[38]

Taking into account the available options of anchor groups, the SAMs constitute a feasible approach to fine-tune the surface of a material. At the other side of the molecules, the rest or tail group used to form SAMs can be virtually any functional group, allowing us to design the surface energy or chemistry of a solid substrate at our best convenience. There have been reported a wide range of functional groups for the modification of solid substrates in different applications. The most used have been amines-, alkenes-, carboxylic acids- and hydroxy- terminated molecules, but also fluorinated alkyl, alkanes, aryl and imidazole rings have been widely employed.[33]

An example of what can be done by surface modification via SAMs is the shifting of hydrophobic character of a surface. This has been portrayed in the work on functionalization of gold films with two different thiols, dodecanethiol and 11-mercapto-1-undecanol. The combination of thiols fine-tune the hydrophobicity and by this, drastically changes the adhesion of Escherichia coli flagella as a function of the hydrophobic character of the surface.[39] Figure 7 shows all the relevant figures of the work, including

the water contact angle of the surfaces with SAMs of the mixed thiols. 11-mercapto-1-undecanol confers hydrophilicity to surface as a result of the hydroxy-terminated thiol. The higher the amount of 11-mercapto-1-undecanol in the surface the smaller the water contact angle.[39] By measuring the adhesion of isolated flagella using a quartz crystal microbalance, the authors observed a higher adhesion of flagella in hydrophobic surfaces. The findings contribute to the understanding of live-cell adhesion mechanism on surfaces.[39]

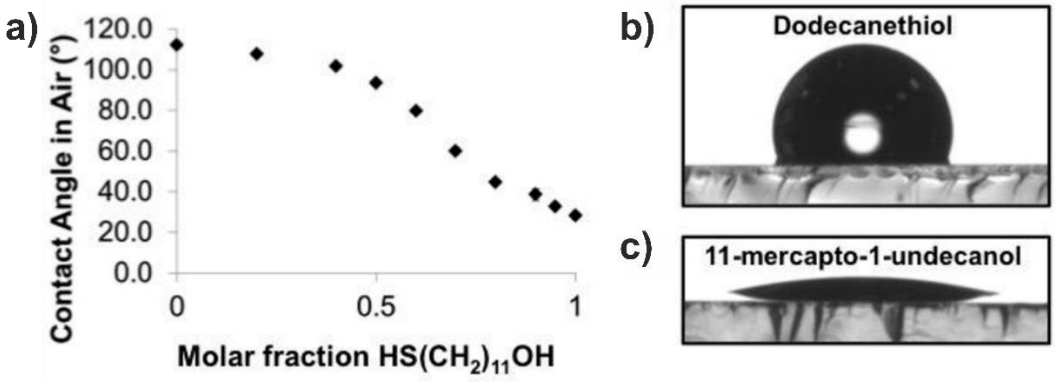

Figure 7 (a) Contact angle of a water droplet on mixed tiol SAM surfaces, in air; averaged over 5 measurements on two separate simples. SAMs are composed of a blend of 11-mercapto-1-undocanol and dodecanethiol in the fractions indicated. Water droplets are shown (b) on the most hydrophobic (100% dodecanethiol) SAM surface, and (c) the most hydrophilic (100% 11-mercapto-1-undecanol) SAM surface. Adapted from reference [39]

Relevant to the confinement of liquids (lubricants) in solid surfaces, the selection of the functional group to anchor to the solid surface is entirely based on the chemical structure of the lubricant. A high affinity is ensured by matching the surface chemistry with the chemical structure of the lubricant.[21,27] For example, the optimal surface chemistry for a silicon oil that contains hydrocarbon chains is a hydrocarbon chains-containing SAMs. In the same way, for a fluorinated oil, the optimal surface chemistry is a fluorinated surface chemistry compound (Figure 8).The intermolecular interactions at the boundary of a solid surface resembles the intermolecular interactions at the boundary of the liquid, consequently the interfacial energies are minimized.[40]

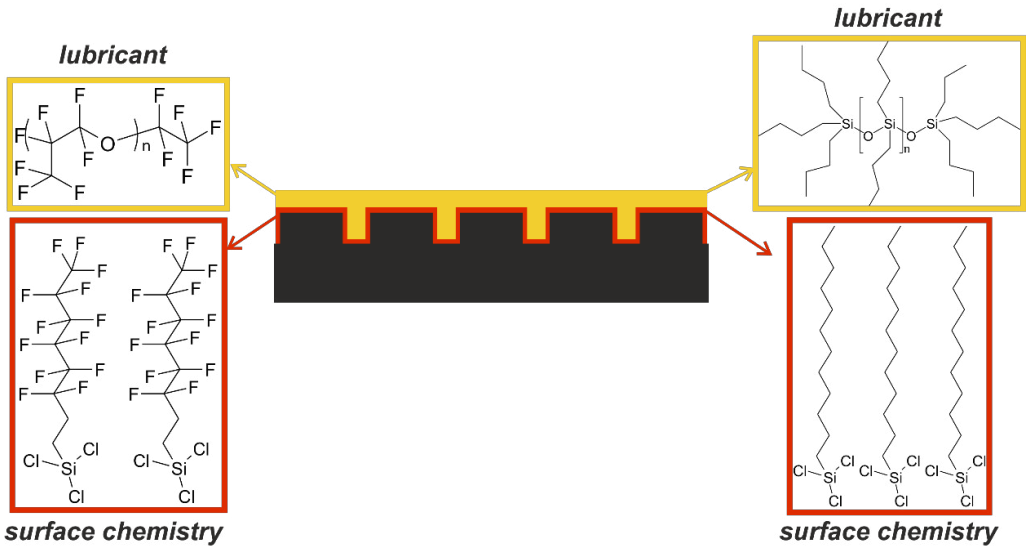

Figure 8. Two examples of optimal surface chemistries compounds for SAMs based on the chemical structure of lubricant to confine. (left) chemical structure of fluorinated oil (Krytox) and trichloro-(1H, 1H,2H, 2H,-perfluoroctyl)-silane. (right) chemical structure of a silicon oil and trichloro(dodecyl)silane.

2.2.1.3 Roughness and capillarity

Capillary effects on a rough surface plays a crucial role both in the wetting and the retention of the lubricant on the surface.[21]In applications involving hierarchical porosity i.e. additional topography over an already porous structure, an increment of the capillary effects and the retention of the lubricant is generally observed.[41–43]

This phenomenon is expected and described by looking at the wetting behaviour of a liquid on rough surfaces. According to the Wenzel model of wetting either the hydrophobic or hydrophilic character of a liquid on a surface is magnified by the presence of roughness.[44] The Wenzel model is based on the Young's equation (chapter 2.1.1), and takes into consideration the roughness of the surfaces by implementing a roughness factor, *R*. This factor defines a ratio between the actual surface area and a projected surface area.[44]

$$\cos\theta_{rough} = R\cos\theta_{flat}$$

The θ_{rough} indicates the Wenzel contact angle on the textured surface, and θ_{flat} is the apparent contact angle on a smooth, flat surface. For liquids wetting the surface and forming a contact angle below 90°, cos θ_{flat} results in a positive value, which makes cos θ_{rough} a bigger value (multiply by *R*), thus θ_{rough} is decreased, and the hydrophilic character enhanced. For liquids unable to wet the surface, forming contact angles above 90°, the cos θ_{flat} is a negative value, when it is multiplied by *R*, the cos θ_{rough} is a smaller value, the θ_{rough} increases to a more hydrophobic character.[44]

The capillary forces that keep the liquid in place can be explained by starting with the general Young-Laplace equation, also referred as the Laplace equation, that describes the pressure difference between two phases at a curved interface.

$$\Delta P = \gamma \left(\frac{1}{R_1} + \frac{1}{R_2}\right)$$

R_1 and R_2 are the two principal radii of an arbitrary curvature and ΔP is the Laplace pressure. A liquid in a solid and air interface forms a curve since the surface tension tends to minimize the area. The Laplace pressure has implications in the changes of vapor pressure of liquids, in capillary condensation and capillary rise of liquid.

The action of capillary forces is easily observed in the capillary rise phenomena (Figure 9), the meniscus (within the tube) is a portion of a sphere. The radius of curvature *R* of the sphere is equal to the radius *r* of the tube when the contact angle is equal to zero, and more generally to $r/\cos\theta$. The pressure of the curved liquid is given then by the Laplace equation (the curvature of a sphere of radius *R* is $2/R$)

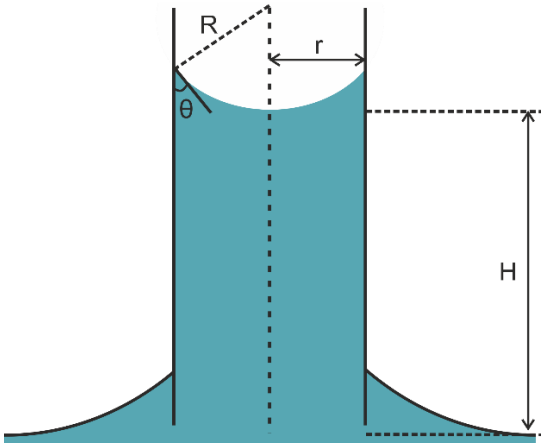

Figure 9. Capillary rise in a capillary tube. R is the radius of curvature of the meniscus formed by the interface, r represents the radius of the capillary tube, θ is the contact angle and H the capillary elevation.

$$\Delta P = \frac{2\gamma \cos\theta}{R}$$

The curved part of the interface is subject to a difference of pressure, in the case of a concave shape as shown in the figure, a lower pressure compared to the surrounding. This decreased pressure is precisely what acts as a pump on the bath and causes the liquid to rise until the pressure is equilibrated by the increased hydrostatic pressure. As the pressure in the capillary is purely hydrostatic the capillary elevation can be obtained from the capillary expression,

$$\frac{2\gamma \cos\theta}{R} = \rho g H$$

Where ρ is the density, g is gravity and H liquid depth.

It is worth noting that the cosine connects the contact angle with the curvature. In an ideal spherical interface with a radius r, the contact angle is $\theta = 0$, indicating a perfect wetting. A neutral wetting is then when $\Delta P = 0$ and $\theta = 90°$. And a non-wetting scenario is when there is a higher pressure in the tube, $\theta > 90°$ and the interface has a convex curvature (Figure 10).

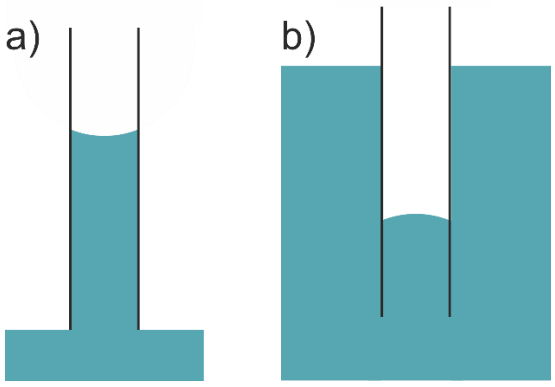

Figure 10. Capillary in different scenarios. a) interface concave curvature of a liquid in contact with a capillary tube when the surface energy of the tube is lower wet than dry and b) convex curvature in the interface of a liquid in contact with a capillary, the molecular interaction between the liquid and the tube are repulsive and the liquid level decreases.

An interpretation of these scenarios at the molecular level is that low contact angles denote attractive molecular interactions, the minimal energy configuration is a solid-liquid interface. High contact angles denote repulsive molecular interactions, where the minimal energy configuration is avoiding the solid-liquid interaction and the liquid level decreases.

For a liquid (lubricant) wetting partially or completely a solid substrate, the contact angle is below 90°, the capillary pressure is then inversely proportional to the radius of the liquid curvature formed in the surface with topography (roughness in the surface),

$$\Delta P \; \alpha \; \frac{\gamma}{R}$$

As a result, for lubricants wetting a solid substrate, the capillary pressure increases with decreasing the size of interstices. That is to say, the smaller the interstitial space of the rough surface, the higher the capillary pressure and the higher the pressure difference keeping the lubricant in the surface.

2.2.1.4 Methods to increase surface roughness

There are many techniques to provide a surface with micro- or nano topography, the selection of the technique is according to the nature of the surface and the application. Among the techniques are deposition of colloids,[45] self-assembled colloidal monolayers,[46] etching,[47] mechanical abrasion or sandblasting[41], temperature treatments,[48] laser lithography, deposition of mesoporous materials, porous polymers or polymeric fibres.[49] Figure 11 shows diverse topographies fabricated using some of these methods.

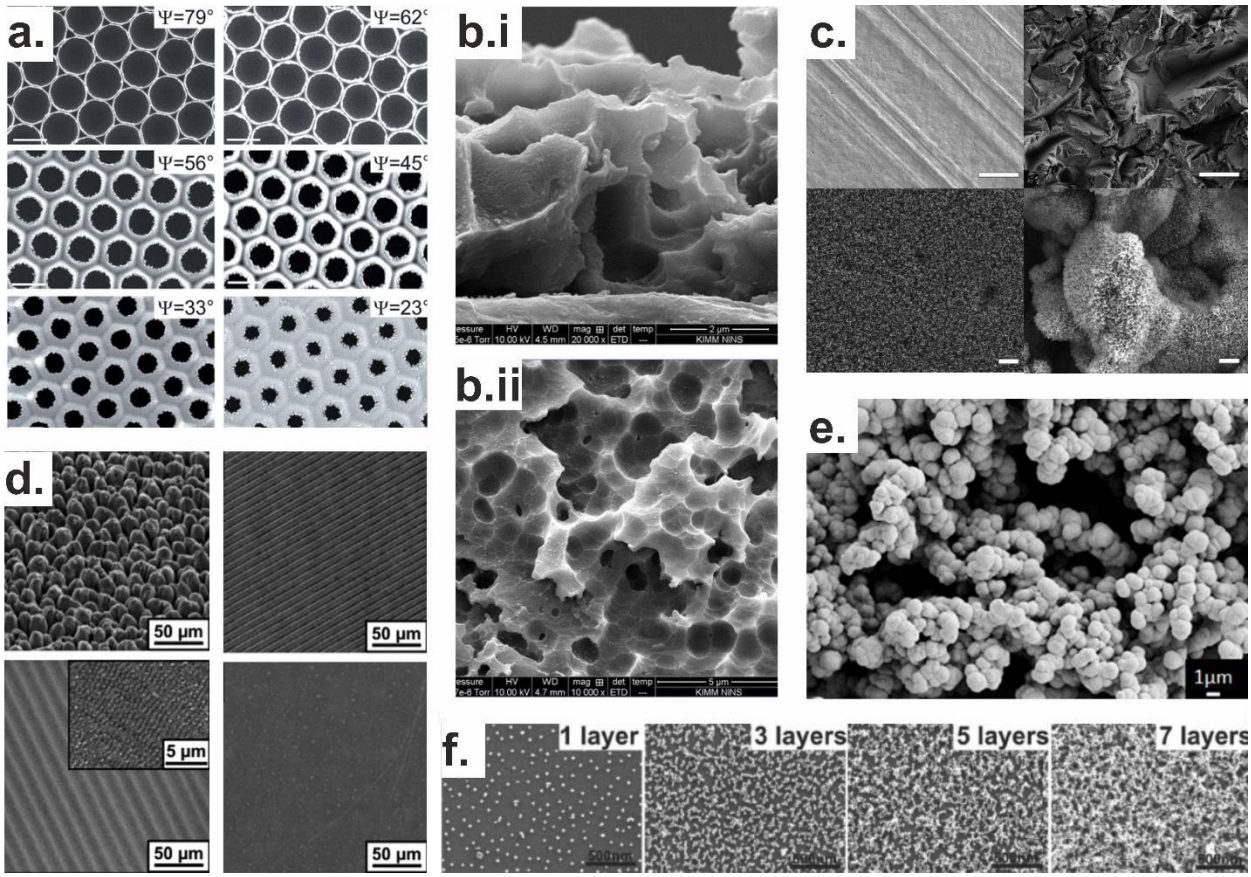

Figure 11. SEM images of topographies in solid surfaces. a) SEM images of self-assembled inverse colloidal monolayers, the colloids were deposited in the surface together with a silica precursor, then the colloids were calcined to form pores with different pore opening angles varying the amount of silica precursor applied. Reproduce from reference [46]. bi and ii) Aluminium plates after etching in a solution of HCl, isopropanol and water at 200°C, reproduced from reference [47]. c) Clockwise, untreated aluminium, sandblasted microstructure aluminium, nanoscale boehmite in flat aluminium and hierarchical texture of sandblasted aluminium with bohemite reproduce from reference [41]. d) Clockwise, laser-generated spikes, grooves and ripples, and unstructured titanium, reproduce from reference [48]. e) Thin porous poly(butyl methacrylate-co-ethylene dimethacrylate films generated through radical polymerization in a glass surface, reproduce from reference [49]. f) Deposition of silica colloidal of 20 nm using Layer-by-Layer deposition, reproduce from reference [45]

Two exemplary methods that are relevant for the work in this thesis will be described in more detail. The first technique is the formation of inverse opals, that are highly ordered porous scaffolds formed by evaporative co-assembly process.[50] A substrate is placed in a suspension of polystyrene colloidal particles and pre-hydrolysed tetraethyl orthosilicate, a precursor for the formation of silicon dioxide (SiO_2), as shown in Figure 12a. The water in the suspension is evaporated very slowly. During the evaporation, the colloids self-assemble in a crystal template on the surface of the substrate and hold in the gaps of the colloids the freshly formed SiO_2.[50] The substrate is then calcined to remove the colloids leaving a highly ordered porous structure. The periodic structure of the inverse opals at the nanoscale provides the

material with structural colour as a consequence of reflected light in interference conditions from the high contrast in the refractive index of the interconnected network and the air-fill pores (Figure 12b).[51–53]

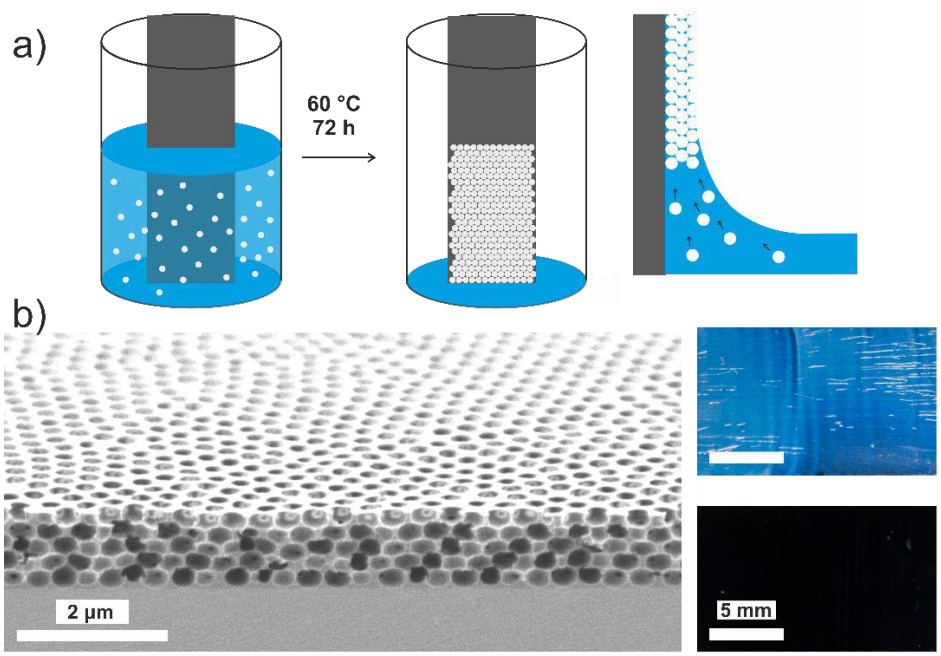

Figure 12. Inverse opals. a) schematic representation of evaporative vertical self-assembly process and b) SEM side view image of an inverse opal and photographs of the structural coloration of an inverse opal (up) and an inverse opal filled with a liquid and losing its coloration (down).

The second technique is the Layer-by-Layer (LbL) deposition of colloidal particles.[54,55] The LbL approach comprises the coating of a surface with different materials of inherently mutually attractive properties.[56–58] The deposition of colloidal particles can be performed using the electrostatic attractive interactions between a positively charged polymer and negatively charged colloidal particles.[54]

The coating is carried out by alternately submerging the surface in a solution of positively charged polymer, like poly(diallyldimethylammonium) chloride (PDADMAC), and in a suspension of negatively charged colloidal particles, such as colloidal SiO_2.[59] The submerging cycles can be repeated iteratively with the certainty of depositing a single layer with each immersion, since the electrostatic attraction is self-limiting.[54,60] Once the electrostatic pair if formed and the surface charged is reversed there is no absorption of more material from the solution or suspension. The multilayer coating is then calcined to remove the polymer, as shown in Figure 13. The result is a surface with a disordered nano topography.[54]

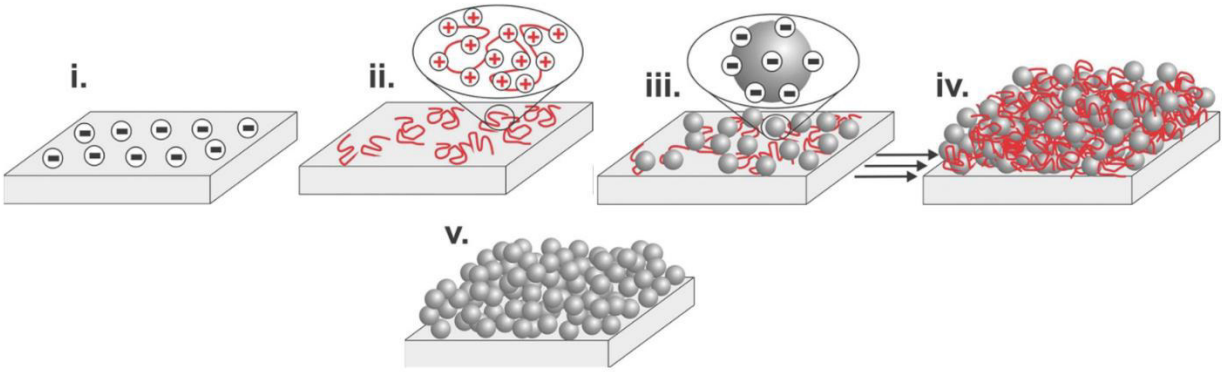

Figure 13. Schematic illustration of the layer-by-layer method to coat surfaces with nanoscale particles. i. the surface is negatively charged, ii. subsequent layers of positively charged polyelectrolyte and negatively charged silica nanoparticles (iii.) are absorbed to form a hybrid thin film (iv.) that then is calcined to produce a porous silica coating (v.).Reproduced from reference [45]

In addition to being exceptionally simple experimentally, the LbL approach offers several attractive features, among them is the controllability of the film thickness by varying the number of immersions in the solution and suspension.[60] It is scalable and objects of any shape can be coated, provided they can be submerged into the solution and suspension.[57]

2.2.1 Approach B: Organogels

The second general approach to confine a liquid to a surface is using organogels (Figure 3b). Organogels are formed by crosslinked polymer networks. In presence of a compatible solvent, polymers reach a thermodynamic equilibrium that can be described by the Flory-Huggins theory of polymer solubility. In presence of crosslinkers, this model is complemented in the Flory-Renher theory and considers an elastic contribution of these crosslinking units. In a three-dimensional polymeric network in contact with a compatible solvent swelling occurs and an elastic retractive force arises containing the solvent in the network.[61]

A thoroughly studied organogel in the context of repellent surfaces is polydimethylsiloxane (PDMS). PDMS is formed by alternating atoms of silicon and oxygen, and methyl groups as side groups on the silicon atom. PDMS can be crosslinked by the addition of chemical crosslinking units or by radiation.[62–64] A

crosslinked PDMS follows the general rule of 'like dissolves like' of solubility and swells in contact with nonpolar solvents like hydrocarbons, dichloromethane, toluene or silicone oil.[64,65] Benefiting from the PDMS swelling properties, technologies using liquid-infused materials have widely employed PDMS swollen with silicone oils (*Figure 14*). The PDMS ensures the immobilization of the oil phase since the chemical composition of the silicon oil is formed by silicon, oxygen and hydrocarbon chains.[20,66–68]

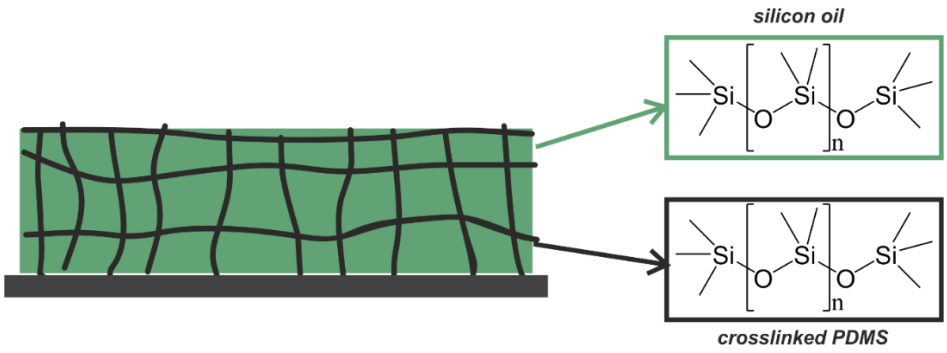

Figure 14. Schematic representation and chemical structure of crosslinked PDMS swollen with silicon oil.

In the same way that the silicone oil can swell the PDMS, other liquids of different compositions can swell different polymers of appropriate solubility. The confinement of a specific liquid via organogels is possible by tailoring the polymer solubility that forms the organogel. The solubility of a polymer in a specific solvent can be designed through the selection of the functional groups forming the polymer.[69]The use of polymer-analogous reactions is a feasible way to synthesize polymers containing in their structure precise and specific functional groups.[70]

2.2.3.1 Polymer-analogous reactions

Polymer-analogous reactions, also referred as post-polymerization modification, are processes by which deliberate changes of the functional groups in a polymer are performed, without affecting the polymer architecture.[71] The post-polymerization modification represent a transformation of a polymer chain into derivatives of functional groups without modifying the polymerization degree.[69,71,72]

Polymer-analogous reactions provide significant advantages and have great technological value since they allow the polymerization of functional units that otherwise could not be obtained, either because the functional units are not compatible with polymerization techniques, the functionality is damaged during the process or there are steric limitations.[69,73–76]

In addition, by making use of polymer analogous reactions, the preliminary polymerization step can be performed using a single monomer, which also simplifies the polymerization process itself, and makes it compatible with a wide variety of different polymerization techniques.

The formation of functional polymers by analogous reactions after polymerization requires the use of active monomers, thus obtaining reactive polymers that are easy to functionalize. In this sense, the so-called active esters represent the active monomers *par excellence*. Active esters easily produce functional amides by allowing an efficient reaction with amines. Polymers such as poly (hydroxysuccidimide acrylate) or polymers containing pentafluorophenol groups can react with amines under very mild reaction conditions (under stirring at room temperature) resulting in functionalized polymers.[69] Figure 15a shows a schematic representation of the post-polymerization modification process to form a functionalized polymer. The left (Figure 15a) corresponds to the polymer chain formed with pentafluorophenyl acrylate, to which a functional molecule with the amine group in its structure is added under mild reaction conditions (right).

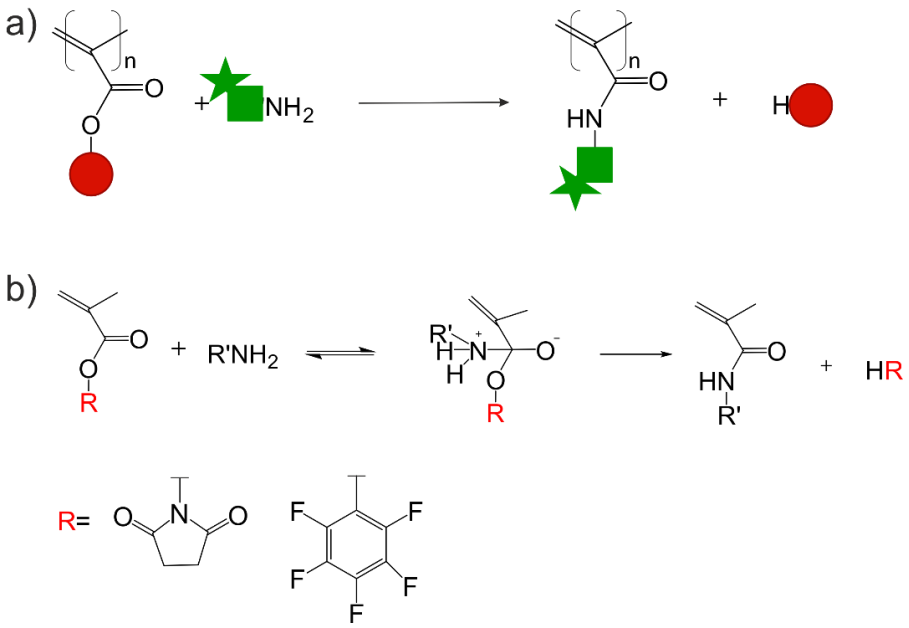

Figure 15. a) Schematic representation of post-polymerization reaction of active ester polymers with an amine to obtain a functional polymer. b) Reaction mechanism of nucleophilic substitution of the amine with an active ester to form an amide. Adapted from reference [77]

At the beginning of the study and development of polymer-analogous reactions, the options involving such reactions were rather limited i.e. only few analogous reactions were known and used.[76] In 1972 Ringsdorf and Ferruti independently reported work using active ester polymers as precursors of functional polymers,[78,79] both are known as the pioneers of functional polymers based on active esters.

2.2.3.2 Active esters

Active esters are carboxylic acid esters that have a good leaving group with high electron density in their structure,.[80] Active esters react with nucleophilic groups, mainly with amines to form the corresponding amides. The reaction mechanism is a nucleophilic substitution, where the amine attacks the carboxylate carbon that is susceptible to such attack due to the presence of the electro-attracting group,[77] as shown in Figure 15b.

Such reactions proceed under very mild reaction conditions, i.e., under stirring at room temperature, and are usually quantitative. Furthermore, it has been shown that amines react with these active esters selectively, even in the presence of weak nucleophiles such as alcohols.[75,77,81–83]

Two examples of active esters quantitative reactions are shown in Figure 16. The first example is the reaction of poly(pentafluorophenyl 4-vinylbenzoate) with isopropyl amine. The conversion of the active ester to form the amide is tracked using time-resolved FTIR spectroscopy. The intensity of the peak at 1760 cm^{-1} associated to the carbonyl carbon of the pentafluorephenol active ester completely vanishes withing less than 5 min, indicating the entire substitution of the pentafluorophenyl group for the isopropyl amine and the formation of the analogous amide (Figure 16a).[75] The second example is the reaction of a poly-norbornene-pentafluoro phenyl ester with hexylamine. The reaction was tracked and the time - resolved FTIR measurements are shown in Figure 16b. The peak at 1777 cm^{-1} (1) decreases at the same rate than the increment of a new peak assigned to the formed amide bond at 1657 cm^{-1} (2), denotating a quantitative polymer analogous conversion.[84]

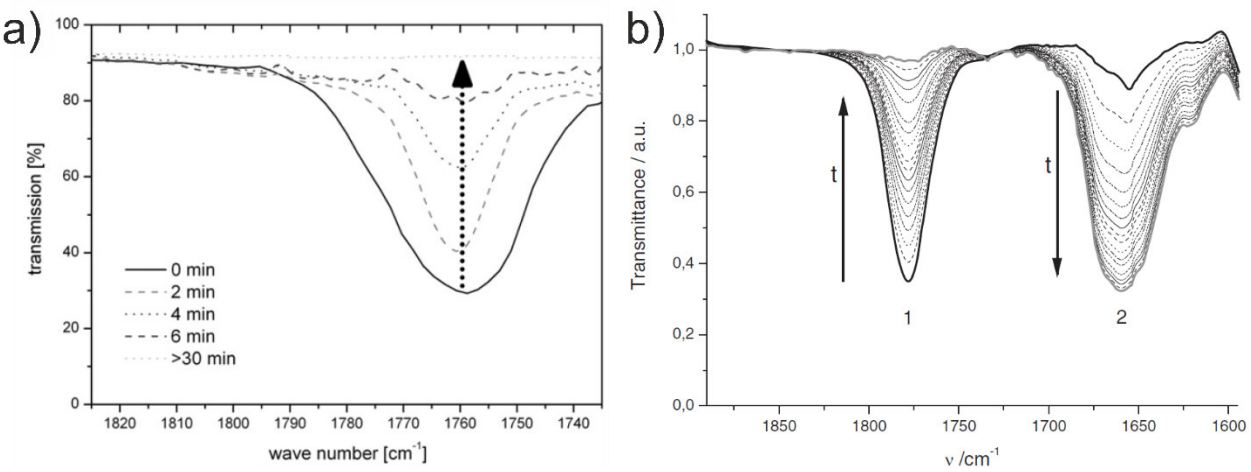

Figure 16. Examples of quantitative polymer-analogous reactions of active esters. a) Time-resolved FTIR measurements of the reaction of poly(pentafluorophenyl 4-vinylbenzoate) with isopropyl amine. The disappearance of peak at 1760 cm^{-1} indicates a complete conversion of the active ester. Adapted from reference [75] and b) time resolved FTIR measurements of the reaction of poly-norbornene-pentafluoro phenyl ester with hexylamine. The disappearance of the peak at 1777 cm^{-1} and appearance of the peak at 1657 cm^{-1} indicates the quantitative conversion of active ester to amide. Adapted from reference[84]

The synthesis and use of a great variety of active esters has been reported, including both vinyl and benzylic esters, and making use of n-hydroxysuccinimide and fluorophenyl groups as electron-attracting leaving groups. However, vinyl esters have been considerably more widely used, because they are compatible with a larger number of polymerization techniques.[83] Regarding the electron-attracting group, the use of n-hydroxysuccinimide presents solubility limitations, since the polymers containing this group are soluble only in dimethylsulfoxide and dimethylformamide, so it is usually co-polymerized with groups soluble in a greater variety of solvents.[83] However, the addition of non-attracting groups to increase the solubility reduces the functionality of the resulting polymers. Therefore, pentafluorophenyl groups represent a convenient choice of electron-attracting group.[83]

In 2005, Theato et al. reported the synthesis of pentafluorophenyl acrylate and methacrylate.[85] These syntheses start from an acid chloride, the methacryloyl chloride, which is attacked by an oxygen atom in pentafluorophenol in an alcoholysis process. The reaction is carried out in the presence of an impeded pyridine, the 2,6-lutidine, in order to avoid Michael addition reactions on the vinyl part of the ester, which would result in its polymerization.[86] Figure 17a shows the proposed reaction mechanism of the alcoholysis of the acid chloride to form pentafluorophenyl (meta)acrylate.

The active ester can be polymerized by a free-radical polymerization, using azobisisobutyronnitrile (AIBN) as initiator. The AIBN forms a radical when is activated with temperature, to then undergo a propagation reaction with the double bond of the vinyl group in the active ester (Figure 17b).[70,87]

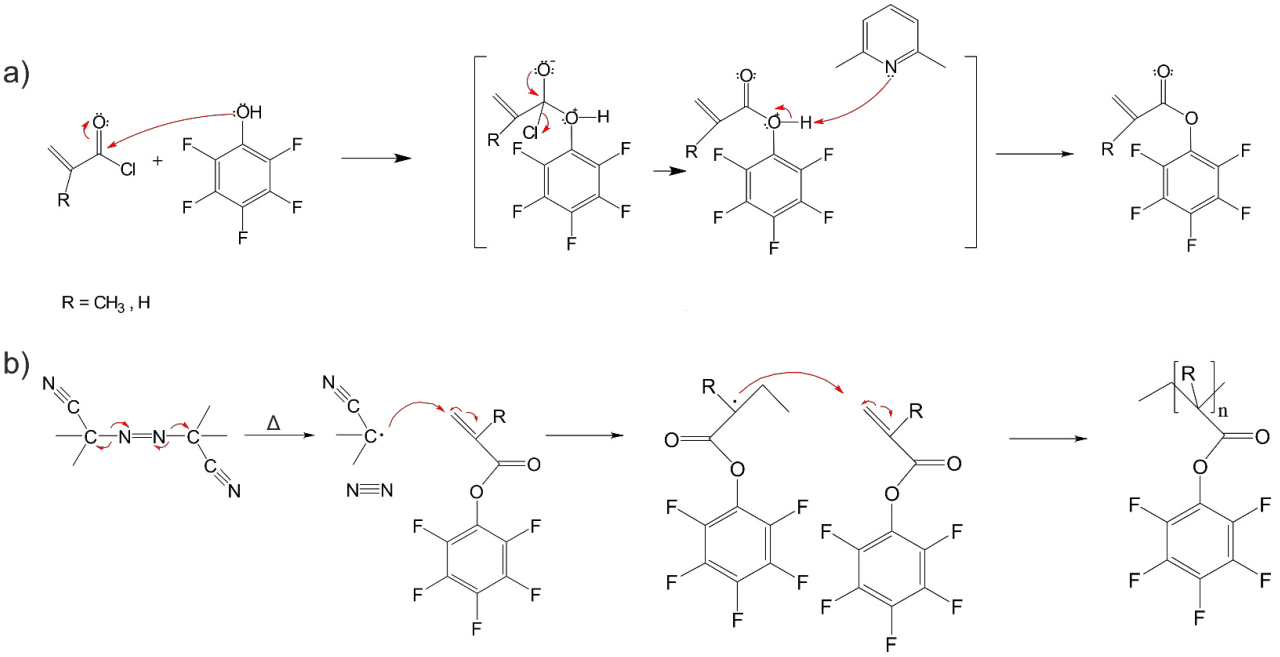

Figure 17. Reaction mechanism for a) the formation of pentafluorophenyl (metha)acrylate from methacryloyl chloride and pentafluorophenol in presence of 2,6-lutidine. Adapted from references [70,88]b) the free radical polymerization of the active ester using azobisisobutyronnitrile.

2.2.3.3 Crosslinker: Benzophenone

The active ester monomer, pentafluorophenyl acrylate can be co-polymerized with benzophenone methacrylate (BP) as co-monomer, the BP is a photoactive crosslinker able to link aliphatic chains and form the networks. The crosslinking reactions are induced by activation of benzophenone units by UV radiation. During the polymerization the vinyl part of the benzophenone methacrylate participates in the radical polymerization without affecting the functionality of the benzophenone group.[89–93]

The mechanism by which the crosslinking of the polymeric chains takes place starts with the irradiation with light in the UV range (350 nm), which induces an electronic transition to the antibonding π orbital

($n\pi^+$) of the benzophenone group leading to the formation of a biradical that is able to extract a hydrogen atom from any aliphatic C-H bond. This, in turn, forms a radical pair and leads to the formation of a stable C-C bond,[94,95] The proposed mechanism is shown in Figure 18.

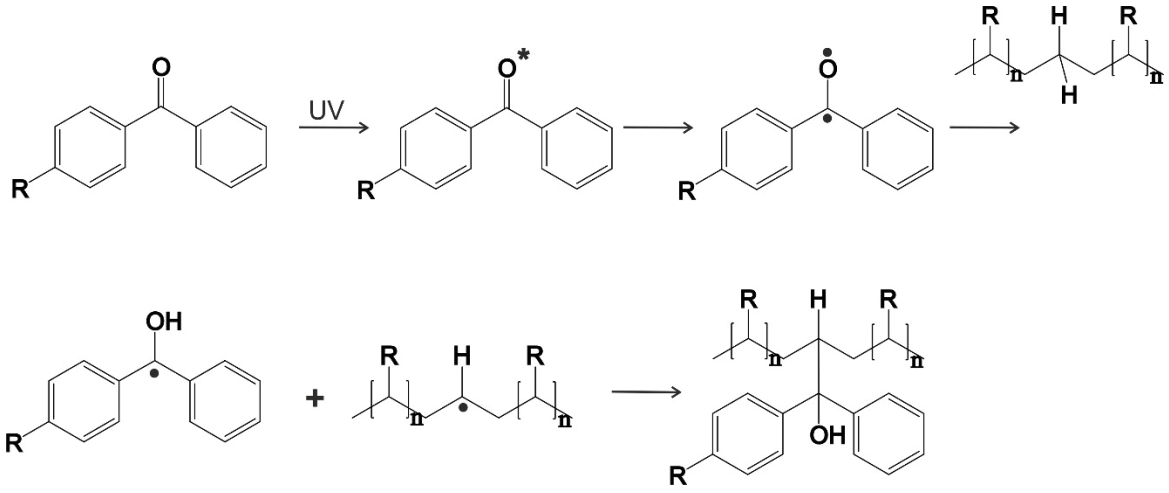

Figure 18. Reaction mechanism of benzophenone crosslinking to an aliphatic carbon atom.

The degree of crosslinking is controlled by the number of crosslinking units added to the chain during polymerization, or by the irradiation time in the crosslinking reactions.[94,96]

2.2.3.4 An amine-containing IL

Interesting for the development of this thesis is the synthesis of the IL containing an amine group in the structure. The amine-containing IL is performed through the alkylation of N-methylimidazole with 3-chloropropylamine hydrochloride, as is shown in Figure 19. The nucleophilic substitution results in 1-(3-aminopropyl)-3-methylimidazolium chloride,[97] that afterwards is dissolved together with a salt of lithium, the lithium bis(trifluoromethylsulfonyl)imide, to carried out an ion exchange and formed the amino-functionalized IL.

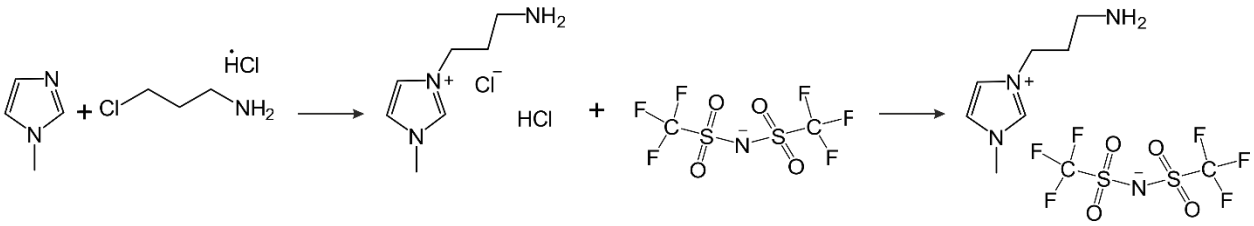

Figure 19. Alkylation of N-methylmidazole and ion exchange to form 1-(3-aminopropyl)-3-methylimidazolium bis(trifluoromethylsulfonyl)imide

2.3 Application I: Repellent Surfaces

The conventional approach to fabricate repellent surfaces consist of mimicking the design of nature from the lotus leaf that possess excellent self-cleaning and water repellency properties.[98,99] The lotus leaf achieves its repellency properties by minimizing the contact area between the surface and a contaminating liquid droplet (Figure 20).[100–102] By combining a hydrophobic surface chemistry and topography at the micro- or nanometer scale the contaminating droplet is prevented from coming in contact with the surface completely. Instead, it forms a liquid/solid/air composite in the upper area of the topography in a Cassie-Baxter wetting state.[101]

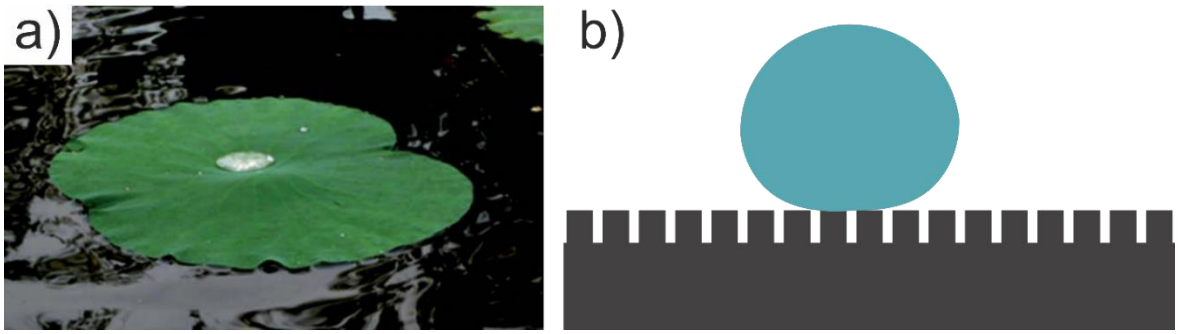

Figure 20. The lotus effect. a) optical image of a lotus leaf in water. Reproduced from reference [103]. b) A droplet is prevented from contact the entire surface as a result of the topography in the surface represented with the black pilars.

The lotus effect has been widely used and very successful in creating surface coatings able to repel water.[104,105] However, the design presents important limitations, including failure at high pressures or during droplet impact due to the compressibility of the air pockets in the air/solid/liquid composite.[106] Complex fluids are not repelled since the direct contact with the solid surface is not fully prevented, leading to contamination of for example proteins and formation of biofouling.[59,107] Additionally, the coating is unable to self-heal, once it is damaged the contaminant can be pinned in the damaged area.[108]

To avoid such limitations, an alternative approach to impart repellency was developed, where a fluid lubricant replaces the air pockets of the lotus leaf. A lubricant-infused surfaces separates the surface completely from the contaminating liquid, circumventing the limitation of the lotus leaf approach.[21,27]

Also inspired by nature, lubricant-infused surfaces mimic the Nepenthes pitcher plant,[21] that uses a prey-trap mechanism for making insect to fall into its digestive cavity (Figure 21a). Such mechanism consists of microstructures that retain an intermediary secreted liquid, the secretion causes the insects to slide off to the cavity filled with digestive juices.[109,110]

The technological analogues to the pitcher plant have been termed slippery lubricant-infused porous surfaces,[19] and are formed by creating nano- or micro topography in a surface and infusing a lubricating liquid in the pores or interstitial spaces of the topography (Figure 21b). The lubricant must be immiscible with other contaminating liquids, must wet the surface and remain locked in place in presence of another liquid.[21,27]

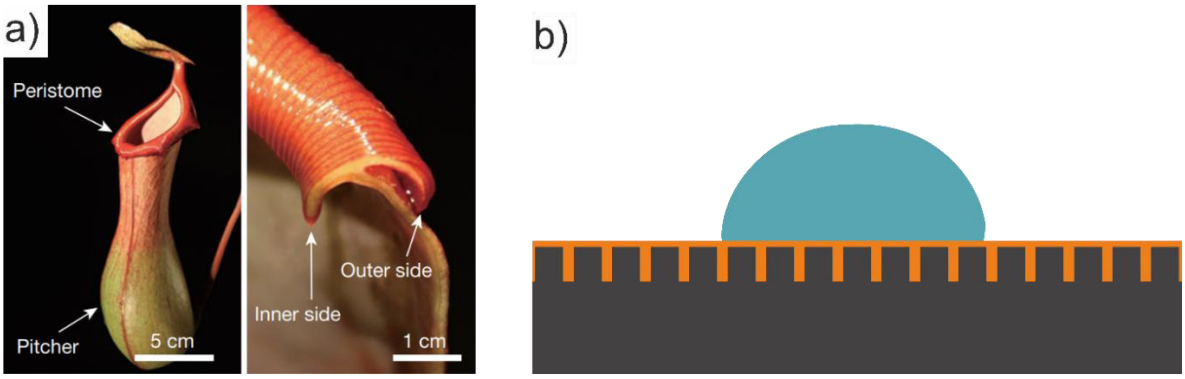

Figure 21. Pitcher plant. a) Optical images of the pitcher Nepenthes alata, showing the pitcher and the prey-trapping rim (left), and a cross-sectional image of the microstructure peristome (right), reproduced from reference [111]. b) schematic representation of a lubricant-infused surface, the confined lubricant is preventing the droplet to touch the surface.

The stability of lubricant-infused surface is determined by the combination of surface topography and a suitable surface chemistry. The topography at the nano or micro scale stabilises the lubricant by capillary forces.[41] The surface chemistry dictates the affinity of the lubricant to the surface, the surface chemistry can be adjusted to make a lubricant wet the surface and continue wetting the surface in the presence of another contaminating liquid by minimizing the interfacial energy between the lubricant and the solid surface. [19,112,113]

In their pioneering work on lubricant-infused surfaces, Tak-Sing Wong et al.[19] described the thermodynamic conditions for the stability of a lubricant-infused system, which is described in Figure 22. Liquid A represent the fluid to be repelled, Liquid B is the lubricant, and the black pillars represent the surface topography. The Figure describes 3 different configurations, Configuration A represents the state where the solid is completely wetted by Liquid A. Configuration 1 represent the state when the solid is wetted by Liquid B in presence of Liquid A, and Configuration 2 represent the solid wetted by the Liquid B in absence of Liquid A. The formation of a stable system is achieved by finding the conditions where the Configuration A is always at a higher energy state than configurations 1 and 2. The selection of a stable combination of solid substrate and Liquid B is performed by comparing the energy states of the different configurations. E1, E2 and EA represent the total interfacial energies per unit area of the wetting configurations 1, 2, and A, respectively. γ_{AB}, γ_{SA}, γ_{SB}, γ_{A}, and γ_{B} represent the interfacial energies of Liquid A-Liquid B, solid-Liquid A, solid-Liquid B and the surface tension of Liquid A and Liquid B, respectively. *H* and *h* are the thickness of the fluid layer and the height of the topography, respectively. *R* is the roughness factor of the textured solid. All the parameters are measurable through the Young equation, discussed in section 2.1.1 and Wenzel model discussed in section 2.1.3. By satisfying $\Delta E_1 > 0$ and $\Delta E_2 > 0$ is ensured a stable lubricant film formation.[19]

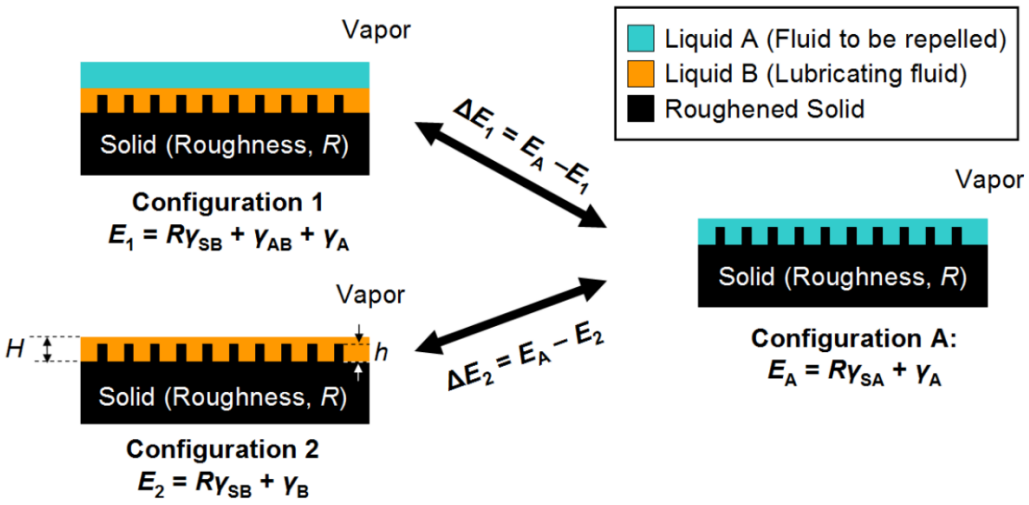

Figure 22. Schematic representation of the thermodynamic condition to form a stable lubricant-infused system. Reproduced from reference [19]

Lubricant-infused surfaces have been extensively studied for the last 10 years since their development due to their valuable contribution to a wide range of technologies.[25,43] Significant contributions have been made regarding the techniques for the formation of lubricated surfaces, including facile methods to add topography to the surface[59] and the formation of organogels both to build-up topography and enhance affinity of the lubricant with the substrate.[67,68,114] Additionally, there are comparisons between different scales of topographies, where the nano-scale presents higher retention of the lubricant.[42,115–117]Another contribution shows the formation of self-replenishing systems.[66,68] Among the applications which benefit the most from lubricant-infused surfaces are anti-biofuling[20,107,118–120] and anti-icing,[25,42,115,121]. Some of the applications are shown in Figure 23.

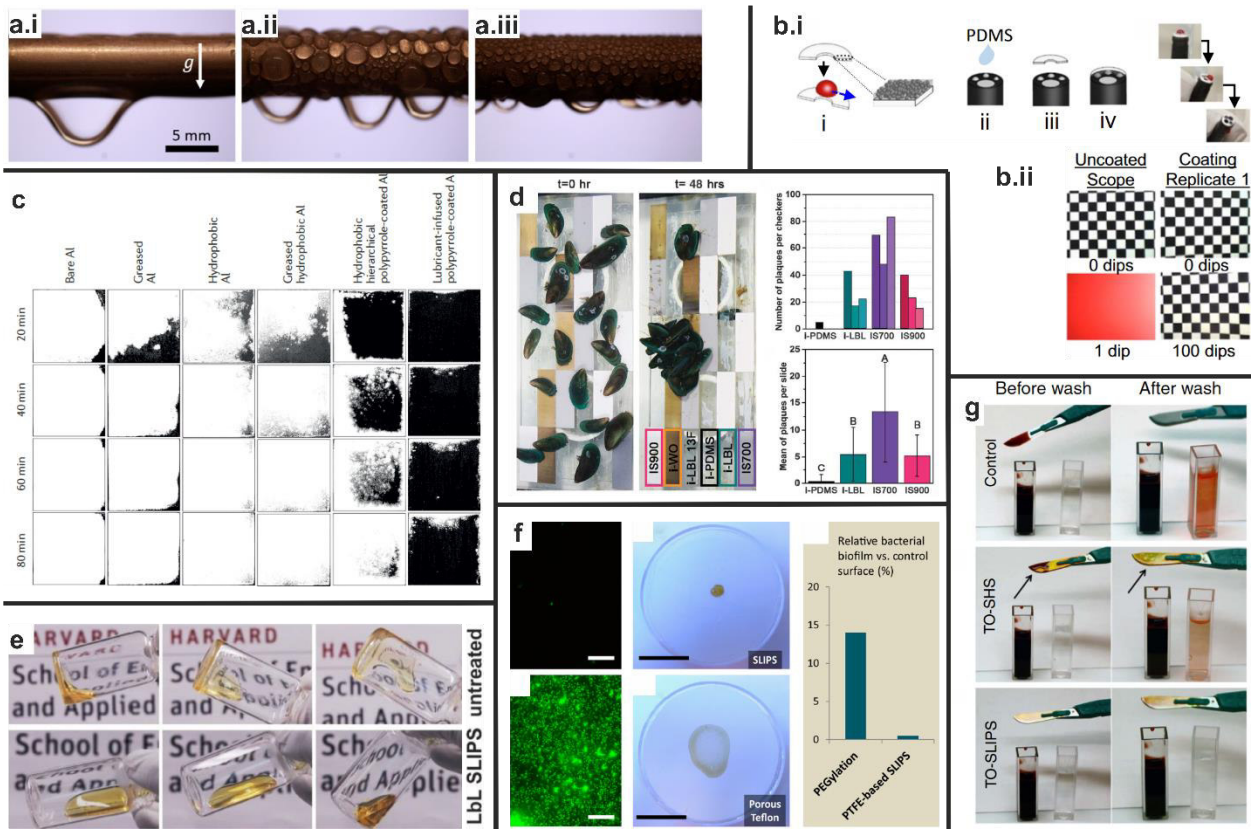

Figure 23. Some applications of lubricated-infused surfaces. a) For heat transfer application. Optical images of copper tubes with different surface treatment placed inside a chamber with control humidity (60% relative humidiy) and below the dew point at 5°C: a.i. condensation forming a film over an untreated copper tube a.ii. drop-wise condensation of hydrophobic nanostructured tube, the condensate forms discrete water droplets that depart when they reach the capillary length.a.iii. Lubricant-infused porous surface condensation enhances droplet mobility and departure. Due to the absence of contact line pinning condensate droplets reside on a defect-free liquid-liquid interface. Adapted from reference [116]. b) Coating endoscopes b.i. schematic representation of the coating process of an endoscope with a disposable, glass coverslip coated with silica nanoparticles and infused with silicon oil, the slide is fixed in the endoscope lens with PDMS. The endoscope repels a drop of blood. b.ii. Comparison of visual field of an uncoated and a coated endoscope after dipping it in blood. The uncoated endoscope fails immediately after one dip (left), whereas the coated endoscope allows for repellence up to 100 dips with no fouling (right). Adapted from reference [122] c) Anti-ice and anti-frost performance. Time lapse images of ice formation at -2°C in high-humiditiy conditions on different aluminium surfaces, the ice-covered areas are white and uncovered areas are black. Adapted from reference. [123] d) Preventing mussel adhesion, mussels over a checkboard of a selection of different materials coated with SLIPS, the mussels were allowed to move for 48 h to then the adhesive plaques per slide. Adapted from reference [118]. e) repellency of complex fluids, time-lapsed images showing the sliding of honey in the inside of a coated glass vial (lower row) in contrast with highly sticky honey in a untreated glass vial. Adapted from reference[45]. f) Biofilms prevention. SLIPS coated surfaces were compared with the hydrophobic porous Teflon. Fluroescence micrographs of attached bacteria and optical microphase showed that after 48 h of incubation of P. aeruginosa the biofilm on SLIPS is minimum. Adapted from reference [107] g) A surgical-grade steel scalpel blade was nanostructured with tungsten oxide (TO) films and infiltrated with perfluoropolyether lubricants to form the lubricant-infused coating (TO-SLIPS), which was compared with a control non-coated blade and a super hydrophobic blade (TO-SHS). The three blades were immersed in a cuvette with blood and then in a cuvette with DI water. The colour of the cuvette with water correlates the amount of blood that remains on every sample. Adapted from reference [124].

2.4 Application II: Supported Ionic Liquid Phase Catalysis

Ionic liquids offer crucial benefits to catalytic processes, however their use in volumetric quantities has important limitations. The first limitation is their high cost (compared to conventional solvents) which raises production costs making such production processes unaffordable.[125] Another relevant limitation of the use of ILs in large quantities is their relatively high viscosity, which makes the mass transfer phenomena involved in the process much slower, which makes the reagents hardly come into contact with the catalyst.[16,125]

To overcome such limitations and make use of ILs as solvents in industrial processes, a technology known as Supported Ionic Liquid Phase (SILP) catalysis was developed, which has been conceived and described by its pioneers as an ideal catalytic system, where the medium (IL) should be the size of a layer that obeys the diffusion layer model, in this way the diffusion distances are shortened, and the mass transfer problems are solved. Additionally, the required amount of IL is minimal.[125–128]

SILP catalysis consists of placing a very thin layer of IL with a catalyst dissolved on the internal surface of a highly porous material or particle,[8,15,16] as shown in the schematic representation of Figure 24. In addition to overcoming the limitations of volumetric ILs, this technology combines the advantages of homogeneous and heterogeneous catalysis. High activity is presented in mild reaction conditions since the catalyst is dissolved (in the IL), which is the main characteristic of homogeneous catalysis. On the other hand, the solid support facilitates the separation processes after the reaction, which characterizes heterogeneous catalysis.

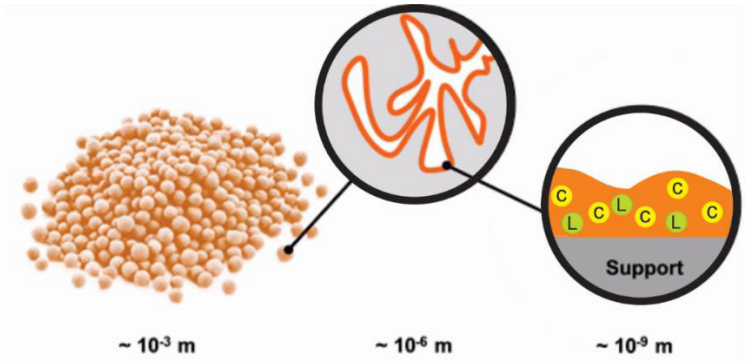

Figure 24. Schematic representation of Supported Ionic Liquid Phase particles. Adapted from reference [129]

SILP catalysis has been successfully used using transition metals, which are reported to be homogeneously dissolved, as well as in acid catalysis with chloroaluminates.[16] Some of the reported reactions with exceptional catalytic performances using SILP catalysis include Rh-catalysed hydroformylations, carbonylations and hydrogenations, hydroamination catalysed with Pd, Zn and Rh independently, W-catalysed epoxidations and Pd-catalysed Heck reactions.[126]

The wide range of possible anion-cation combinations that can form ILs provides the possibility of synthesizing ILs specifically designed to fulfill certain functions, in this way it is possible to design ILs that stabilize specific catalytic species, for example, in asymmetric catalysis SILP systems that immobilize high cost chiral catalysts have been successfully reported.[125] In the same way, it is possible to design ILs in which the reactants of a reaction present good solubility and at the same time the solubility of the products is reduced, with the purpose of facilitating the subsequent necessary separation processes.[130]

The confinement of ILs on solid supports is carried out by capillary forces, electrostatic interactions and hydrogen-bonds or covalent bonds (Figure 25).[16,125,131]

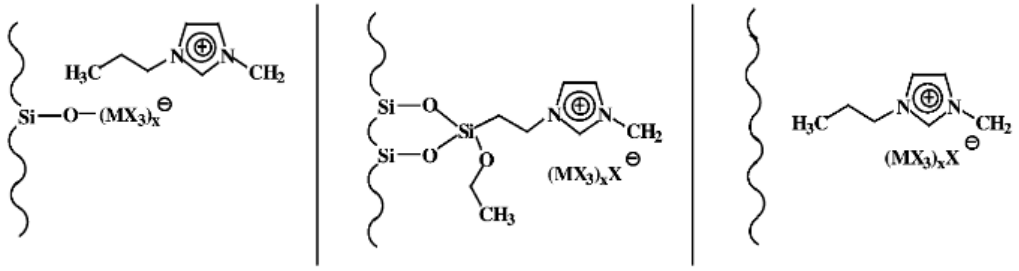

Figure 25. Immobilization of ILs via covalent bond of the surface with the anion or cation. And as a supported liquid phase. Reproduce from reference [131]

Currently, SILP catalysis has been successfully applied in several processes resulting in transcendental improvements for a great variety of chemical reactions. Such improvements concern low-cost catalytic optimizations, simplifications in unit operations of separation processes and important decreases in environmental impact.

The main obstacle of SILP catalysis involves liquid-phase reactions, where there is the potential removal of the IL layer from the solid support due to mechanical forces i.e. the IL can be washed away and replaced by another liquid involved in the reaction, either liquid reagent or a solvent. Cases of significant leaching have been reported in SILP systems even with confinement of the IL by covalent bonds.[130]

3. Motivation

The distinctive characteristics of the ILs make available the use of liquid fluids that practically do not evaporate, can endure high temperatures without going through decomposition, and are good solvents for catalytic compounds. However, to be able to benefit from the ILs in practical technological applications it is required to partially immobilize them in the form of films deposited in solid surfaces or supports. The use of volumetric quantities of ILs is, apart from unaffordable, extremely impractical, and complicated.

The term partial immobilization is perhaps the closer describing our efforts since we intent to attach the ILs to solid surfaces, importantly, preserving their fluid dynamics regime. In this way, the remarkable advantages that ILs offers are fully exploited. In other words, our interest is to maintain the liquid-like flow of the ILs in the confines of a solid surface. Therefore, attaching ILs covalently to the surface as a way of complete immobilization is not in the scope of this research.

We have witnessed emerging technologies involving a liquid confined in solid supports while keeping intact its liquid nature, like the lubricant-infused surfaces developed for applications in repellent coatings. There, the method to confine the lubricant is based on the analysis of its wetting behaviour and the manipulation of such wetting. This in turn is done through a combination of the control of the interfacial interactions between the lubricant and the solid surface and capillary forces.

The control or tuning of interfacial interactions is performed by the functionalization of the solid surface. The addition of functional groups that promote the wetting of the lubricant in the surface is possible using surface chemistry. The key is the addition of functionality in the surface resembling the chemical structure of lubricant. By having the same functional groups in the lubricant and in the surface, interfacial interactions of low energy are ensured. For example, in the case of having fluorinated oil as the lubricant, the best choice for the surface functionalization is a surface compound containing fluorine, the affinity of the lubricant to the surface is maximized, so its wetting behaviour is optimized.

Benefitting from this technology and transfering it to manage the confinement of ILs in solid surfaces requires taking into consideration the complexity in the chemical structure of the ILs. In Chapter 2.1 we have learned that the inherent properties of the ILs are the result of their ionic nature combined with hydrogen bonding and Van der Waals forces. This then implies that there is never only one functionality

or functional group present in the structure of an IL. The challenge relies on finding the suitable functionality for the solid surface to maximize the affinity of the IL and the surface.

The first step to address the challenge of finding a suitable functionality to confine ILs in solid surfaces is testing several functionalities. The test is done by adding surface compounds resembling the functional groups present in the IL. In Chapter 5.1 we took imidazole-based ILs a sample of common ILs, we functionalized surfaces with silanes with functional groups present in the chosen ILs. We analysed the wetting behaviour of the ILs in the functionalized surfaces and used the optical properties of inverse opals to observe the wetting and stability of ionic liquid-infused porous surfaces as a function of the functionality of the surface. We corroborated that the retention of ILs in porous surfaces is feasible with the appropriate surface chemistry and developed a repellent ionic-liquid infused coating.

In Chapter 5.2 we aimed to increase the capillary effects of porous materials by depositing additional topography. We gained a deeper insight into the complexity of using the Layer-by-Layer approach to coat porous materials. We used the findings on circumventing the physical limitations of coating porous materials to coat SiC monoliths for the confinement of ILs, which is a set up commonly used in the catalytic water-gas shift reaction.

We further increased the affinity of the ILs with the surface by fabricating a polymeric network with the chemical structure of the ILs. We used polymer-analogous reactions, described in Chapter 2.2.2, to functionalize a pre-polymerized chain with IL in each of the monomeric units. The result was an organogel with higher retention of the IL since a large number of IL-polymer pairs increases the IL affinity to the surface.

We used active ester chemistry to fabricate the functionalized organogels. We co-polymerized pentafluorophenyl acrylate to anchor ILs containing an amine group, and benzophenone methacrylate to crosslink the chains and form the gels. Chapter 5.3 displays the formation of the organogels with their characterization and application as repellent coatings. For this, the organogels were attached to surfaces using benzophenone functionality and UV irradiation, then the gels were infused with IL to create the slippery repellent coating.

In Chapter 5.4 we extended the applicability of the IL-organogels to form polymer-based coating supports for the supported ionic liquid phase (SILP) catalysis. We coated SiO_2 particles with customized IL-gels and infused them with an IL and catalytically active species to then test their retention in leaching tests.

4. Experimental Methods

4.1 Materials

All reagents were obtained from Sigma-Aldrich. MilliQ water was used for all experiments and nitrogen or argon to dry all substrates.

4.2 Assemblies and coatings

4.2.1 Inverse Opal Fabrication

Inverse opals were prepared following a protocol from literature. [50] In brief, a solution of tetraethyl ortosilicate (TEOS), hydrochloric acid and ethanol (1:1:1.5 by weight) was prepared and stirred for 1 h in order to pre-hydrolyze the TEOS. 1.25 mL of 1.16 % v/v suspension of monodispersed colloidal particles of polystyrene (232 nm diameter) was added to 18.75 mL of milliQ water to prepare a 0.1 % w/v polystyrene solution, to which 140 µL of pre-hydrolyzed TEOS solution was also added. Substrates were cleaned in base piranha (1:1:5 ratio of ammonia solution (25% in water) to hydrogen peroxide (33% in water) to milliQ water) at 80°C for 0.5 h and then rinsed in milliQ water.

Cleaned and dried substrates were vertically suspended in a vial containing the colloid/TEOS suspension. The solvent content was evaporated slowly in an oven at 65°C to form a thin film on the suspended substrate. The substrates were subsequently heated at 500°C for 2 h with a 5 h ramp time to remove the polystyrene particles and sinter the SiO_2 structure to form the inverse opal structure.

4.2.2 Fabrication of Layer-by-Layer-based Surface Nanostructures

Layer by layer samples were prepared following a protocol from literature. [45] In brief, substrates were cleaned by base piranha treatment as described above and subjected to oxygen-plasma for 5 min to activate the surface. The layer-by-layer deposition was performed by complete immersion of the substrates in a 0.1% w/w solution of poly(diallyldimethylammonium) chloride (PDADMAC) for 5 min, followed by thorough rinsing in DI water by immersion into three consecutive water-filled vials. The next layer was deposited by immersion of the substrate into a solution of 0.1 % w/w Ludox silica colloids for 5

min followed by rinsing in water. This cycle was repeated 10 times to deposit a multilayer. Afterwards the polyelectrolyte PDADMAC was removed by combustion at 500ºC for 2 h with a 5 h ramp time.

4.2.3 Surface Functionalization of Inverse Opals

The substrates were cleaned in an oxygen-plasma for 10 min at 10 sccm oxygen flow and 100 W plasma power to activate the surface. Silanization of the surfaces with trichloro-dodecylsilane and butyl(chloro)dimethylsilane were carried out by vapor phase deposition for 24 h at reduced pressure (approximately 1 mbar) and room temperature, following a protocol from literature. [132] Dry substrates were placed in a desiccator adjacent to a vial with 1 mL of silane. Then, the desiccator was closed, and a vacuum pump was used to reduce the pressure for 10 min. The desiccator was then sealed, and the substrates were incubated for 24 h and washed with ethanol afterwards to remove unbound silane.

Silanization of the surfaces with N-(3-triethoxysilylpropyl)-4,5-dihydroimidazol was performed by liquid phase deposition, in which the substrates were placed in a 1 % v/v solution of the silane in ethanol for 24 h at room temperature, followed by thorough rinsing with ethanol to remove unbound silane.

Mixed monolayer substrates were prepared by a sequential approach. First, liquid phase silanization was performed with N-(3-triethoxysilylpropyl)-4,5-dihydroimidazol as described above. The substrates were then dried and subjected to a vapor phase deposition of trichloro-dodecylsilane or butyl(chloro)dimethylsilane for 24 h as described above. The number ratio between the functional groups could be altered by changing the immersion time in the liquid imidazole-silane solution. For all experiments shown in the manuscript, an incubation for 6h was used.

All substrates were heated to 95 °C on a hotplate for 1 h to complete the condensation reaction and to covalently bind the silane molecules to the surface.

4.2.4 Infusion of Ionic Liquids and Measurement of Contact Angles

Static contact angles were measured using a goniometer (Data Physics model OCA 30) under ambient conditions at five different areas per substrate and averaged. For water contact angles on lubricated inverse opal samples, 10 µL/cm^2 of each ionic liquid was added to each type of inverse opal substrate, and uniform coverage was achieved by tilting. All samples were placed vertically for 10 min in order to drain the excess lubricant film by gravity. Sliding angles were measured using a tilted stage and the angle necessary to induce sliding of a 5 µl droplet was recorded as the sliding angle. Wettability of inverse opals with ionic liquids was determined by optical microscopy.

4.2.5 LbL Coating of Micro-Scale Porous Materials

Silicon carbide (SiC) monoliths with a pore size average of 3 µm were activated with oxygen plasma for 5 min. The LbL deposition was performed similarly to the coating of flat surfaces, with an additional drying step between each immersion. The first immersion used 0.1% w/w solution of PDADMAC for 10 min, followed by rinsing in DI water, and drying with nitrogen. The second immersion step used a solution of 0.1 % w/w of Ludox silica particles for 10 min, followed by rinsing in water and drying with nitrogen. The cycle was repeated 5 times and the PDADMAC was removed by combustion at 500°C for 2 h with a 5 h ramp time.

For infusion of the IL and leaching test, the coating solutions were exchanged as follows: After activation of SiC monoliths with plasma, the first immersion was in 0.1 % w/w solution of Al_2O_3 (average size: 50 nm, Alfa Aesar). After the rinsing and drying steps, the second immersion was in 0.1 % w/w solution of poly (sodium 4-styrensesulfonate) (PSS). We coated SiC monoliths with 5, 10, and 15 cycles, respectively. The PSS was removed by combustion at 500°C for 2 h.

4.2.6 Coating Nano-scale Porous Materials (Inverse Opals)

The inverse opals were activated with oxygen plasma for 5 min. The LbL deposition was performed similar to the coating of micro-scale porous materials but using solutions containing NaCl. The first immersion was into a solution 0.1% w/w of PDADMAC with NaCl (1 mM, 10 mM, 30 mM, 50 mM, and 100 mM) for 10 min, followed by rinsing in DI water and drying with N_2. The second immersion was into a solution of 0.1 % w/w of Ludox silica particles with NaCl (1 mM, 10 mM, 30 mM, 50 mM, and 100 mM) for 10 min, followed by rinsing in water and drying with N_2. The cycle was repeated 5 times and the PDADMAC was removed by combustion at 500°C for 2 h with a 5 h ramp time.

4.2.7 Infusion of Ionic Liquid in SiC Monoliths

Before infusing the SiC monoliths, both the monoliths and the IL were dried. 1-butyl-2,3-dimethylimidazolium chloride [BMMIM][Cl] (99%, solvent innovation) was place in a desiccator together with silica gel in vacuum for 24 h. The SiC monoliths were dried at 110°C for 2 hours just before the infusion. A solution of 10 % v/v of dried [BMMIM][Cl] in dichloromethane was prepared. The SiC monoliths were immersed in the solution for 5 min and dried under vacuum for 24 h.

4.2.8 Leaching Test of SiC Monoliths

[BMMIM][Cl]-infused SiC monoliths were weighed before and after every 5 hours of compressed air streaming. Non-coated and coated with 5, 10, and 15 coating cycles monoliths were compared.

4.2.9 Surface Functionalization of Glass Slides

Glass slides were cleaned in piranha solution (1:1:5 ratio of ammonia solution (25% in water) to hydrogen peroxide (33% in water) to MQ-water) at 80°C for 0.5 h and then rinsed with MQ-water. The surface was activated with oxygen plasma for 10 min at a 10 sccm oxygen flow and 100 W plasma power. Then the substrates were immersed in a 0.002 molar solution of CSB in toluene for a liquid-phase deposition silanization at room temperature for 48 h, followed by rinsing with ethanol to remove unbound silane.

4.2.10 Coating Substrates with IL-gel

Polymer films were deposited on the surfaces by drop-casting 500 µl of 10wt% of PIL solution in butanone on a silanized glass substrate surface. The polymer films were dried overnight at 110°C.

4. 2.11 Crosslinking of IL-gel in surface

Coated substrates were irradiated in a BioLink crosslinker from Vilber with a peak wave of 365 nm. The energy input to form a stable film varied based on the PIL. Poly([APMIM][NTf2]A-co-BPMA) was irradiated with 10 J/cm2, and poly([APTBP][NTf2]A-co-BPMA) with 100 J/cm2. The coated substrates must be free of solvent during the irradiation for a successful crosslinking. After irradiation, the substrates were immersed in acetone for two hours to removed non-crosslinked polymer.

4.2.12 Infusion of free ionic liquid in IL-gel

40 µL/cm2 of dissolved ionic liquid (IL) in butanone (1:9) was added to the substrates and left horizontally overnight in a closed petri dish. Then the substrates were tilted vertically overnight at 85°C to drain the excess of IL by gravity and evaporate the remaining solvent. Substrates containing poly([APMIM][NTf2]A-co-BPMA) were infused with 1-methyl-3-propylimidazolium bis(trifluoromethylsulfonyl)imide

([MPIM][NTf2], Iolitec, >99%) and substrates containing poly([APTBP][NTf2]A-co-BPMA) were infused with methyltributylphosphonium bis(trifluoromethylsulfonyl)imide ([MTBP][Ntf2], Iolitec, >98%).

4.2.13 SLIPS and Infiltrated PDMS Coated Substrate

The SLIPS and PDMS-coated substrates were formed according to Sunny et al. [45,122] Microscope glass slides were activated with oxygen plasma for 10 min at 10 sccm oxygen flow and 100 W plasma power. The SLIPS were formed by layer-by-layer deposition, immersing the slides alternatingly in a 0.1 wt% solution of poly(diallyldimethylammonium) chloride (PDADMAC) and a 0.1 wt% solution of Ludox 40T silica colloids. Before change of solutions, the samples were immersed in pure water twice to avoid cross-contamination. 10 multilayers were deposited. The organic material was removed by calcination at 500°C and the slides were again activated by oxygen plasma for 10 min. Then, they were functionalized via vapor-phase deposition with (1H,1H,2H,2H-perfluorooctyl)-trichlorosilane to be infiltrated with Krytox PFPE GPL 100 and with n-decyltrichlorosilane to be infiltrated with 10 cSt silicone oil.

The poly(dimethylsiloxane) (PDMS) was formed using a Sylgrad 184 Silicone Elastomer Kit at a 10:1 ratio of elastomer to curing agent [122]. The mixture was added to an activated microscope slide and cured for 48 hours. Then, it was infiltrated with an excess of 10 cSt silicone oil for 48 hours. The PDMS film used for the durability measurements was around 2 mm thick after swelling.

4.2.14 Formation of IL-gel Support

Silanization of porous SiO2

Silanization of porous SiO2 (63-230 µm, pore size 6 Å, 500 m2/g) was performed in liquid phase. SiO2 was calcined at 500°C for 24 hours before silanization to eliminate water. 0.6 g of APTES for 5 g of SiO2 was stirred in 50 mL of toluene under reflux overnight. After refluxing, the SiO2 was filter with a slit-sieve filter funnel. Then the SiO2 was washed in toluene stirring for 1 hour to dissolve the non-attached APTES. After a second filtration the silanized SiO2 was dried overnight in vacuum (0.1 mbar) at 45°C.

Addition of crosslinking units to the silanized SiO2 via polymer-analogous reactions

Silanized SiO2 (5g) was stirred with of poly (pentafluoro phenyl acrylate-co-benzophenone methacrylate) (poly(PFPA-co-BPMA)) (0.75g) in THF (40 mL) overnight at 50°C. Afterward the powder was filter and washed in THF (30 mL) for 1 h. After a second filtration the functionalized SiO_2 was dried overnight in vacuum (0.1 mbar) at 45°C.

Polymerized IL coating of functionalized SiO2 and crosslinking

Functionalized SiO2 (5g) was stirred with poly([APMIM][NTf2]A-co-BPMA) (0.5g) in THF (40 mL) overnight. The THF was evaporated slowly and the coated SiO2 was dried overnight. The dried coated powder was placed and scattered in a glass petri dish and was irradiated in a BioLink crosslinker from Vilber with a peak wave of 365 nm, with 100 J/cm2, moving the sample every 10 J/cm2.

4.2.15 IL Leaching Test and Quantitative NMR

0.1 g of infiltrated IL-gel support with IL was placed in a vial with 3 mL of solvent (cyclohexane, n-heptane, 1-butanol, ethanol, acetone). The mixtures were shaken for 48 h at room temperature. Afterwards, the support was filtrated, and the solvent was concentrated in a rotary evaporator for its analysis in quantitative NMR. ECX-400-NMR from JEOL was used for the NMR measurement. ^{19}F NMR spectra were obtained with a signal-to-noise ratio of 12000:1 and a scan count of 32 of samples prepared as follows: using a precision scale, 0.02 g of trifluroro toluene was weighted in a NMR tube, 0.2 g of deuterated acetone was added as well as the concentrated solvent mixed with 0.8 mL of dry acetone, all the 4-digits exact weights were registered for further analysis. The amount of IL in the solvent was obtained through the integration and comparison of the ^{19}F NMR signals assigned to the trifluoro toluene (-64 ppm) and the NTf2 anion of the IL ([MEIM][NTf2]) (-80 ppm). The same procedure was followed using non-coated SiO_2 as reference.

4.2.16 Infiltration of IL, catalyst, and ligand in the IL-gel support

The IL, [MEIM][NTf2] (0.025 g), was weighted in a round bottom Schlenk flask. The flask with the IL was inserted in a glovebox of inert atmosphere were the IL-gel support, catalyst and ligand were weighted in

the following quantities: support (2.5 g), dicarbonyl (2,4-pentanedionato) rhodium(I) (Rh(acac)(CO)2) (0.0125 g) and bis(pentafluorophenyl)-phenylphosphine (0.04 g). The mixture was placed in a flux of Argon and 30 mL of dry acetone was added. The solution was stirred using a rotary evaporator (connected to Ar) for 1 h at 800 mbar. Then the temperature was set at 42° and the pressure was decreased very slowly to 450 mbar to evaporate the acetone. The same procedure was followed using non-coated SiO_2 as reference.

4.2.17 Catalyst and Ligand leaching test in Soxhlet column

A Soxhlet column was fluxed with Argon before placing 0.5 g of support infiltrated with IL and catalyst in the sample holder. 100 mL of heptane was refluxed in an oil bath at 120°C for 72 h. Afterward, the IL-gel supported was dried overnight in vacuum (0.1 mbar). The same procedure was followed using non-coated SiO_2 as reference.

4.3 Synthesis

4.3.1 Monomers synthesis

4.3.1.1 Pentaflurophenylaacrylate (PFPA) (Figure 17)

Pentafluorophenylacrylate (PFPA) was synthesized following a protocol from Eberhardt et al. [133] Briefly, pentafluorophenol (54 g) and 2,6-lutidine (35 mL) were dissolved in dichloromethane (DCM) (400 mL). The mixture was cooled down in an ice bath and acryloyl chloride (26 mL) dissolved in DCM (100 mL) was slowly added and stirred for 2 h at 0°C. The reaction mixture was stirred at room temperature overnight. Then the reaction mixture was filtrated, washed with HCl and MQ-water twice and dried over $MgSO_4$. Pure PFPA was obtained by distillation at 45°C and 0.02 mbar.

PFPA: 1H NMR (CDCl3): δ/ppm: 6.68 (1H, dd), 6.36 (1H, dd), 6.17 (1H, dd)

19F NMR: (CDCl3): δ/ppm: -153.0 (2F, dd), -158.5 (2F, t), -162.5 (2F, dd)

4.3.1.2 Benzophenylmethacrylate (BPMA) (Figure 18)

Benzophenylmethacrylate (BPMA) was synthesized according to Huang et al.[134] 4-hydroxybenzophenone (20 g) and triethylamine (20 mL) were dissolved in DCM (200 mL). Methacryloyl chloride (11.7 mL) dissolved in DCM (50 mL) was added dropwise under cooling and stirred for 3 h at 0°C and then stirred overnight at room temperature. The reaction mixture was filtered and washed twice with MQ-water (100 mL), twice with a saturated solution of NaHCO3 (125 mL) and twice with a saturated solution of NaCl (125 mL). Finally, it was dried over MgSO4 and recrystallized with hexane.

BPMA: 1H NMR (CDCl3): δ/ppm: 2.08 (3H, t), 5.80 (1H, t), 6.38 (1H, t), 7.26-7,86 (9H, arom)

4.3.2 Polymer synthesis (Chapters 5.3 and 5.4)

Poly(pentafluorophenyl acrylate-co-benzophenone methacrylate) (poly(PFPA-co-BPMA)) was synthesized according to an adopted protocol from Eberhardt et al.[133]. In a typical reaction, a mixture of monomers, pentafluorophenyl acrylate (15.0 g, 0.063 mol) and 4-benzophenyl methacrylate (0.84 g, 0.0031 mol for 5 mol% BPMA content) was dissolved in dried toluene (90 mL) together with azobisisobutyronitrile (AIBN) (106 mg, 0.65 mmol) using a Schlenk-flask. The mixture was degassed via freeze-thaw cycles three times. Afterwards, the mixture was placed in a preheated oil bath at 80°C for 24 hours. The polymer was purified by precipitation in methanol twice, centrifuged and dried with vacuum at 50°C overnight. The content of BPMA was changed between 1 mol% to 10 mol% in different syntheses.

GPC: MW = 2.25 ± 0.26 X 104 g/mol , Mn = 1.14 ± 0.16 X 104 g/mol

poly(PFPA-co-BPM): 1H NMR (CDCl3): δ/ppm: 2.16 (2H, br s), 3.13 (1H, br s), 7.45-7.74 (9H * %BPM, br s)

19F NMR: (CDCl3): δ/ppm: -153.0 (2F, br s), -157.0 (2F, br s), -161.5 (2F, br s)

The content of BPMA in the polymer was characterized using 1H NMR, by relating the signals associated with the 9 H nuclei present in the benzophenone molecule between 7.36-7.94 ppm (±0.03) to the

normalized signal associated with the H nuclei of the acrylate backbone chain at 3.12 ppm (±0.02). NMR integrals determined the content of BPMA to be within ±10 mol% of the molar amount added during the synthesis, in samples containing between 1 mol% and 10 mol% of BPMA.

4.3.3 Ionic liquids synthesis (Figure 19)

4.3.3.1 Aminopropylmethylimidazolium-bis(trifluoromethylsulfonyl) imide

Aminopropylmethylimidazolium chloride [APMIM][Cl] was synthesized according to Yue et al[97]. Briefly, 3-chloropropylamine HCl (26 g) and 1-methylimidazole (16.4 g) were mixed in ethanol (100 mL) and refluxed for 3 days to form 1-(-3-aminopropyl)-3-methylimidazolium chloride [APMIM][Cl]. The product was dissolved in 200 mL of MQ-water and the pH was adjusted to 8.2 by addition of KOH. In a second step an ion exchange with an equimolar amount of Li[Ntf2] was carried out in aqueous solution to obtain [APMIM][NTf2] (55 g) as an immiscible liquid phase of yellow color.

[APMIM][NTf2]:1H NMR (DMSO-d6): δ/ppm: 2.02 (2H, quintet), 2.46 (1H, s), 2.77 (2H, t), 3.81 (3H, s), 4.20 (2H,t), 7.68 (2H, dd), 9.02 (1H, s)

19F NMR: (DMSO-d6): δ/ppm: 78.6 (6F, br s)

4.3.3.2 Aminopropyl tributylposphosponium bis(trifluoromethylsulfonyl)imide (Chapter 5.3)

Aminopropyl tributylposphosponium bis(trifluoromethylsulfonyl)imide [APTBP][NTf2] was synthesized by alkylating tributylphosphine with 3-chloropropylamine HCl, followed by ion exchange with Li[Ntf2]. 3-Chloropropylamine HCl (15.62 g) was dissolved in a 1:1 mixture of 140 mL ethanol and isopropanol at 70°C. Subsequently, tributylphosphine (30 mL) was added and refluxed for 8 days in inert conditions. The solvent and residual tributylphosphine were evaporated at 50°C and 0.02 mbar overnight. The product [APTBP][Cl] was redissolved in MQ-water (200 mL). For the ion exchange, Li[NTf2] (27.6 g) was added to the aqueous solution while stirring at 80°C. The resulting [APTBP][NTf2] (37.6 g) is a clear, viscous liquid immiscible with the reaction mixture.

[APTBP][NTf2]: 1H NMR (DMSO-d6): δ/ppm: 0.83-0.87 (9H, br s), 1.37 (14H, br s), 1.55 (2H, br s), 2.14 (8H, br s), 3.36 (4H, br s, +H2O)

31P NMR (DMSO-d6): δ/ppm: 34.73 (1P, s)

19F NMR: (DMSO-d6): δ/ppm: 78.74 (6F, s)

4.3.4 Functionalization of polymer chain with ionic liquid (Chapter 5.3 and 5.4, Figure 38)

For a typical functionalization we added an equimolar mixture (0.01 mol) of [APMIM][NTf2] or [APTBP][NTf2] and poly(PFPA-co-BPM) to 50 mL dried THF. The reaction mixture was placed in an oil bath at 50°C in N_2 atmosphere. After 1 and 2 hours of reaction triethylamine (1.5 mL/each time) was added. Then, the reaction mixture was stirred for 24 h. Afterwards, the solution was concentrated by evaporation of the solvent. For the [APMIM][NTf2]-containing polymer, the resulting concentrated solution was phase separated with n-hexane (100 mL), washed with chloroform (100 mL), two times with 0.1N hydrochloric acid (100 mL) and MQ-water, and then dried in vacuum overnight. The purification of [APTBP][NTf2]-containing polymer was performed by the same procedure except washing with chloroform.

poly([APMIM][NTf2]A-co-BPMA): 1H NMR (DMSO-d6): δ/ppm: 1.7-2.1 (4H, br t), 2.46 (1H, br s), 2.80-3.60 (3H, br d), 3.82 (3H, br s), 4.10-4.21 (2H, br d), 7.69 (2H+BPM%*9, br s), 9.03 (1H, br s)

19F NMR (DMSO-d6): δ/ppm: 78.67 (6F, s)

poly([APTBP][NTf2]A-co-BPMA):1H NMR (DMSO-d6): δ/ppm: 0.83-0.87 (9H, br s), 1.37 (14H, br s), 1.55 (2H, br s), 2.14 (8H, br s), 3.36 (4H, br s, +H2O), 7.4-7.9 (9H*BPM)

19F NMR (DMSO-d6): δ/ppm: 78.64 (6F, s)

31P NMR (DMSO-d6): δ/ppm: 34.73 (1P, br s)

4.3.5 Benzophenone silane synthesis

4-(3'Chlorodimethylsilyl)propoxybenzophenone (CSB) was synthesized according to Prucker et al.[135]. First, 4-alloxybenzophenone was synthesized by dissolving 4-hydroxybenzophenone (39.6 g, 0.2 mol) and allyl bromide (26.5 g, 0.22 mol) (Alfa Aesar) in acetone. Afterwards potassium carbonate (28 g) was added and

the mixture was refluxed overnight. Then, MQ-water (90 mL) was added, and the solution was extracted with diethyl ether (150 mL) twice. The organic phases from the extractions were combined, washed twice with aqueous NaOH (10%) (100 mL), and dried over MgSO4. The solvent was evaporated. The product was recrystallized from methanol to obtain a transparent crystalline 4-alloxybenzophenone (27.3 g).

4-ABP: 1H NMR (CDCl3): δ/ppm: 4.6 (2H, d), 5.3-5.5 (2H, 2dd), 6.0 (1H, oct), 6.9-7.9 (9H, arom)

To synthesize CSB, 2 g of the produced 4-alloxybenzophenone was added to 20 g of freshly distilled dimethyl chlorosilane (Alfa Aesar) together with 10 mg of Pt-C (10% Pt) (Alfa Aesar) as a catalyst. The mixture was refluxed for 5 hours. Afterwards, the excess of dimethyl chlorosilane was removed by evaporation in vacuum (0.02 mbar) and the Pt-C was filtered. The CSB was stored as a solution in toluene.

CSB: 1H NMR (CDCl3): δ/ppm: 0.19 (6H, s), 0.7 (2H, m), 1.9 (2H, m), 3.9 (2H, t), 6.9-7.9 (9H, arom)

4..4 Characterization

4.4.1 Scanning electron microscopy (SEM)

A Zeiss Gemini instrument was used and samples deposited onto a silicon wafer substrate were used for the investigations. Cross-sectional samples were fabricated by carefully breaking the wafer along its crystal plane using a diamond cutter.

4.4.2 X-ray photoelectron spectroscopy (XPS)

XPS measurements were performed using a Thermo Scientific K-Alpha XPS system. Low resolution survey scans were taken followed by high resolution scans with a dwell time of 50 ms and a resolution of 0.1 eV for the individual elements. The high resolution N 1s and C 1s scans were used for quantification.

4.4.3 Characterization of repellency properties

Static contact angles, contact angle hysteresis and sliding angles were measured using a goniometer (Data Physics model OCA 30). Sliding angles and droplet sliding speed were measured using a tilted stage as well. 5 µL water droplets were used in each measurement. The durability tests were performed by measuring substrates stored at 85°C over a period of 150 days.

4.4.4 Confocal Microscopy

Confocal microscopy was performed on a Leica confocal microscope (model TCS SP5 II). All images were taken using a 543 nm excitation laser, the emission was recorded between 600 nm and 756 nm. The images were captured at 2 µm intervals in stack to obtain the thickness of the PIL film in a glass slide by subsequent image analysis. The PILs were labelled using Nile Blue chloride. For this, an ion exchange was carried out with equimolar Li[NTf2] in an aqueous solution at 80°C to obtain Nile Blue-[NTf2]. The labelled PILs were formed by a typical functionalization reaction, where 99 mol% of [APTBP][NTf2] and 1 mol% of Nile Blue-[NTf2] were mixed with poly(PFPA-co-BPM) in dried THF at 50°C, under inert conditions, and purified as described above.

The polymer films were measured before and after depositing a drop of ionic liquid (10% in butanone). The stacked images were processed with ImageJ to obtain side views of the samples and determine their thickness.

4.4.5 Thermogravimetric analysis (TGA)

A Q50, TA Instruments was used to determine the composition of coating particles, in a temperature range 25–1000 °C, with a heating rate of 1 K min^{-1}.

4.4.6 Nuclear magnetic resonance (NMR)

All the synthesis were characterized by NMR of ^{1}N and ^{19}F (if applicable) using an ECX-400-NMR from JEOL. Different deuterated solvents were employed based on the solubility of the measured samples. The detail of all NMR measurement for every synthesis is located at the end of synthesis description in this same chapter.

4.4.7 Fourier-transform infrared spectroscopy (FTIR)

FTIR spectra were obtained with a FTS3100 FT-IR spectrometer. For polymer-analogous reactions attenuated total reflectance (ATR) was used. Samples in form of powders (coated SiO_2) were measured by using KBr pellets. Typically, 200 mg dry KBr and 2 mg of sample were mixed and pressed (10 Tons).

4.4.8 Gel permeation chromatography (GPC)

The molecular weight and molecular weight distribution of poly(pentafluorophenyl acrylate-co-benzophenone methacrylate) (poly(PFPA-co-BPMA)) were determined by size exclusion chromatography on an Agilent PL-GPC-220 coupled with a multiangle light-scattering device Dawn Eos from Wyatt Technology. The values reported at the end of the description of the synthesis (Chapter 4.3.2) are mean values and standard deviations of four different measurements of 6 different synthesis. The eluent used was TFH and the flow rate was 1 mL/min at 25°C.

4.4.9 Inductively couple plasma Optical emission spectrometry (ICP-OES)

ICP-OES was used to determine the content of Rh and P on the IL-gel supports before and after leaching test using the Soxhlet extraction column. The analysis was performed with a plasma 400 Perkin Elmer. Dry IL-gel supports were dissolved and added to 0.1 L of water for their analysis. Infiltrated SiO_2 with IL was also analysed as standard.

5. Results and Discussion

5.1 Slippery ionic - liquid infused porous surfaces: confinement via interfacial energy and capillary effects

In this chapter we explore the confinement of ILs by means of the interfacial energy and capillary forces. We used the concepts introduced in Chapter 2.2.1 as the foundation to use ILs as lubricant in the repellent slippery liquid infused porous surfaces (SLIPS). We aim to address the depletion of the lubricant in SLIPS by evaporation. As discussed in chapter 2.2 the use of ILs as lubricant represents a challenge for the design of an optimal surface chemistry to keep them in place due to the diversity in the chemical structure of the ILs. The ILs holds a variety of chemical functionalities, and a predominant kind of intermolecular interaction is difficult to identify.

All the experiments were performed by Yaraset Galvan, building on preliminary work performed in the master thesis of Yaraset Galvan. The analysis, discussion, complementary experiments were performed, and the manuscript was written by Yaraset Galvan during the PhD program, the manuscript was corrected by all co-authors.

The results obtained have been published in Langmuir, 2018, which are partially reproduced from reference [136] with permission of the American Chemical Society.

5.1.1 Introduction

As described in Chapter 2.3, the main criteria for the design of a SLIP surface relies on the choice of the lubricant and the rough surface. The surface roughness provides a strong support and mechanical stability to the lubricant for its retention. This increased affinity is provided through capillary forces. Roughness can be formed on a surface in several ways and can be ordered or disordered at the nano- or micrometre scales [26,112,113] .

The surface chemistry of the rough surface must be chosen so that a minimum energy state is obtained, so the lubricant wet the surface both in absence and presence of an immiscible contaminating liquid. [19,112,113]. To ensure such an energy state, the interfacial energy between the solid surface and the lubricant must be minimized.

A straightforward way to adjust the interfacial energy is by modifying the surface chemistry of the solid support [26]. By matching the chemical structure of the lubricant with the surface chemistry we foster low interfacial interactions. The chemical affinity between the lubricant and the solid support is maximized if the chemical structure of both is alike. In this way, the molecules in a volume of lubricant at the boundary to the solid support are matched by similar intermolecular interactions to those of the surface-bound layer of molecules in the solid support [40]. This can be regarded as low efforts for the lubricant to wet the solid surface. In this manner, an ideal surface chemistry to keep in place a fluorinated lubricant is a fluorinated surface, while to keep in place a lubricant formed mainly of hydrocarbon chains, such as commercial silicon oils, the ideal surface chemistry consists of hydrocarbon chains.[108]

We used ILs as a lubricant to create a SLIP surface with long-term stability. We benefited from the ultralow vapor pressures (approximately 10^{-12} mmHg) to avoid the potential lubricant evaporation, which is the main cause of lubricant depletion and degradation of the coating over time or at elevated temperatures.

To fabricate a lubricant-infused repellent surface using ILs as lubricants, it is necessary to take into consideration the different functional groups in the ionic liquids. As an example, the widely used imidazolium-based ionic liquids involve Coulombic interactions from the ionic groups, hydrophobic interactions from the alkyl side chains and π-π interactions from the aromatic imidazolium group. We therefore look on the design of the surface chemistry to match the diverse functional groups present in the IL.

We investigate the wetting features of three imidazolium based ILs in surfaces containing imidazole and aliphatic groups as surface chemistry, both individually and mixed. To observe the wetting behaviour of the ILs as a function of the surface chemistry, we used inverse opals as nanostructured surfaces and take advantage of their optical properties.

Inverse opals structures are materials with highly defined and ordered nano- or micro-pores that present structural coloration as a result of the periodic light diffraction in the ordered structured with different refractive indices. [137] The high refractive index contrast between the matrix and air-filled pores is reduced when the pores are filled with a liquid, leading to disappearance of structural colour.[138] In this fashion, we

can verify the surface chemistry needed to make the ionic liquid wet and fill the inverse opals pores, by observing a shift of colour in the inverse opal.

5.1.2 Results and Discussion

The inverse opals were formed using a co-assembly evaporative method, where sacrificial polystyrene colloidal crystals are formed in a self-assembled fashion. The colloids are suspended in a solution of hydrolysed sol-gel precursor, tetraethyl orthosilicate (TEOS), which is slowly evaporated. The colloids then form consecutive rows that are embedded in freshly formed SiO_2. After the evaporation of the solution, the polystyrene particles are calcined, leaving behind the inverse replica of the formed polystyrene crystals, as shown in Figure 26a.The final material is a highly ordered porous surface that macroscopically exhibits structural coloration.

We chose functional groups that are present in the molecular structure of the ionic liquid to modify the surface chemistry of the inverse opals and test the wetting behaviour as a function of the surface chemistry.

The ionic liquids tested in this study are all imidazole-based varying their hydrocarbon chain length. 1-ethyl-3-methylimidazolium bis(trifluoromethylsulfonyl)imide, [EMIM][NTf2], 1-butyl-3-methylimidazolium bis(trifluoromethylsulfonyl)imide, [BMIM][NTf2], 1-hexyl-3-methylimidazolium bis(trifluoromethylsulfonyl)imide, [HMIM][NTf2], Figure 26bshows their chemical composition.

The selection of the optimal surface chemistry to match the ionic liquid is not a trivial choice because of the diversity of functional groups in their structure. We selected three silanes that resemble some of the functional groups present in the ILs for these experiments. Figure 26c shows the chemical composition of trichloro-dodecylsilane (Dod), butyl(chloro)dimethylsilane (But) and N-(3-triethoxysilylpropyl)-4,5-dihydroimidazole (Imi), which are the silanes used in this chapter.

We tracked the wetting behaviour of the ILs using the structural colour of the inverse opals, as described in chapter 2.1.1. When the IL is able to completely wet the inverse opals, its colour disappears due to the reduction of refractive index contrast. Additionally, in a successful system the lubricant must not be

replaced by other liquid, and we observed this by the same mechanism of the variation of colour in the inverse opal.

Figure 26d shows a schematic representation of the possible scenarios when an IL is placed in an inverse opal functionalized with the different silanes. In the dry state, the inverse opal shows structural colour as a result of the high refractive index contrast between the matrix and air-filled pores that leads to strong interference conditions of reflected light (i). When a liquid is added to the inverse opal, it can be prevented from wetting the pores, infiltrate the pores, or partially infiltrated by wetting just the first layer of pores (ii). This depends on the pore-opening angle and the contact angle of the liquid with the solid surface, which in turn depends on its surface chemistry [46,52].

Low contact angles indicate low interfacial energy, which benefits wetting, high contact angles prevent pores infiltration. For intermediate contact angles, the partial wetting of the first layer is a consequence of the change in the pore opening angle between the top layer, which has a pore opening angle close to 90°, and the underlying three-dimensional pore network with a pore opening angle around 23°, as is shown in the side view SEM image of Figure 26a.

Analogously, a change in the appearance of the inverse opal when is infiltrated enables the observation of the stability of the lubricant layer upon exposure to an immiscible contaminating liquid (figure 1d.iii). We used water as contaminating liquid, as its refractive index is lower that the imidazole-based IL[139]. Therefore, if the water replaces the IL in the pores a change in the color of the infiltrated inverse opal is observable.

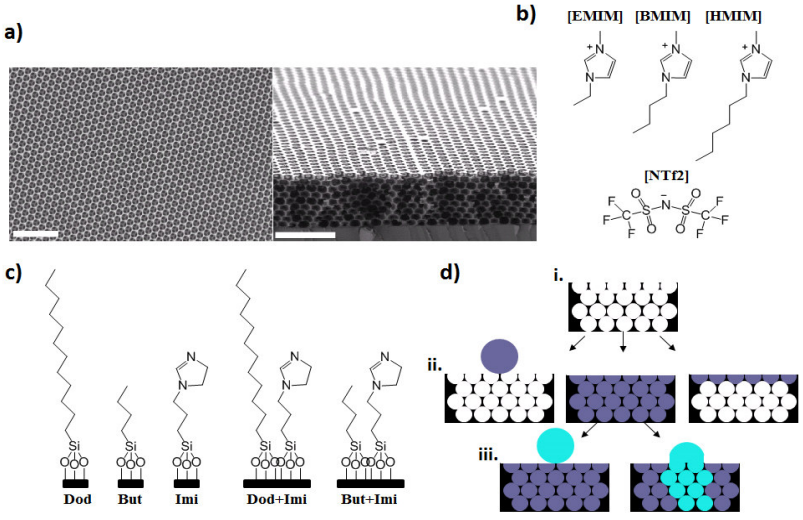

Figure 26. Fabrication of an ionic-liquid infused repellent coating from nanoporous coatings.
a) SEM images of an inverse opal showing the long range periodicity of the pores in top-view (left) and side-view (right), scale

bars = 2µm; b) Chemical composition of the imidazolium-based ionic liquids tested in this study: 1-ethyl-3-methylimidazolium bis(trifluoromethylsulfonyl)imide, [EMIM][NTf2], 1-butyl-3-methylimidazolium bis(trifluoromethylsulfonyl)imide, [BMIM][NTf2], 1-hexyl-3-methylimidazolium bis(trifluoromethylsulfonyl)imide, [HMIM][NTf2]; c) Chemical composition of the tested silanes used to modify the surface chemistry: trichloro-dodecylsilane (Dod), butyl(chloro)dimethylsilane (But) and N-(3-triethoxysilylpropyl)-4,5-dihydroimidazole (Imi);
d) Schematic representation of the possible wetting states of an inverse opal in a lubricant-infused coating. Depending on the contact angle of the surface with the ionic liquid (dark blue), the ionic liquid cannot infiltrate the pores of the inverse opal or can infiltrate them totally or partially (ii). Addition of a second, contaminating liquid (light blue) can either create a stable coating in which the ionic liquid is not replaced by the second liquid or failure of the coating when the IL is replaced by the second liquid. The refractive index-dependent structural coloration of inverse opals enable the observation of the different wetting scenarios directly from the change in macroscopic coloration.

We first used flat silicon wafers as substrates and silane chemistry for the functionalization of the surface to investigate the wetting characteristic of the different imidazole-base ionic liquids as a function of the surface chemistry. We used an imidazole-based silane (Imi) and two hydrocarbon silanes with different chain lengths, butyl (But) and dodecyl (Dod), as well as a mixed monolayer combining the Imi with But and Imi with Dod, as moieties of the functional groups in the ILs.

Figure 27 shows the characterization of the surface functionalization using X-ray photoelectron spectroscopy (XPS) and the wetting behaviour of the ILs in the functionalized surfaces by contact angle measurements. We measured the N 1s peak to confirm the presence of the nitrogen atoms of the imidazole ring. For the samples functionalized exclusively with Imi, a clear nitrogen signal can be seen corresponding to an overlap of the two N signals expected for imidazole [140]. All the ILs presented a small contact angle in the Imi functionalized surfaces, which indicates a good wettability.

In Figure 27b, the surface functionalized with Imi and Dod presented a very weak signal of N 1s, indicating that the influence of the imidazole-base silane is poor even though the silanization with Imi took place prior the silanization with Dod. We corroborate this with the contact angle of water and the ILs in the mixed (Imi+Dod) functionalized surfaces.Figure 27a shows no difference in the contact angles of Dod-functionalized surfaces. We attribute the poor influence of Imi to the larger dimensions of Dod silane that shields the adjacent Imi silane on the surface.

We then functionalized new samples with But as it is the same functional group than the Dod yet with a shorter chain length and cannot be expected to sterically shield the imidazole groups. The XPS spectra in Figure 27d shows a clear N 1s signal for both the Imi and mixed (Imi+But) self-assembled monolayer on flat surfaces, confirming the presence of the imidazole ring in the surface. As expected, Figure 27c shows

smaller contact angles of water on But-functionalized surfaces, as But has a lower hydrophobic character. Nevertheless, the still hydrophobic contact angle (101±1°) indicates a successful functionalization. Importantly, the contact angles of water and ILs clearly decrease in the mixed (Imi+But), confirming the influence of the Imi-silane that is no longer shielded.

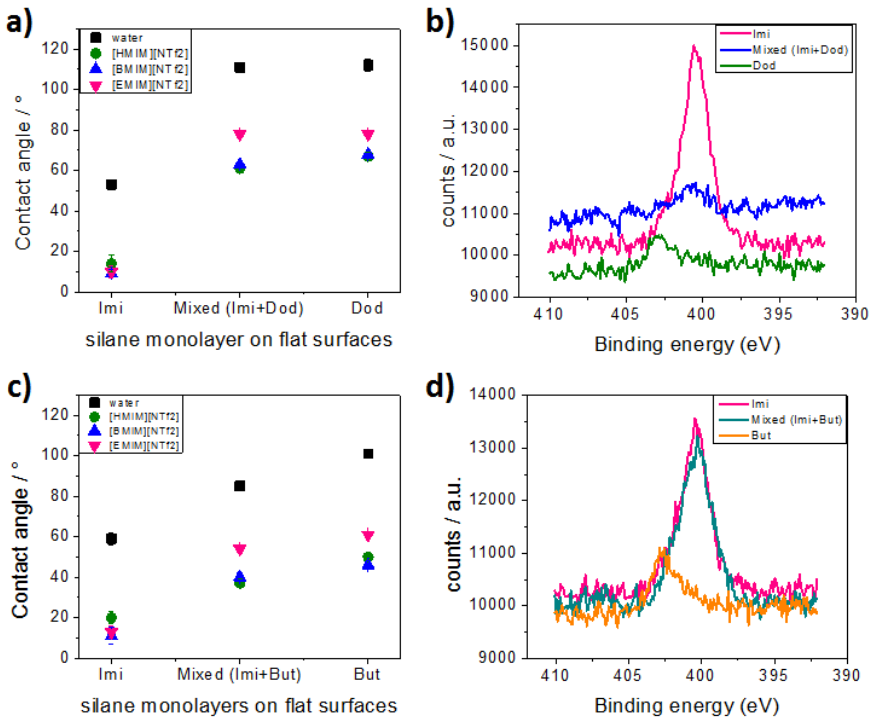

Figure 27.Surface functionalization and wetting properties. a) Contact angle of water and ionic liquids on a flat silicon wafer surface with self-assembled monolayers of Imi, Dod, and mixed composition (Imi and Dod). b) XPS spectra in the N1s region of Imi-, Dod- and mixed monolayers. c) Contact angle of water and ionic liquids on a flat silicon wafer surface with self-assembled monolayers of Imi, But, and mixed composition (Imi and But). d) XPS spectra in the N1s region of Imi-, But- and mixed monolayers. All contact angles were averaged over five separate measurements.

Once the different surface chemistries were examined, we prepared the inverse opals and functionalized them to next investigate the wetting properties of the ILs as a function of the surface chemistry applied in the inverse opals.

Figure 28 shows the infiltration or wetting states of the ILs in the inverse opals. Loss of colour indicates that the IL fills the pores completely, which eliminates the contrast of refractive index. We assigned the infiltrated wetting stage as state 1 in Figure 28. The infiltration of the IL in the uppermost layer of pores is the result of the considerably larger pore opening angle. It can be observed by the presence of a liquid

film, yet the structural colour is still visible. We refer to this case as wetting stage 2 in Figure 28. The complete hindrance to liquid infiltration, which leads to a liquid drop residing on top of the substrate, which keeps its structural colour, is assigned as the wetting state 3.

Generally, the wetting states of the inverse opals reflect the contact angles of the ILs on the flat surfaces. In Figure 28, the wetting state 1 (complete pore infiltration) is observed in the Imi functionalized inverse opals with all the ILs tested, in agreement with the low contact angles of the ILs in the flat Imi-functionalized surface.

Therefore, the Imi functionalization fulfills the first criterion to form a repellent coating with all the ILs. The Dod functionalization, which present the highest contact angle values impede the infiltration of all the ILs showing the wetting state 3 and cannot form an IL-infused coating. But-functionalized inverse opals display the wetting state 3 for the most hydrophilic IL ([EMIM][NTf2]) that is inhibit from filling the pores. In contrast, the same But-functionalized inverse opal presented an intermediate wetting state 2 when infiltrating both the more hydrophobic [BMIM][NTf2] and [HMIM][NTf2].

The combination of silanes in the mixed monolayers both (Imi+But) and (Imi+Dod) modified the wetting behaviour of the ILs and showed a remarkable sensitivity to the applied IL. The most hydrophilic IL ([EMIM][NTf2]) did not infiltrate the pores of either of the mixed monolayers, while the slightly more hydrophobic [BMIM][NTf2] could partially infiltrate the two mixed monolayers (Imi+But) and (Imi+Dod). The most hydrophobic [HMIM][NTf2] could completely infiltrate (Imi+But) and (Imi+Dod).

According to the contact angles, we were not expecting a change in the wetting behaviour of the mixed monolayers using Dod and Imi, as the contact angle of Dod and the Dod+Imi are very similar (figure 2a). However, there is a clear change in the wetting behaviour between these two surfaces chemistries in the inverse opals (figure 3). We attribute this change in wetting to effects caused by surface roughness. Steric shielding of long chains of the Dod-silane may be efficient in flat substrates, in contrast to rough surfaces where there are sharp edges and curved geometry that may exposed imidazole groups, allowing the Imi-silane to influence the overall surface properties.

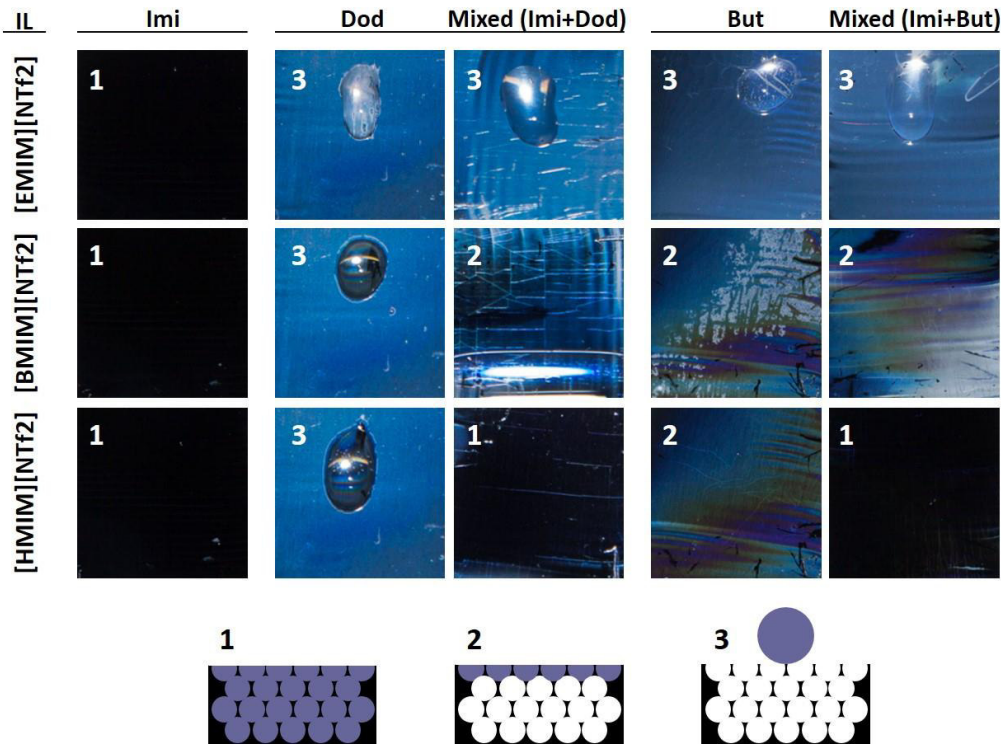

Figure 28. Visual identification of the wetting state of the different ionic liquids on inverse opals with different surface functionality, observed via the structural coloration of the inverse opal. Complete liquid infiltration eliminates the refractive index difference and thus the structural color (assigned as "1"); partial infiltration, caused by a different pore opening angle between topmost layer and underlying pores ("2") leads to a wetted substrate with retained structural color. Complete prevention of wetting leads to a droplet sitting on the nanoporous structure (3).

We then used the same control of pore wetting characteristics of the tested ILs to evaluate their performance as repellent surface coatings. We analysed the successfully infiltrated inverse opals, using the ILs with the surface chemistries that enable wetting of the pores (Figure 28). We added a drop of water as the contaminating liquid to be repelled. We observed whether the drop of water replaced the IL, leading to failure of the repellent coating, or the coating was able to repel the water, making it slide off the surface. As described before, we exploited the structural coloration to monitor the efficiency of the formed IL-infused systems.

The apparition of colour indicates a change in the infiltration medium, such as the replacement of the IL with water. We observed that the inverse opals functionalized with Imi failed as infused coating, the drop of water clearly displaced the IL and left in the substrate an area with colour back (Figure 29)a. In contrast, the mixed functionalization made of Imi and But silanes, make the drop of water to slip off the coating

without replacing the IL, enabling a stable repellency using the hydrophobic ILs [BMIM][NTf2] and [HMIM][NTf2]. Interestingly, we noticed that stable repellency can be achieved without a completely wetted inverse opal. In Figure 29a the IL in the uppermost layer of the inverse opal can be seen, as indicated by the liquid film and the remaining of the structural colour. in such a sample the drop of water also slid off the surface without leaving behind any stains.

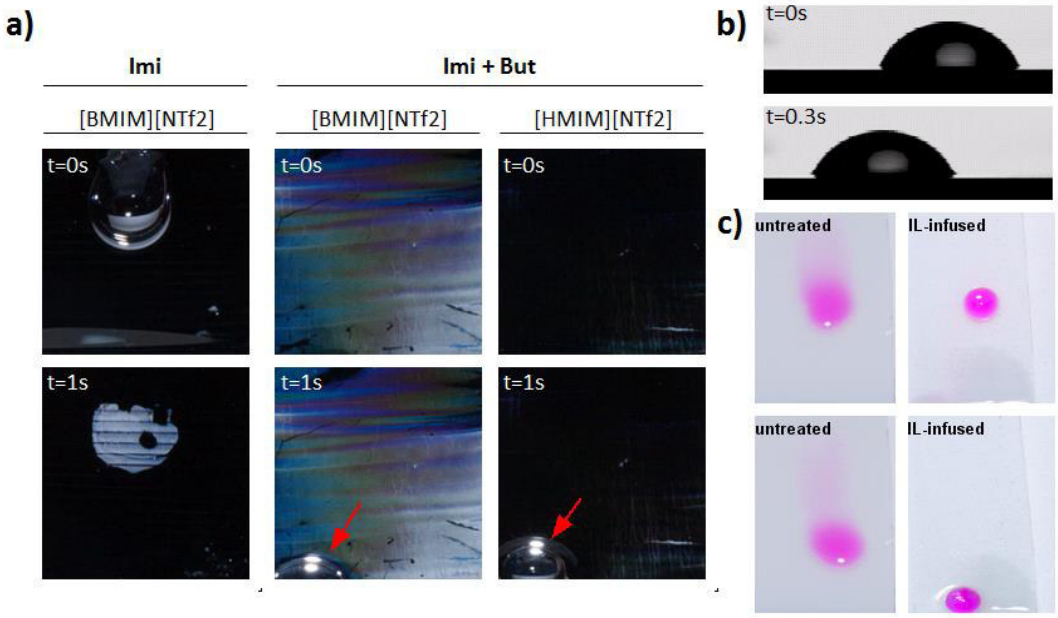

Figure 29. Water-repellency properties of ionic-liquid infiltrated surface nanostructures. a) Time-lapse images of a water droplet on an inverse opal surface nanostructure with different surface functionalities infiltrated with different ILs. The wetting state of the IL and the water droplet can be followed by changes in structural color: with an imidazole functionalization (Imi), the ionic liquid is replaced by water, while a stable film can result from mixed self-assembled monolayers (Imi + But); b) Time-lapse image of a water droplet show sliding under an angle of 2° on an ionic liquid ([HMIM][NTf2])-lubricated substrate with a mixed surface chemistry (Imi + Dod); c) Transparent ionic liquid-infused nanoporous coating based on silica nanoparticles enables efficient water repellency: A droplet of Rhodamine B colored water stains an untreated glass slide (left) but slides down without staining the substrate for the ionic liquid-infused sample (right).

Finally, to demonstrate the universal applicability of the stable ionic liquid-infused repellent surfaces, we prepared a transparent coating formed with disordered silica nanoparticles as a rough surface. We coated a glass slide with 20 nm SiO_2 particles using the layer-by-layer method,[45] then we functionalized it with a mixed self-assembled monolayer of Imi and But silanes. We used an aqueous dye to monitor the repellency in the transparent particulate coatings. Figure 29c shows a drop of rhodamine in water solution

that did not stain the IL-infused repellent surface, indicating a stable repellency and a glass slide completely protected from the contaminant.

5.1.3 Conclusions

To tackle the depletion of lubricant in the SILPs we propose the use of ILs. The extremely low vapor pressure and high thermal stability of ILs avoid the loss by evaporation. However, the design of the optimal surface chemistry to retain the ILs stably is challenging as a result of the structural chemical complexity.

Here we selected different functional groups resembling those in the molecular structure of the ILs for the surface functionalization. We analysed the wetting behaviour as a function of the surface chemistry.

We observed a maximal wetting contrast with water when we used mixed self-assembled monolayers containing aliphatic hydrocarbon chain and imidazole for the surface functionalization.

We used the structural colour of the nano porous inverse opals to study the wetting behaviour of the IL in the different surface chemistries applied. We detected three different scenarios based on the pore opening angles of the inverse opal, the contact angles of the ILs measured in the flat surfaces, and on the steric shielding in mixed monolayers on the coating with surface curvatures.

Subsequently, we identified the suitable conditions for infiltration and for a stable IL-infused coating with a drop of water as a contaminating test liquid. We concluded that stable repellent coating can be formed using 1-butyl-3-methylimidazolium bis(trifluoromethylsulfonyl)imide ([BMIM][NTf2]) or 1-hexyl-3-methylimidazolium bis(trifluoromethylsulfonyl)imide ([HMIM][NTf2]), and mixed monolayer of silanes as surface chemistry: the aliphatic hydrocarbon and imidazole functionalities. These surface functionalities create a favourable interfacial energy between the surface and the IL compared to the same surface functionalities and water.

Generally, these results confirmed that the surface chemistry needed to confine ILs as lubricant in nanostructures needs to be tailored based entirely on the chemical structure of the IL. We formed stable IL-infused repellent surfaces.

5.2 Porous materials with hierarchical porosity prepared by the layer-by-layer process enhance the stability of infused liquid films

In this chapter, we used the layer-by-layer technique to create defined thin films for coating porous materials. As this chapter will show, the complex geometry, long diffusion pathways and small sizes of necks connecting individual pores all contribute to difficulties to reliably coat such materials. We analysed the necessary conditions for using this technique in porous materials with different pore sizes.

The goal of the treatment is to deposit a nanoscale topography on top of a microscale topography to create hierarchical surface roughness to enhance capillary effects required for the confinement of a liquid on top of a solid material. This hierarchical porosity increases the surface area of an already porous material and with this the contact area between the material and the supported liquid increases in turn.

Then, as a proof-of principle, we use our findings to coat SiC monoliths with aluminum oxide nanoparticles for the confinement of ionic liquids, a setup commonly used in the water-gas shift reaction.

This study was designed by Nicolas Vogel and Yaraset Galvan, the experiments involving inverse opals were performed by Yaraset Galvan. The experiments involving SiC monoliths included in this chapter were performed by Johannes Bauernfeind as part of his Master thesis, supervised by Yaraset Galvan.

5.2.1 Introduction

The layer-by-layer (LbL) technique for coating surfaces consists in submerging a charged surface in a solution of a polymer with opposite charge, rinse it to get rid of the excess of polymeric solution and submerging it in another solution of opposite charge in turn.[55,141] This cycle can be repeated indefinitely, and because of the ionic nature of the polymers deposited, the process is self-limiting and every immersion leads to the absorption of a single monolayer of the next polymer, resulting in fuzzy films with a defined thickness. A desired film thickness and molecular composition can then be obtained by varying the nature of the polymer and the numbers of iterations.

The layer-by-layer technique has been extensively employed to coat different materials, and it has shown to be a versatile method for the formation of controlled thin films in a wide range of applications [142–144]. Virtually any surface can be coated with films of different functionalities, as long as the surface and the coatings have opposing charges. The LbL process provides a range of attractive features: it is scalable and experimentally simple to apply, objects of any shape can be coated, provided they can be brought in contact with a liquid, and the film thickness and composition can be readily adjusted, even at smallest length scales.

In the context of lubricant-infused surfaces, one key strategy to enhance the stability of the lubricant-solid interface is the introduction of capillary forces, as mentioned in chapter 2, the Layer-by-Layer technique was employed as an accessible and beneficial technique to create the roughness in the surface.[45]

In addition, the design of nanoscale porosity has been shown to improve on the depletion of lubricant. For example, loss of lubricant during frost formation over lubricated surfaces was lowest for substrates with the smallest interstitial space.[115] Enhanced capillary effects generated by nanoscale roughness or hierarchical features improve retention of the lubricant during frost formation [42] and condensation.[116]

Within the extensive field of porous materials there are other applications that require keeping an immobilized liquid on a surface. As an example, the supported ionic liquid phase (SILP) catalysis process,[125] that uses the relatively good wettability of ionic liquids on inorganic materials and exploits it to form systems that retains ionic liquids films with dissolved catalyst in the porous materials via capillary forces.[145]

Based on the evidence for enhanced lubricant retention in the design of repellent surfaces, we hypothesize that the presence of a nanoscale surface roughness may also stabilize the ionic liquid film within a SILP support. An increased stability of this film, in turn, would potentially reduce losses in a catalytic reactor, where a continuous gas stream is pushed through the SILP catalyst,[127,146,147] and may potentially enhance long-term stability. In addition, enhancing the lubricant/surface interactions may be the first step towards SILP operation in liquid phase, which is currently limited by a rapid loss of the ionic liquid during operation.

In contrast to a lubricant-infused repellent coating, however, increasing the affinity of the lubricant with the underlying solid in such processes requires a homogeneous functionalization of all surface regions within a three-dimensional porous material. Evidence in literature shows that the lbl process can be used to add polyelectrolyte[148–150] or particle layers within the surface of porous materials, such as micro- and

nanopores[151–154] with cylindrical geometry, membranes,[155] fibers,[156] or capillaries.[157] Despite this body of available literature, the successful coating of porous materials is less trivial compared to flat surfaces because of the increased surface area, transport limitations, or small geometric features preventing proper access. While some reports in literature suggest focus on very sparse particles layers [153,155–157] (i.e. for catalysis), others require process modifications such as charge screening by the addition of salt.[148,158,159]

As we focus on exploring the enhanced ionic liquid-support interactions in a SILP system, we set out to coat macroscopic silicon carbide specimens (approximate dimensions 20x2.5cm) typically used in supported ionic liquid phase (SILP)-based water-gas shift (WGS) reaction to produce H2 from fossil fuels.[160,161] These support materials exhibit a porosity at the micron scale, which is much larger than to the dimensions of the nanoparticles used in this study (Ludox silica, d= 20nm). As a second porous material, we therefore investigated a porous material with a much smaller pore size with dimensions in the range of the particles to be deposited. To this end, we used inverse opals as a model platform. These materials are prepared by backfilling a polymer colloidal crystal with an inorganic precursor material.[51,138,162] Upon calcination, the templating particles are combusted to give rise to a well ordered, interconnected porous structure. In our case, the pores had a dimension of 320nm and the necks approximately 120nm.

Surprisingly, we found that for both types of samples, the typical coating process did not allow a functionalization of the interior of the pore walls, but merely creates a coating on the outer surface of the material. We therefore analyzed in detail the limiting factors preventing accurate coatings in our systems and then re-designed a suitable LbL procedure according to the specific requirements of the porous materials for a successful coating of the entire porous material.

5.2.2 Results and Discussion

We employ the LbL process to create layers of SiO_2 nanoparticles to enhance the nanoporosity of a surface.[45,60,136,163] To this end, we create negative charges on the surface by means of plasma treatment. Subsequently, the substrate was immersed in a 0.1% w/w solution poly(diallyldimethylammonium) chloride (PDADMAC) as positively charged polyelectrolyte. Subsequently, the sample is rinsed with water and immersed in a 0.1% w/w solution of Ludox silica colloidal particles. These steps were then iterated to

create the coating. After having completed 5 cycles the surface was calcined to completely remove the PDADMAC. Figure 30a shows a planar silicon wafer successfully coated with five layer of 20 nm SiO_2.

Interestingly, when coating a porous material with SiO_2 following the same procedure, the coating exclusively deposited at the outer surface of the material, whereas the inner pores of the material remained uncoated. The size of the pores showed not to have any influence on the limitation of the LbL method for coating porous materials. We first tried to coat silicon carbide (SiC) monoliths with an average pore size of 3 µm as shown in Figure 30b. The top SEM image (i) shows a high magnification image of the outer surface, which was successfully coated with the SiO_2 particles. The bottom image (ii) was taken of an inner section of the same monolith after breaking and shows a pristine, uncoated surface.

Similarly, an inverse opal coated with the same procedure was only functionalized at the top layer (Figure 30c). This material was formed by an evaporative co-assembly approach resulting in an inverse replica of a colloidal crystal and exhibited a regular, interconnected porosity[50] with an average pore diameter of 320 nm.

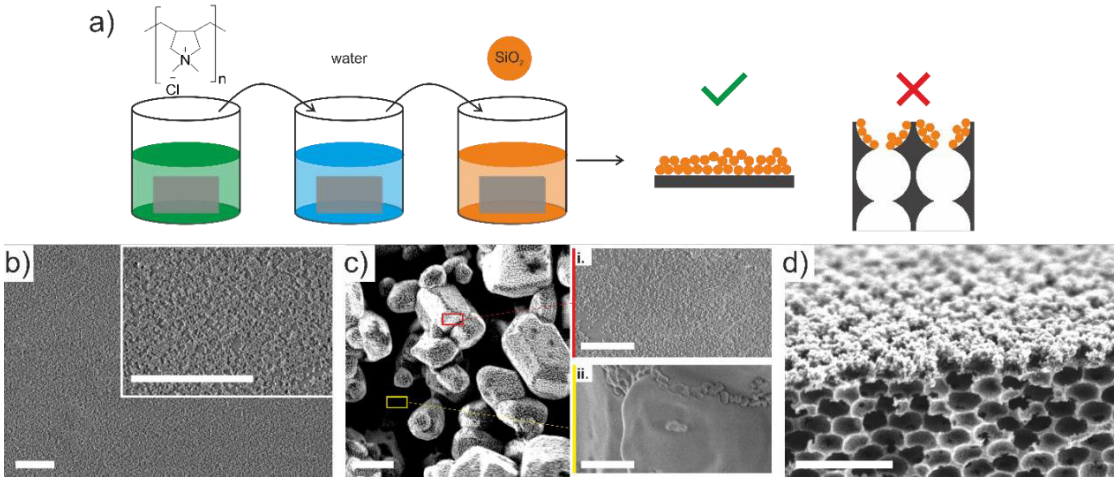

Figure 30. Layer-by-Layer coating of different surfaces by SiO_2 particles. a) Schematic representation of the LbL process that consists in the immersion of a substrate (flat or porous) in the positively charged PDADMAC, followed by water to get rid of excess of polymer and then in a solution of negatively charged SiO_2 particles. A homogenous coating is obtained in flat surfaces, but in porous material the particles cannot coat the inner pores. b) of a flat Si wafer, c) of a porous SiC (3 µm pore average) monolith, i. magnification in the outer surface of the SiC monolith, ii. Magnification in an inner pore of the SiC monolith, d) of SiO_2 inverse opals (350 nm pore average). All scale bars= 1 micrometer.

To address the limitations of the LbL technique in coating porous materials we first investigated several parameters during the coating of the SiC monoliths that may be affected by the nature of the porous materials. As mention above, prior to the actual LbL process, it is necessary to activate the surface to introduce negatively charges hydroxyl groups via oxygen plasma [45]. Here, taking into account the

tortuosity of the porous network, we increased the treatment time to allow the plasma to diffuse further into the porous network. Secondly, we considered the increased surface area in porous materials and increased the concentration in both coating solutions to ensure that all available surface can be coated. A successfully coated flat surface needs only 0.1 wt% solutions either of PDADMAC or colloidal SiO_2.[45] For the porous SiC, we increased the concentration to 1 wt%. Thirdly, we also increased the immersion time of the porous materials in the coating solutions. Since the pores are filled with water after each rinsing step before immersion into the coating solutions, either type of surface functionality to be attached needs to diffuse into the porous system to coat the surface. This diffusion time to reach the surface is greatly increased compared to a flat surface. We therefore increasing the immersion time from 5 min used for flat surfaces to 60 min for the porous surfaces.

We adapted the oxygen plasma treatment, the concentration of the coating solutions and the immersion times, first separately and, in a second attempt, together. Even after implementation of the three different aspects simultaneously, the inner surface was not coated. Since there was a slight increase in coating depth with increasing time, we inferred that diffusion of PDADMAC and SiO_2 into the pores is the limiting step preventing efficient pore functionalization. The difficulties in coating the porous SiC monolith were surprising, given the large pore sizes in the material (Figure 30) and the body of literature suggesting successful LbL coatings or porous materials. Seemingly, and in contrast to typical porous materials used in literature, the macroscopic dimensions (pore diameter = 3 μm) of the monolith lead to transport limitations of the ionic species involved in the LbL process.

Next, we therefore implemented an additional step to circumvent the slow diffusion process of the particles and polymer chains into the wetted porous material. After each immersion of the porous material in the coating solutions, we rinsed it in water and subsequently dried the entire sample with a flow of nitrogen. In this way, when the porous material is immersed into the next coating solution, either the PDADMAC or the SiO_2 particles enter the pores via convective flow along with the solution through the pores. The coating process therefore becomes independent of the diffusion limitations.

Figure 31 schematically shows the difference in coating process, illustrating the concentration profile of a species to be coated (i.e. the silica particles) within a single pore. The top part (i-iii) shows the conventional LbL process without the intermediate drying step. The SiO_2 particles enter the pores from the top. Due to the slow diffusion and continuous adsorption to the wall, the concentration decreases towards the interior of the pore. Figure 31-iv shows the absence of any coated SiO_2 particles on the surface of an inner pore treated using this process. The bottom part (Figure 31v-vii) shows the coating process with the

intermediate drying step between each immersion. The dispersed SiO_2 particles are dragged into the pore by a convective flow and maintain a high concentration. This process modification allowed a reliable coating of the inner pore walls, as shown in the SEM image of Figure 31-viii.

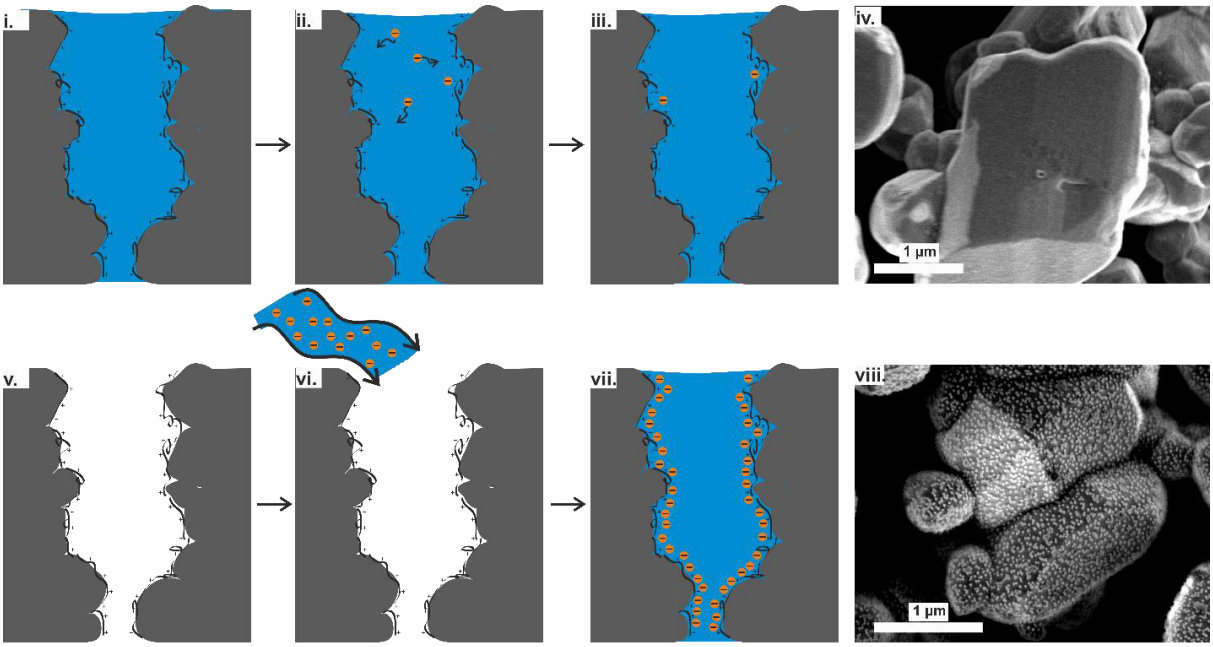

Figure 31. SiC monolith with micron-scale porosity coated with SiO2 particles via the layer-by-layer technique. Schematic representation of the Layer-by-Layer coating process in two different scenarios. The top part depicts the conventional LbL process, while the bottom part shows the modified process with an intermediate drying step in between each immersion. i. represents an inner pore immersed in the PDADMAC solution, ii. depicts the diffusion of SiO2 particles inside a pore flooded from the previous coating step, iii. represents the unsuccessful SiO2 coating with the conventional coating process and iv. shows a representative SEM image of the surface of an actual pore in a SiC monolith unsuccessfully coated. The bottom row shows the modified process. v. represents a dried inner pore coated with a layer of PDADMAC vi. shows the introduction of the SiO2 dispersion by convective wetting into a dry pore, which created a uniform concentration profile and thus achieves a homogeneous coating (vii.). viii. shows a representative SEM image of a successfully coated pore.

Next, we investigated the coating of interior pore walls of an inverse opal, which has an interconnected porous network with pore dimensions around 320 nm.

Figure 32 shows a schematic illustration of the coating strategies to coat the pores of an inverse opal, following the conventional LbL approach (Figure 32a). As expected, the side view SEM image showed that only the outermost pore layer was coated with silica nanoparticles. Similar to the case of the porous monolith, we hypothesized that the 20 nm SiO_2 particles were not able to coat the inner pores because of the diffusion limitations [164,165], which are even more pronounced because of the considerably smaller pores and the necks that connect them. We then applied the developed coating strategy towards the inverse opals, in which we capitalize on convective flow to enhance the mass transport of colloidal

particles into the pore network (Figure 32b). We used the structural coloration of the inverse opal to monitor the process steps.[52,53,136,162] Successful drying of the pores in between deposition steps could be seen by the presence of structural colour, which is caused by the high refractive index contrast between silica matrix and air. In contrast, after immersion, the water-filled pores exhibit a much lower refractive index contrast and thus lose their coloration [52,136]. Even though this structural colour-based monitoring indicated that the entire porous network was dried in between all immersion steps, the developed methodology did not lead to a coating of the inner pore walls. Similar to above, the side view SEM image shows that only the uppermost row of the inverse opal was decorated with silica nanoparticles. Even though the SiO_2 particles (d=20nm) are notably smaller than the necks of the pores (d=119±13 nm), the particles apparently cannot be transported through the pore network.

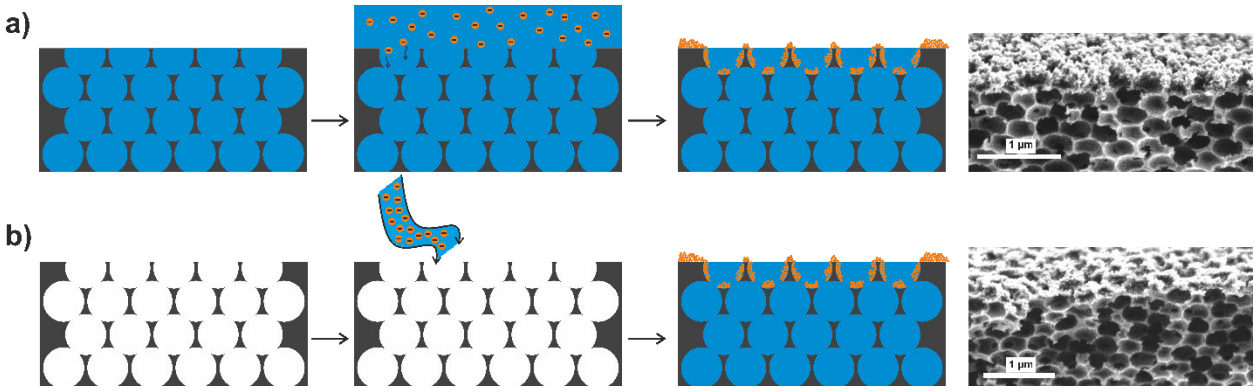

Figure 32. Inverse opals coated with SiO2 nanoparticles (20 nm) using a conventional Layer-by-Layer technique (a) and the modified LbL version with a convective flow of the solutions of PDADMAC and SiO2 colloidal particles (b).

Based on reports on literature that the addition of salt can facilitate the coating efficiency in confinements,[148,149,166] we hypothesize that the inability of the colloidal SiO_2 to penetrate through the pore network may be related to the electrostatic properties of the colloids in our system as well. The potential of a charged surface penetrates into an electrolyte solution and decays as counterions accumulate around the surface. The extend of this penetration is described by the Debye length, defined as the distance from the surface when the electrostatic potential drops to 1/e.[2] The decay of the potential is therefore determined by the ion concentration in the solution. [2] We hypothesize that electrostatic repulsion blocks pore access of the silica particles as follows (Figure 33). Since the surface is charged to induce the LbL process, electrostatic adsorption of silica particles will take place at the outer layer of the

porous surface upon contact, leading to a layer of silica particles being deposited. The surface potential of these adsorbed silica particles, in turn, will extend into the neck region, effectively reducing the available opening for an additional, like-charged silica particle to pass through (Figure 33a). Since the surface potential can be screened by charges, the addition of salt should decrease the Debye length, [2] and thereby increase the accessible pore area for a like-charged particle to pass through (Figure 33b). With increasing salt concentration, however, the electrostatic repulsion of the colloidal silica dispersion itself will be affected, leading to an onset of agglomeration. Such agglomerated particles are larger in size and therefore, when adsorbed onto the outer layer of the inverse opal, physically block pore access by covering the neck (Figure 33c).

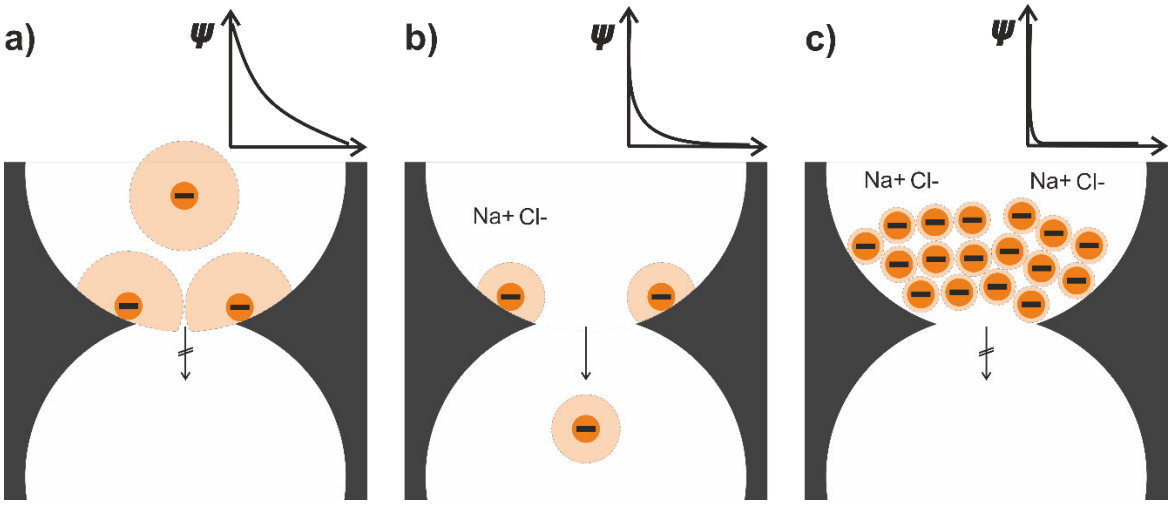

Figure 33. Graphic representation of the possible three scenarios at the neck of two pores of an inverse opal based on the electrostatic profile of colloidal particles in solution, adjusted with the addition of NaCl. a) the electrostatic effect of the colloid restricts the move of the particles into the pores. b) The electrostatic effects of the colloids are limited, so they can pass freely through the neck of the pores. c) the electrostatic effects of the colloids are inexistent, so the particles agglomerate and are unable to move through the neck of the pores.

To test this hypothesis, we carried out a parametric study on the influence of concentration of NaCl addition on the colloidal stability and the coating of inverse opals using the layer-by-layer technique. We prepared solutions of 0.1 wt% of colloidal SiO_2 with 1 mM, 10 mM, 30 mM, 50 mM, and 100 mM of NaCl, respectively. We determined the zeta-potential of the different SiO_2 dispersions as a function of the salt

concentration (Figure 34). As expected, the zeta potential decreased with increasing salt concentration, indicating an increased screening of charges, and thus a decrease in the range of the surface potential. [167]

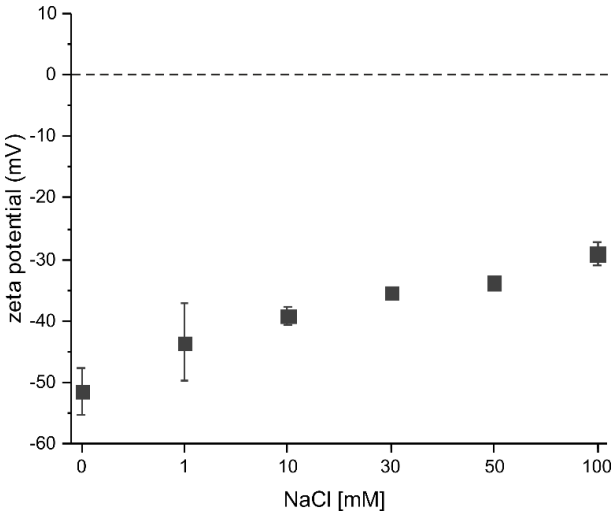

Figure 34. Zeta potential of the colloidal SiO_2 in dispersions with different concentrations of NaCl.

Next, we tested the effect of the screened electrostatic repulsion on the pore accessibility. (Figure 35) To this end, we used our modified LbL process. After the activation with oxygen plasma, we immersed the inverse opal in a positively charged solution of PDADMAC (0.1 wt%) with the different NaCl concentrations. We then rinsed the inverse opal thoroughly with water and dried it completely using nitrogen case. Subsequently, we immersed the sample in a dispersion of negatively charged colloidal SiO_2 (0.1 wt%) with the different NaCl concentrations. In addition to the varying salt concentration, we also varied the exposure time to account for the slow diffusion within the porous network and exposed the inverse opals to the individual solutions for 1 hour and 1 day, respectively.

Figure 35a shows representative side view SEM pictures of the different inverse opals samples coated by LbL using coating solutions with the different concentrations of salt, and the two immersion times. All samples were coated with 3 layers by the previously described procedure, calcined to remove the organic PDADMAC polymer and broken into two parts to reveal the pore interior in the side view images. Using image analysis, we determine the fraction of functionalized pores for samples coated with different salt concentration and immersion times by counting around 500 pores per sample (Figure 35b,c).

Without addition of NaCl, no particles were deposited in the interior pores, even for the extremely long immersion time of 1 day, corroborating with the inability of the particle to access the pores. In contrast, the addition of 10 mM of NaCl, allows at least some silica particles to enter the porous network. For both

immersion times, we determined around 30% of the inner pores coated. Using coating solutions with 30 mM NaCl, we observed a larger pore coverage. Using 1h deposition time, around 50% of all pores are coated. With an immersion time of 1 day, the fraction of coated pores increases to 70%, indicating that the charge screening indeed increased pore accessibility. With increasing salt concentration (50mM), the fraction of coated pores was reduced again, which we interpret as an onset of agglomeration that hinders pore access. For a salt concentration of 100 mM, no particles were detected in the pore interiors and close inspection of the surface structure reveals the presence of agglomerates deposited on the topmost layer. Apparently, a salt concentration of 30 mM provides a compromise between sufficient colloidal stability and decreased Debye length, which optimizes pore accessibility.

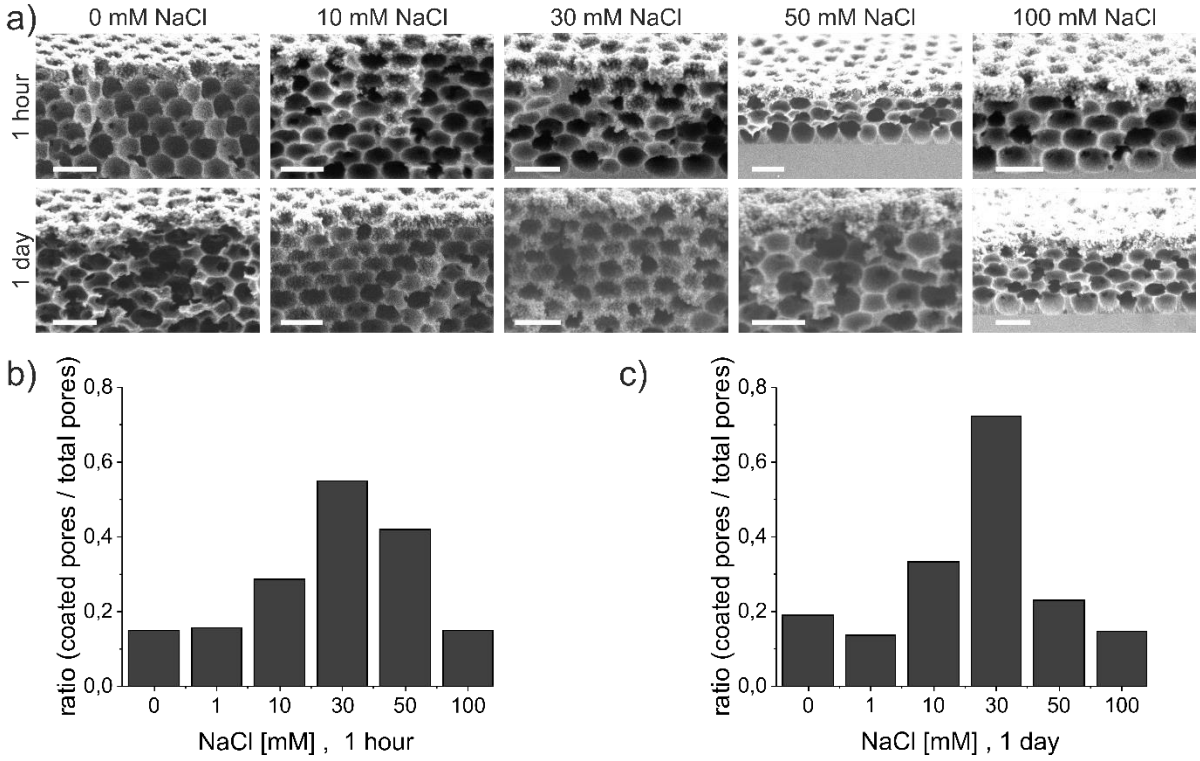

Figure 35. Influence of salt concentration on pore functionalization efficiency of inverse opals by the layer-by-layer method. a) representative side view SEM images of inverse opals coated by a LbL process using dispersions of colloidal SiO2 different NaCl concentrations (columns) and different immersion times (rows), scale bars= 200 nm. b,c) Statistical analysis of the pore functionalization efficiency, showing the ratio of coated pores as a function of salt concentration for immersion times of 1h (b) and 1day (c). Over 500 pores were analysed for each experiment.

Having established a reliable protocol to introduce a nanoscale topography in our porous materials, we tested its effect on the stability and retention of an infused ionic liquid film. Based on the fact that liquid film can be efficiently infused into nanoporous coatings on flat surfaces to design liquid repellent

surfaces,[136] we aimed to transfer this concept to a porous material. We used the SiC monoliths with hierarchical porosity and infused a layer of 1-butyl-2,3-dimethylimidazolium chloride [BMMIM][Cl] as the ionic liquid. This combination of support and ionic liquid is of interest in catalytic applications, for example for a supported ionic liquid phase (SILP)-based water-gas shift (WGS) reaction to produce H2 from fossil fuels.[15,129,168] In this SILP approach, a thin layer of ionic liquid is confined in the pores of a porous material, such as the SiC monoliths. This supported ionic liquid phase further contains a dissolved molecular catalyst and combines the high surface area and ease of operation of heterogeneous catalysis with the selectivity of a homogeneous catalyst.[16,125,127,169]

Recent studies showed that aluminum oxide (γ-Al_2O_3) is an ideal support for the ionic liquid and the catalyst for the WGS reaction [161,170]. Here, we aimed to investigate whether nanoscale alumina particles can be coated onto the porous SIC monolith to create by additional capillary forces acting through the nanoscale porosity. With the coating we anticipate a more stable confinement of the ionic liquid within the SiC monolith.

We subjected the SiC monolith to our modified LbL protocol using a dispersion of positively charged aluminum oxide particles (50 nm, 0.1wt-%)) and negatively charged poly(sodium 4-styrenesulfonate) (PSS; 0.1 wt-%). Figure 36a-c shows the interior of a monolith successfully coated with γ-Al_2O_3 nanoparticles at different magnifications.

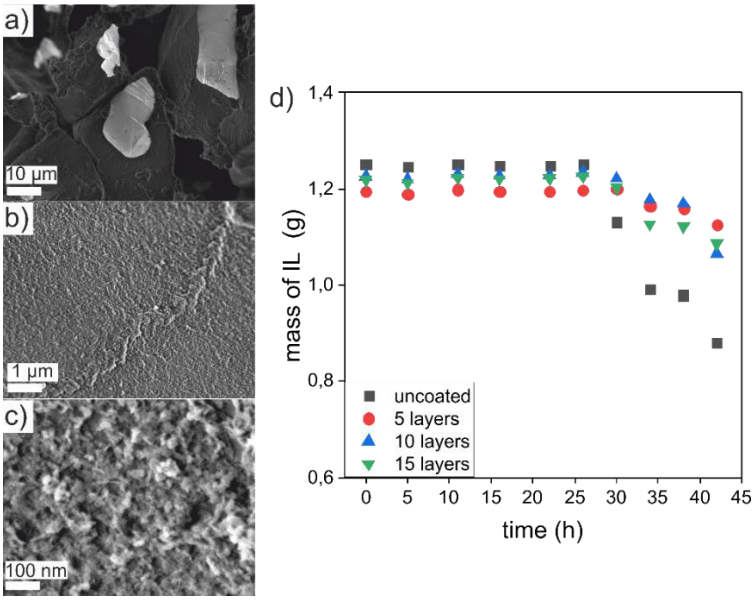

Figure 36. a)-c) SEM images of the inner pores of a SiC monolith coated with 15 layers of γ-Al_2O_3 nanoparticles using the layer-by-layer method with a convective flow of the coating solutions. d) Gravimetric evaluation of the retention of ionic liquid in coated and non-coated SiC monoliths.

Finally, we compared the retention of the ionic liquid film infiltrated in pristine and γ-Al_2O_3 nanoparticle-coated SiC monoliths. To this end, we immersed the monoliths into 10 v/v% solution of 1-butyl-2,3-dimethylimidazolium chloride [BMMIM][Cl] in dichloromethane (DCM) and evaporated the DCM to leave an impregnated IL film within the solid support.

We simulated reaction conditions occurring in a flow reactor by streaming a current of compressed air through the monoliths. We evaluated the IL retention by gravimetrically determining the loss of IL over time (Figure 36d). All coated samples consistently showed lower IL loss compared to the uncoated reference. After 42hours, only 70% of the initial ionic liquid was retained in the reference sample, while the coated monoliths held 95% of the initial ionic liquid. The loss of IL in this simulated reactor setup could thus be decreased by a factor of 6, underlining the potential of employing capillary forces by nanoscale surface roughness.

5.2.3 Conclusions

The Layer-by-layer process is a simple, yet powerful technique to create defined surface coatings for a broad range of applications. Here, we demonstrate that a nanoscale topography can enhance the stability of an ionic liquid film infused in a porous solid support. We first explore strategies to successfully coat the inner pore walls of our porous materials of interest. We realize that a combination of transport limitations and pore accessibility are the main limitations hindering the coating process. We overcome these limitations via two modifications of the coating process. First, adding convective flows by intermediate drying steps overcomes diffusive transport limitations and allows coating of porous materials with a micron-scale porosity. Second, screening electrostatic repulsion effects by the addition of salt overcomes the limited accessibility for pores in the nanometer range.

In a proof of principle, we show how a nanoscale surface roughness created by a LbL deposition of Al_2O_3 nanoparticles within a porous monolith can enhance capillary interactions and thus increases the retention of an ionic liquid film infused into the porous material.

5.3 Ionic-liquid infused organogels for repellent surfaces

In this chapter, we confined ILs to an underlying substrate by means of a functionalized polymeric gel that matches the chemical structure of the ILs and thereby maximizes their molecular interactions. We formed long lasting lubricant-infused repellent surfaces described in Chapter 2.3.

We used pentafluorophenol-based active ester polymers described in Chapter 2.2.2 to provide a versatile platform that allows a convenient post-synthetic functionalization of the polymer network. The matching functional groups to efficiently bind a desired IL can be introduced via their amine-functionalized analogues, which we demonstrate for imidazole- and phosphonium-based molecules.

This project was designed by Nicolas Vogel and Yaraset Galvan. The synthesis and characterization of the polymers, ILs and benzophenone silane were performed by Yaraset Galvan and Tobias Salbaum, who performed his master thesis on the topic under supervision of Yaraset Galvan. The synthesis of phosphonium-based IL and the drop-casting of the polymers in glass slides were performed by Tobias Salbaum during his master thesis. The results of this project have been published in the Journal of Materials Chemistry A, 2021, the results are partially reproduced from reference [171] with permission of the Royal Society of Chemistry.

5.3.1 Introduction

To create robust repellent coatings, we further maximized the affinity of the surface and the lubricant using surface-anchored organogels. As mentioned in Chapter 2.2.2, organogels consist of crosslinked polymer networks that, with proper chemical affinity, can be swollen with a lubricant [20,172,173], where the lubricant is held in place by chemical interaction with the polymer network [66]. More precisely, the affinity of the lubricant to the polymer network is maximized if the enthalpy of polymer-lubricant pairs is minimized. This, in turn, minimizes the interfacial energy of the lubricant to the solid surface. Compared to solid, porous surfaces, the large number of lubricant-polymer pairs in such organogels can increase the lubricant affinity to the surface [25,174,175].

To successfully use the ILs as lubricant in organogels-based repellent coatings we need to maximize the affinity of the polymer network and the free IL. This requires the creation of highly functionalized polymer networks exhibiting chemically similar groups as the IL to be retained in the organogel.

For maximal flexibility, we used a reactive polymer strategy that allows tailoring the functionality of the polymer to any desired IL. As described in Chapter 2.2.2.1, pentafluorophenyl-based reactive polymers react with primary amines under mild reaction conditions [76,176], by which a great variety of functional molecules can be introduced to the polymer backbone.

We tailored the polymer-IL affinity by incorporating amine-functionalized IL molecules with similar chemical composition into the polymer. Additionally, we co-polymerized benzophenone methacrylate to form the crosslinked network.[90]

Once the polymerized ILs were formed, we anchored it to a surface using a photoactive benzophenone silane to covalently attach the polymer to the surface, Figure 37 shows a schematic representation of the formation of the ionic liquid-based repellent coatings.

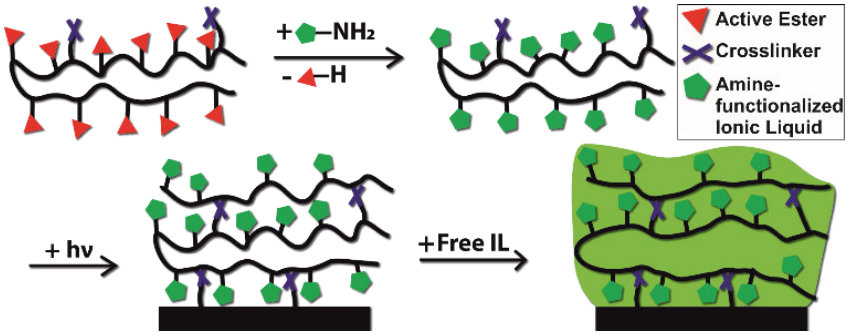

Figure 37. Schematic illustration of the fabrication of repellent surfaces using polymerized ionic liquids. Active ester co-polymers with a crosslinker are functionalized via polymer analogous reactions with a desired, amino-functionalized IL to form an ionic liquid-functionalized polymer, which is attached to an underlying substrate by UV irradiation of the crosslinker present in the polymer and on the surface. The ionic liquid-polymer attached to the surface is then infused with a free ionic liquid to form the repellent IL-infused organogel.

5.3.2 Results and Discussion

To create the functionalized organogels, we first co-polymerized pentafluorophenyl acrylate (PFPA) with 4-benzophenone methacrylate (BPMA) as a photo-crosslinkable moiety, required for subsequent network formation (Figure 38).

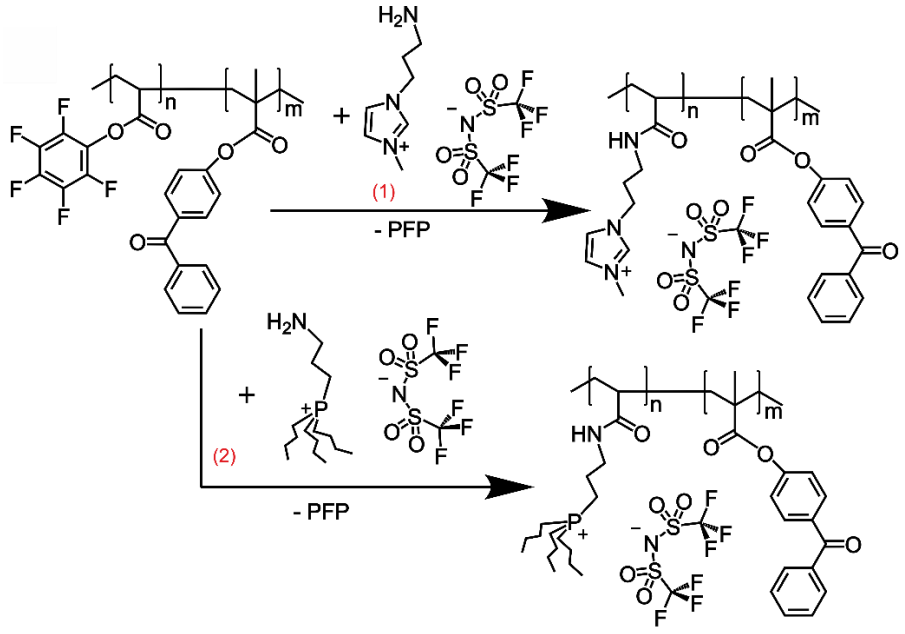

Figure 38. Synthesis of the ionic liquid-functionalized polymers: copolymerization of pentafluorophenyl acrylate and benzophenone methacrylate and its functionalization with the ionic liquids. (1) 1-aminopropyl-3-methyl imidazolium bis(trifluoromethylsulfonyl)imide and (2) aminopropyl tributylphosphonium bis(trifluoromethylsulfonyl)imide

Figure 39 shows the characterization of a typical batch of the co-polymers synthesized in this study. Figure 39a is the NMR spectra of 19F were the signals for the pentafluorophenyl group are present. Figure 39b shows the 1H-NMR spectra. The aromatics from the benzophenone methacrylate (7.26 – 7.86 ppm) and from the acrylate and methacrylate backbone: in 2.5 ppm is the shift of the 2 atoms of H from the aliphatic chain overlapped with 2 atoms of H from the aliphatic chain next to the acrylate group 2.16 ppm. Additionally, the H atom from the acrylate group is present in 3.13 ppm, and the 3 H atoms from the methacrylate in 1.47 ppm. Figure 39c shows the molar mass distribution of typical (7 different) batches of polymers synthesized for this study with Mw= 2.25 ± 0.26 X 104 g/mol and Mn= 1.14 ± 0.16 X 104 g/mol. We varied the BPMA concentration between 1- and 10 mol% to adjust and optimize the network formation.

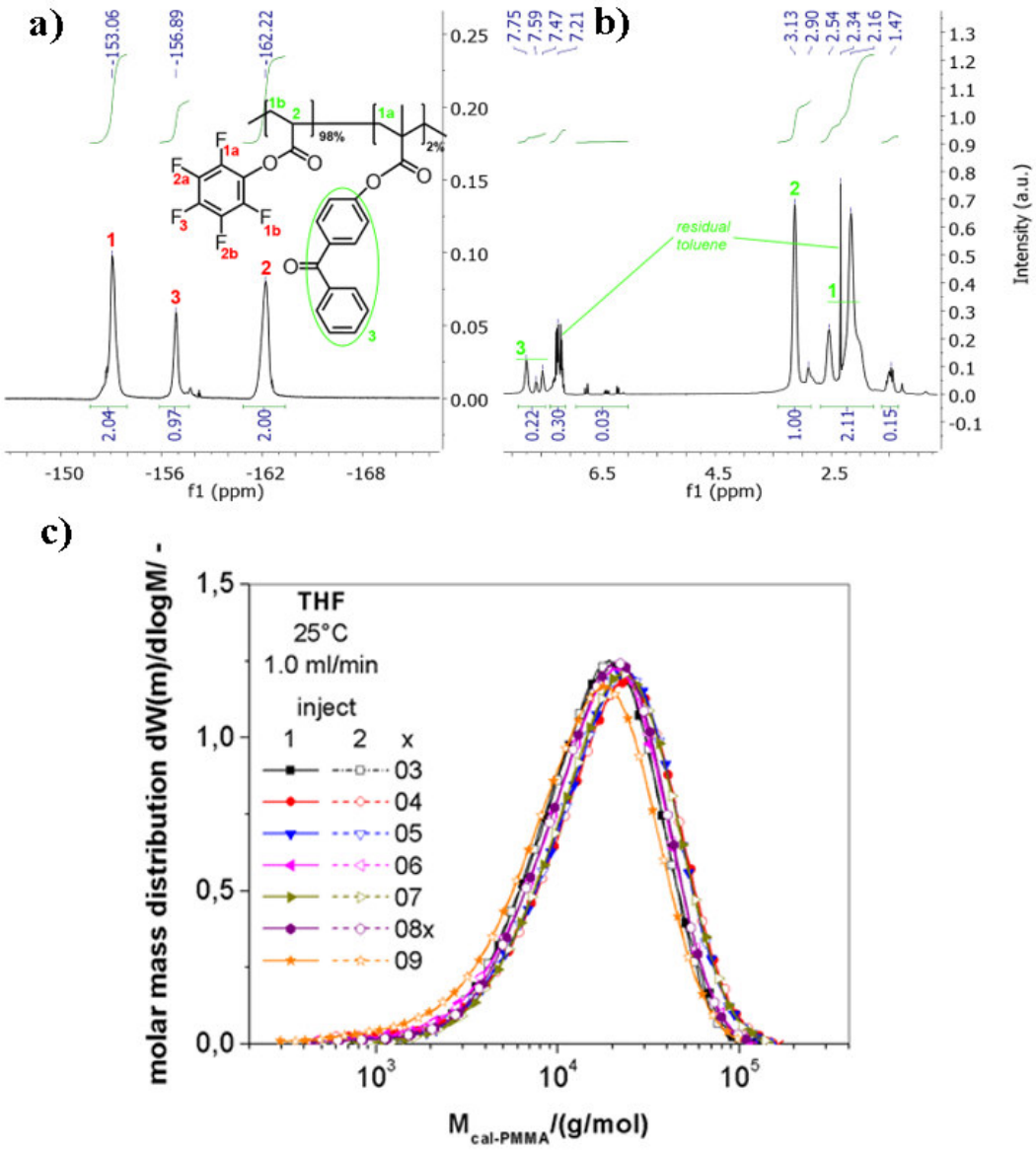

Figure 39. NMR spectra a) 19F-, b) 1H and c) GPC data (Mw) of different synthesized poly(pentafluorophenyl acrylate) polymer batches used in the study.

As a proof of principle of the flexibility in creating tailored IL organogels, we then functionalized the active ester polymer with two different IL species. To this end, we substituted the pentafluorophenyl groups with 1-aminopropyl-3-methyl imidazolium bis(trifluoromethylsulfonyl)imide [APMIM][NTf2] and aminopropyl tributylphosphonium bis(trifluoromethylsulfonyl)imide [APTBP][NTf2], as described in

Figure 38. We confirmed the successful functionalization of the reactive polymer by NMR spectroscopy and FTIR spectroscopy.

Figure 40 shows the NMR spectra the atoms of 1H (a) and 19F (b)of the imidazole-based ionic liquid and Figure 41 shows the NMR spectra the atoms of 1H (a) and 31P (b) of the phosphonium-based ionic liquid.

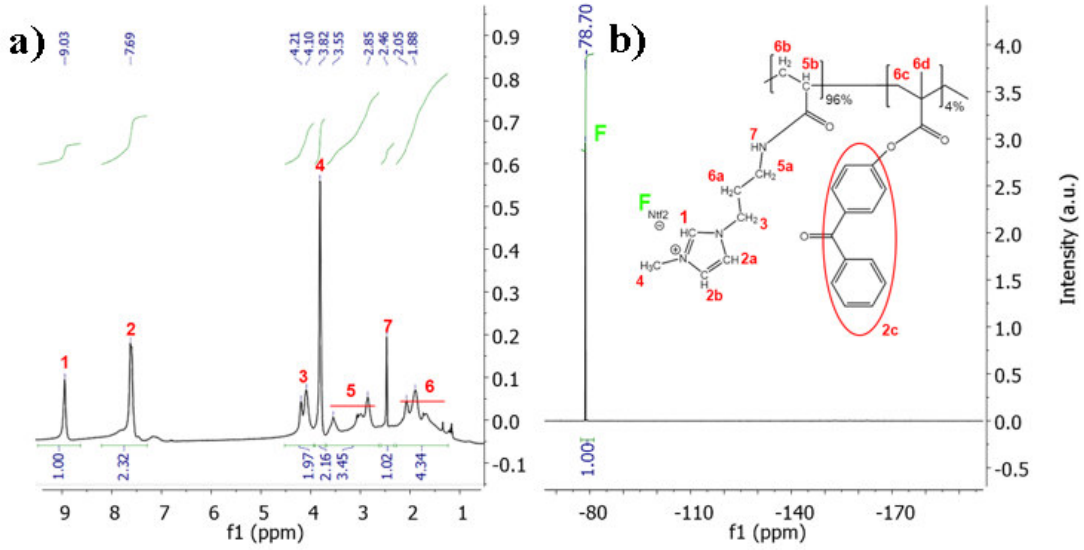

Figure 40. NMR spectra of imidazole-based polymer [APMIM][NTf2] a) 1H and b) 19F.

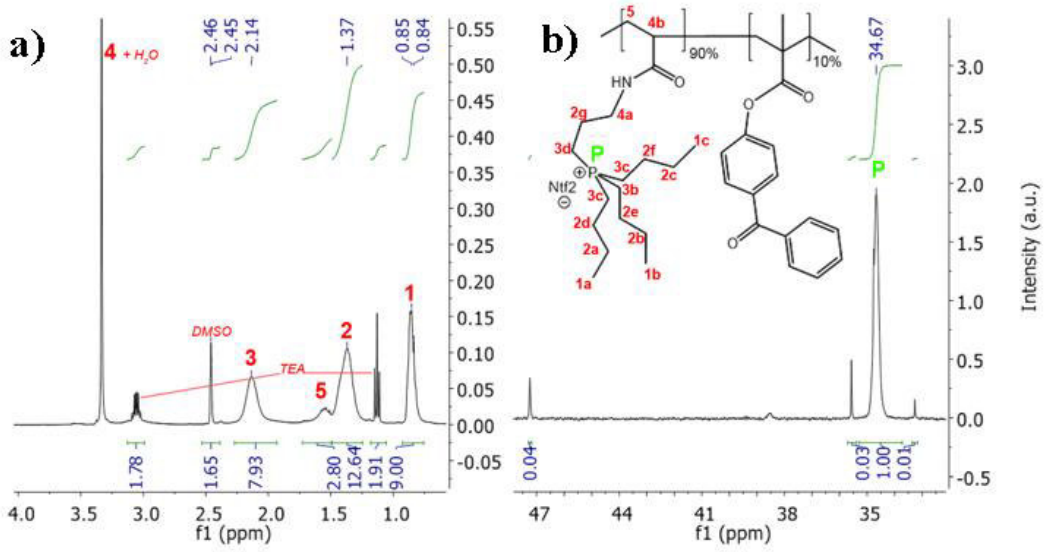

Figure 41. NMR spectra of phosponium-based polymer [APTBP][NTf2] a) 1H and b) 31P.

Figure 42 shows the FT-IR spectra, the carbonyl bond of the pentafluorophenyl ester assigned at 1783 cm-1 disappeared after the polymer-analogous reaction.[177] A new peak appears assigned to the amide bond of the IL containing side chain at 1650 cm-1. This corroborates the successful functionalization of the polymer with the amine-functionalied IL. In addition, new peaks assigned to the IL functionalities appeared, such as the sulfonyl bond (S=O stretching) at 1350 cm-1 and 1195 cm-1 present in the anion of both ILs.

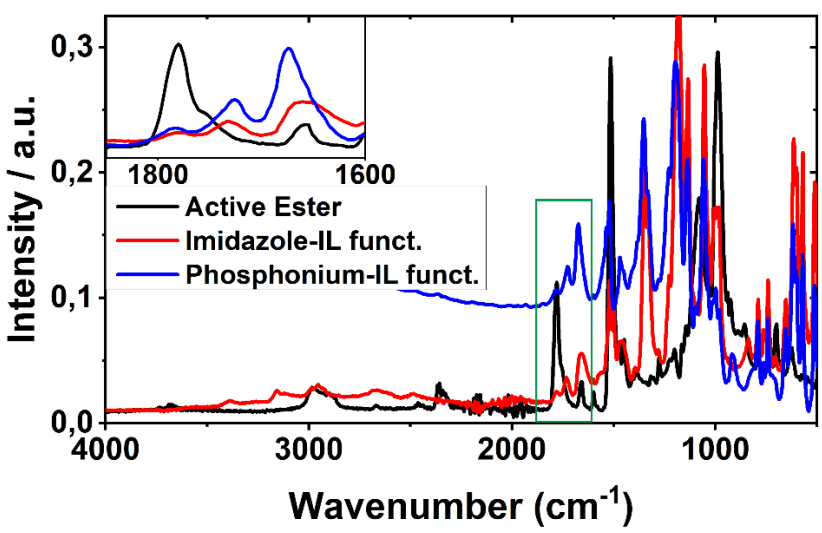

Figure 42. FT-IR of the active ester polymer and the ionic-liquid functionalized polymers. The inset shows the characteristic carbonyl region that shows a shift of the amide peak upon functionalization to form poly([APMIM][NTf2]A-co-BPMA) (red) and poly([APTBP][NTf2]A-co-BPMA) (blue).

Next, we produced thin polymer films on a substrate surface by covalently anchoring the polymers to the substrate. We used the same benzophenone-based crosslinking chemistry as for the polymer network formation. We synthesized 4-(3'-chlorodimethylsilyl) propyloxybenzophenone [135] (Figure 43a) to form a molecular monolayer of benzophenone molecules on a glass substrate via liquid-phase silane chemistry [178–180]. A change in water contact angle from below 5° to 70 ± 4° confirmed the successful formation of the silane monolayer (Figure 43b). We subsequently drop-casted the IL-functionalized polymer dissolved in butanone and carefully removed the solvent in vacuum. We then irradiated the polymer film with UV light (365nm) to simultaneously induce crosslinking and anchoring to the substrate. We immersed the coated surfaces in acetone for five hours to remove any unbound species.

Depending on the functionalization of the polymer, the amount of crosslinker and required irradiation time varied. Imidazolium-based polymers already formed stable gels at 2 mol% BPMA and 10 J/cm², whereas the phosphonium-based polymers needed at least 8 mol% of crosslinker and 200 J/cm² to form non-dissolvable gels. In the case of the polymer functionalized with [AMTBP][NTf2], the presence of a larger number of aliphatic carbon chains requires a higher amount of BPMA and irradiation to overcome the steric hindering and the higher probability of crosslinking of adjacent monomeric units.

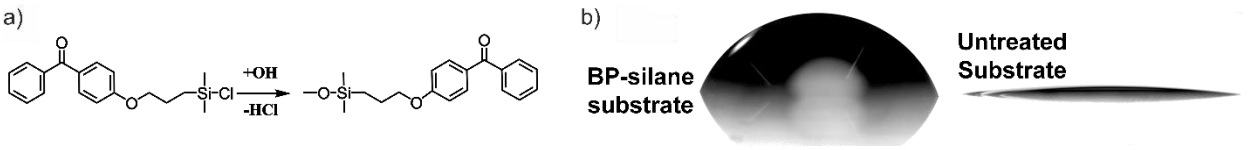

Figure 43. a) Schematic representation of the silanization of a substrate with benzophenone-silane. b) Static contact angle of an untreated substrate and a substrate modified with benzophenone-silane.

Having formed a crosslinked, surface-bound network of the functionalized polymers on the surface, we next formed an organogel by swelling of the network with a desired IL. We matched the chemical structures of the polymers to the desired ILs. As a first system, we formed organogels containing 1-methyl-3-propylimidazolium bis(trifluoromethylsulfonyl)imide [MPIM][NTf2] as the IL and used the [APMIM][NTf2]-functionalized polymers (Figure 38). As a second system, we used the more hydrophobic methyltributylphosphonium bis(trifluoromethylsulfonyl) imide [MTBP][NTf2] as the ionic liquid. In this case, we matched the chemical nature of the polymer network via the synthesized [APTBP][NTf2]-functionalized polymer (Figure 38). Since the ionic liquids are highly viscous, the best strategy to form the organogel was to dissolve the IL in butanone (1:9), swell the polymer network and subsequently evaporate the auxiliary solvent.

We used confocal microscopy to trace the infiltration and swelling of the polymer network with the IL, using the example of the [MTBP][NTf2]-based organogel. We co-functionalized the polymer with 1 mol% of Nile Blue- bis(trifluoromethylsulfonyl)imide to covalently attach a dye molecule to the polymer and therefore allow observation of the polymer network in the confocal microscope. Figure 44b shows the cross-section of the polymer film in the course of the swelling process at different times. Directly after addition of the IL/butanone mixture (1 min), the confocal microscopy images show a broadening of the

fluorescent area and a decrease of fluorescence intensity. Both indicate the successful infiltration of the dissolved IL into the polymeric network, which subsequently expands. After 20 minutes, the fluorescence intensity increased and the film thickness decreased again, indicating evaporation of butanone as auxiliary solvent. From these confocal images, we determine the evolution of film thickness as a function of time using image analysis of the stacked confocal images in ImageJ. The initial thickness of the non-swollen polymer film on the substrate was 50 µm. After addition of the IL/butanone mixture, the thickness increased to 80 µm, and finally stabilized at 75 µm after evaporation of the butanone, giving a swelling ratio of 1.5.

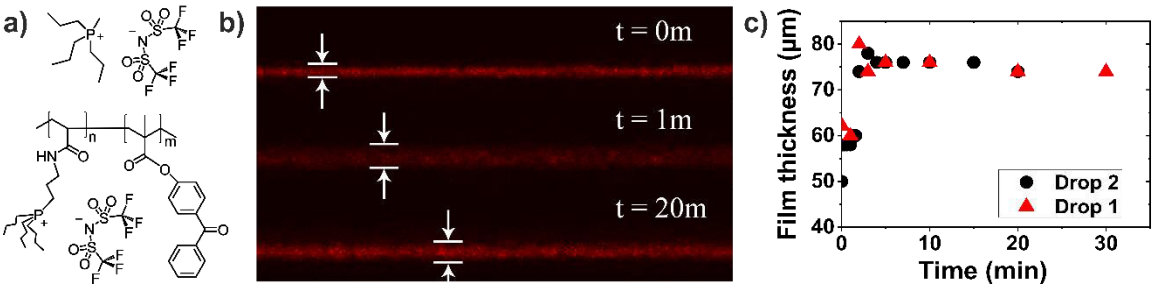

Figure 44. Formation of the ionic liquid-containing organogel using poly([APTBP][NTf2]A-co-BPMA) swollen with [MTBP][Ntf2], as investigated by confocal microscopy. a) Chemical structure of the free and polymerized ionic liquid used in the experiment. b) Cross-sections of the dye-labelled polymer network before (top) and after swelling with the ionic liquid dissolved in butanone (1:9) as a function of time. c) Film thicknesses extracted from the cross-sections in ImageJ for two droplets on separate areas of the substrate. The initial thickness of the polymer film attached to the substrate was 50 µm. This thickness increases upon swelling and stabilizes at ~ 75 µm after evaporation of the auxiliary solvent.

We investigated the self-cleaning and repellency properties of the formed IL-infused organogels. First, we observed the drying process of water on different substrates and used ink to colour the water to increase visibility and to investigate the resulting drying patterns. Figure 45a compares the drying process of an unfunctionalized glass slide, a benzophenone silane-coated glass slide (BPM-silane) and the IL-infused organogel. We used the tributyl-phosphonium-based IL system ([MTBP][NTf2] infused in the matching polymer network because of its more hydrophobic character. Both references showed the expected drying behaviour of the ink droplet in the form of a coffee stain, which is caused by pinning of the solid content of the droplet at the drying edge of the droplet [181,182]. In contrast, the ink droplet continuously shrunk upon evaporation on the IL-infused organogel and only left a very small residue at the droplet centre. This drying behaviour is characteristic for the absence of pinning [183,184] and indicates that there are no direct interactions between solid contaminants and the underlying surface. Consequently, it can be

inferred that the organogel prevents the direct contact with the contaminating liquid and the solid substrate.

This absence of pinning and the resulting liquid repellency is further underlined by the dynamic behaviour of a water droplet on the IL-infused organogels. Figure 45bshows a water droplet sliding down an inclined organogel substrate without pinning. The slow speed of the droplet and the comparably large inclination angle to demonstrate the sliding are caused by the high viscosity of the ionic liquid [185].

The key advantage of using ILs as the lubricating fluid in the design of lubricant-infused surfaces is their enormous temperature stability, which is caused by the extremely low vapour pressure as pointed out in Chapter 2.1 [186]. In Figure 45c, we capitalize on these properties and demonstrate the long-term stability of the IL-infused organogels upon storage at 85°C for extended periods of time, up to 150 days. We compare the retention of the liquid repellency properties against other lubricant-infused coating designs by measuring the sliding angle of a water droplet and the contact angle hysteresis. Two-dimensional coatings consisting of a silane-functionalized layer-by-layer silica nanoparticle coating infused with silicone oil (viscosity 9.3 cP) [122] and a fluorinated liquid (Krytox 100) [59] failed in their repellency properties after exposure to 85°C for 1-2 days, as indicated by a rapid increase in sliding angle and contact angle hysteresis. Polydimethylsiloxane (PDMS) swollen with silicon oil (viscosity 9.3 cP), a widely-used and efficient lubricant-infused coating, [67,68,118] retained its repellent characteristics for much longer times. This improved long-term stability reflects the three-dimensional nature of the swollen PDMS layer and the increased affinity by the matching chemical functionalities of the polymer network. However, both the water sliding angle and the contact angle hysteresis of a water droplet continuously increased with storage time at 85°C. After 150 days, the sliding angle of this type of coating exceeded 40°, indicating reduced liquid repellency. In contrast, the IL-infused organogels retained its repellency throughout the tested period without showing any signs of reduced performance. After 150 days at 85°C, the contact angle hysteresis remained below 5°. This long-term stability under demanding conditions underline that the attractive properties of ILs can be efficiently incorporated in a lubricant-infused coating, provided that the physicochemical properties of the polymer network are properly matched to the desired IL.

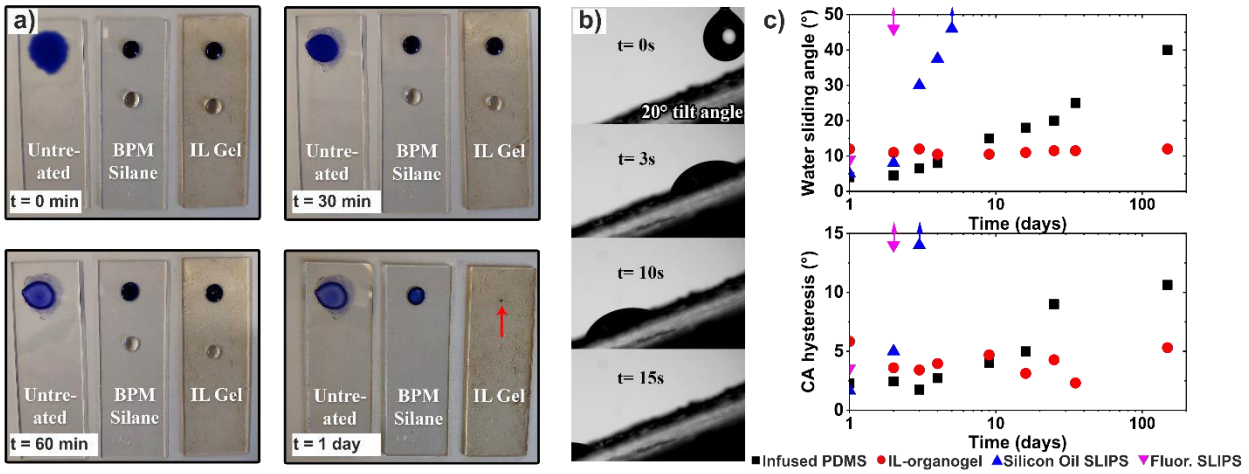

Figure 45. Liquid-repellency and long-term stability of the ionic liquid-based organogels. a) Prevention of pinning and self-cleaning capacities of the IL-infused organogels probed by drying of a contaminated liquid. Comparison of the drying process of a blue ink droplet (up) and pure water (down) added to an untreated glass substrate, a BPM-silane functionalized glass substrate and an IL-infused organogel (poly([APTBP][NTf2]A-co-BPMA infused with [MTBP][Ntf2]). The efficient repellency of the organogel is seen by the continuous shrinkage of the droplet. This lack of pinning and absence of any drying patterns indicate that the organogel prevents any surface attachment of the contaminating liquid. b) A 4 µL water droplet sliding down an organogel-coated substrate with a 20° inclination without pinning indicates its slipperiness. c) Comparison of Sliding angles and contact angle hysteresis for different lubricant-infused repellent surfaces upon storage at 85°C. The water sliding angle and the contact angle hysteresis remain constant for the ionic liquid-based organogel even after storage for 150 days at 85°C.

5.3.3 Conclusions

We have demonstrated how lubricant-infused coating with long-term stability at elevated temperatures can be design via IL-infused organogels.

To take advantages of the properties of IL, especially their negligible vapour pressure, we confined them efficiently by maximizing their chemical affinity to the polymer network. We used an active ester-based approach that provides a versatile platform to introduce such tailored surface functionalities.

In polymer-analogous reactions, amine-functionalized IL species can be directly bound to the polymer network.

In contrast to existing IL-based repellent surface coatings that operate via infusion of surface-functionalized porous coatings or commercial polymer structures, our approach allows adjusting the polymer architecture precisely to a desired IL. As a result, these optimized organogel coatings show robust liquid repellency properties that outperform existing systems in temperature tolerance and long-term stability.

5.4 Polymerized ionic liquid gels as scaffolds for SILP catalysis

In this chapter, we investigate the application of formed polymer-based coatings supports for the supported ionic liquid phase (SILP) catalysis. Polymerized ionic liquids were employed for coating porous silica to enhance the retention and stability of an ionic liquid (IL) film containing catalytically active species After a detailed characterization of the formation of the surface-bond polymer film, we focus on the leaching of the IL and therefore the ability of the polymer coating to enhance retention and stability.

Yaraset Galvan synthesized and characterized the polymers and the surface-bound polymer films. The experiments of the leaching tests shown in this chapter were performed by Yaraset Galvan with the collaboration of Markus Schörner (Lehrstuhl für Chemische Reaktionstechnik), who also performed the ICP-OES measurements. Figure 52 and Figure 53 were taken from the master thesis of Helene Kaleeva. This thesis, supervised by Marco Haumann and Markus Schörner at the Chair of Chemical Reaction Engineering included a study of different catalysts and ligands using the surface-bound IL films synthesized by Yaraset Galvan. These figures are necessary for the discussion of this chapter.

5.4.1 Introduction

As described in chapter 2.4, in a Supported Ionic Liquid Phase (SILP) catalysis system, a molecular catalyst dissolved in an IL is confined to a porous solid support. This system combines the advantages of both homogeneous and heterogeneous catalytic processes and it has been used in different reactions, yet it is still technologically challenging since it requires preventing the IL from being washed out of the porous solid support when is in contact with reactants and solvents at reaction conditions.[130,187]

In a typical SILP catalysis, the IL is impregnated onto a porous support and is considered to form a thin film. [125] However, different studies have pointed out discrepancies and inhomogeneous wetting, which may compromise the performance.[187] Noteworthy, controlling the surface wettability is important for a broad range of other applications, especially the design of repellent surfaces. In this field, a clear understanding of the importance of controlling the interfacial energy has emerged (see chapter 2.3). As we have shown in chapter 5.1, minimizing the interfacial energy allows the use of ILs for the design of such repellent surfaces. Here, we suggest that a transfer of the concept developed for such repellent

surfaces may be beneficial for the performance of a SILP material as well. We therefore investigate the use of customized polymer gels to be used as polymeric support for the SILP catalysis.

The use of polymeric gels to entrap IL has been previously employed in different applications including solar cells,[188–190] Lithium-ion batteries,[191] fuel cells, [192,193] antifouling materials[175] and catalysis membranes [194,195]. Most of the mentioned applications employ fluorinated polymers like poly(vinylidene fluoride)-hexafluoropropylene as a suitable polymer to retain fluorinated ILs. [191,196]

We propose to maximize the chemical affinity of the IL to the solid support by creating polymeric gel supports with a chemical composition matching that of the IL, thereby strongly confining the IL inside the supporting polymeric scaffold.

We used surface-anchored organogels previously described (Chapter 2.2.2 and 5.2) that with proper chemical affinity, can be swollen with an IL. Using similar chemical compositions for IL and polymer, we maximize the affinity and thus reduce the interfacial energy of the IL with the solid support. This, in turn, may increase the retention of the IL to be used in the SILP catalytic process.

First, we synthesized pentafluorophenol-based active ester polymers and functionalized them with amine-containing IL to match the chemical nature of the IL. Subsequently, we coated mesoporous SiO_2 with the polymerized IL via a combination of silane chemistry, active ester and photoactive benzophenone units and investigate the retention of the IL, especially in contact with a continuous liquid environment.

5.4.2 Results and Discussion

We followed a three-step process for the formation of our catalytic supports, starting from porous SiO_2 powder to provide the supports with mechanical stability. The porous SiO_2 was calcined to remove traces of water in the surface. After calcination, the first step consisted of the functionalization of the porous SiO_2 powder with a widely used amine-containing silane, (3-aminopropyl)triethoxysilane (APTES) (Figure 46-1). The amine group in the surface of the SiO2 (Figure 46a) serves to anchor crosslinking units via active ester chemistry in the second step.

As described in chapter 2.2.1, in presence of amines the pentrafluorophenyl-based ester undergoes a nucleophilic substitution where the pentafluorophenyl group is replaced by the amine forming an amide bond. Here, we use this reaction to bind our previously synthesized co-polymer poly(pentafluorophenylacrylate-co-benzophenone methacrylate) (Figure 46-2) to the surface of the

silanized silica particles. This polymer binding results in the formation of a polymer layer that contains benzophenone units at the surface, which can undergo crosslinking to subsequently polymer chains (Figure 46b). For practical purposes we will refer to this layer as BPMA, referring to the benzophenone units.

In the third step, we added the previously described poly(aminopropylmethylimidazolium-bis(trifluoromethylsulfonyl) imide-co-benzophenone methacrylate) (Figure 46-3). This IL polymer has the same chemical structure of the IL we want to retain. The polymer and IL synthesis, the organogel formation and their characterizations have been previously described in chapter 4 and 5.2. The benzophenone units from the second and third step are activated to covalently attached the IL-organogel to the SiO_2 and crosslink the polymer layers (Figure 46c). Once attached to the SiO2, the organogel is swollen with the IL.

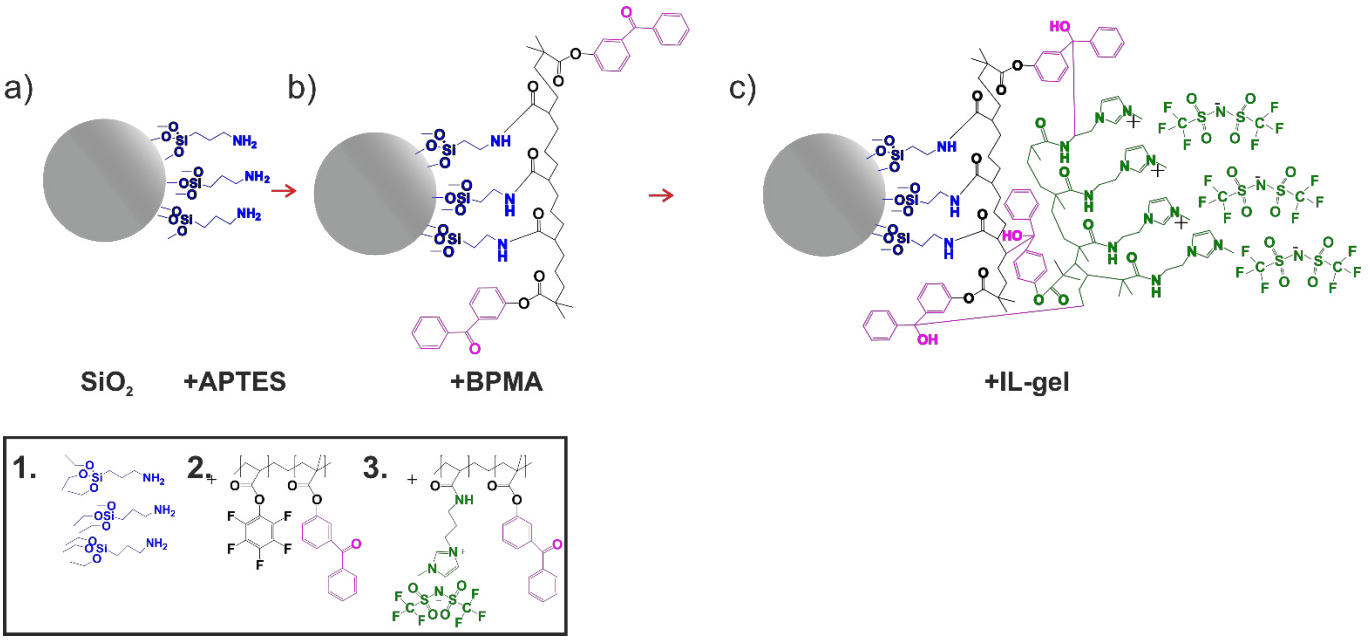

Figure 46. Schematic representation of the formation of the polymeric supports and chemical structure compounds used. a) silanized SiO_2 with APTES, b) functionalization via active ester chemistry for the addition of benzophenone units, c) IL-gel coating. 1. 3-aminopropyl triethoxysilane (APTES), 2. poly(pentafluorophenylacrylate-co-benzophenone methacrylate (BPMA) and 3. poly(aminopropylmethylimidazolium-bis(trifluoromethylsulfonyl) imide-co-benzophenone methacrylate) (IL-gel)

We characterized the polymeric supports along the three-step process using X-ray photoelectron spectroscopy (XPS), fourier-transform infrared spectroscopy (FTIR), thermogravimetric analysis (TGA), and scanning electron microscopy. We used XPS for the determination of the support surface chemical composition in each step of the coating by detecting N 1s and C 1s atoms. Considering the presence of N

and C in the silane and the IL-gel, their detention in each step is an indication of a satisfactory coating. Figure 47 shows the XPS spectra of the supports in the different stages. The different stages show different XPS signals as a consequence of the different chemical composition at the surface. In Figure 47a the XPS spectra for the C 1s atom shows 3 peaks, the peak at 284.8 eV corresponds to C atoms with C or H neighbors.[197] We observed this peak in the 3 steps of the support's formation (lines green, blue and red), the alkyl C is present in the silane, the active ester-polymer and the IL-organogel. The peak at 286.6 eV is assigned to the C atom of the carbonyl group,[198] observed in the second step, when the functionalization with the benzophenone-containing polymer takes place (blue line). Finally, the peak at 292.5 eV is assigned to C 1s with polar bonds belonging to the [NTf2] anion of the IL-organogel, which, is only observed in the last step of the functionalization.[199]

In Figure 47b the N 1s belonging to the amine group of the silane is located at 399.5 eV [200] and it can be seen in the first, second and third step of the formation of the supports. The red line overlaps the signal assigned to the silane ant the N 1s assigned to the N of the IL-gel anion. The N 1s of the support coated with the IL-organogel (Figure 46c) exhibits two different signals, 401.9 eV is assigned to the two nitrogen atoms in the imidazolium ring. The second peak at 399.3 eV is attributed to the N atom of the IL [NTf2] anion that compose the IL-organogel. [197]

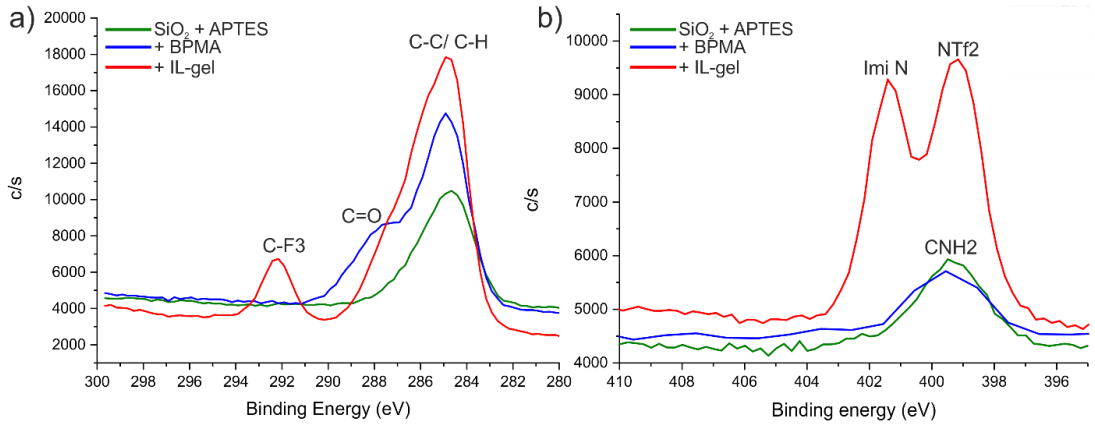

Figure 47. XPS spectra of the support surface during the different steps of its formation. a) C 1s region and b) N 1s region. The green line corresponds to the porous SiO_2 functionalized with APTES, the blue line corresponds the second step: the support coated with acrylate polymer containing crosslinking units (BPMA), and the red line corresponds to the support coated with the IL-gel.

During the second step of the coating, we used FTIR spectroscopy to confirm the covalent attachment of the BPMA-layer to the surface via the functionalization of the polymeric chain with the amines on the

surface. Figure 48 shows the FTIR spectra of the porous SiO_2 powder functionalized with APTES (black curve) and the appearance of a signal at 1650 cm^{-1} (red curve) assigned to the amide bond formed in the functionalization of the active ester polymer with the amines in the surface of the silanized SiO_2.[84] The a smaller signal at 1750 cm^{-1} corresponds to the carbonyl group of the benzophenone units present in the polymer (5 mol%).

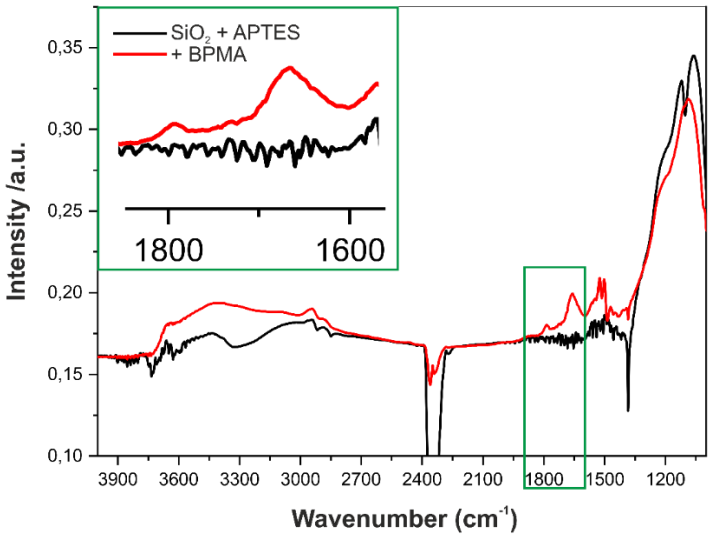

Figure 48. FTIR spectra of SiO_2 functionalized with APTES (black line) and coated with the BPMA (red line). The appearance of the peak at 1650 cm^{-1}indicates the formation of amide bonds between the amine of APTES and the active ester units in the BPMA polymer.

Next, we used TGA to determine the amount of material deposited in the porous SiO_2 powder in each step of the coating, including the infiltration of free IL after the coating was completed. Figure 49 shows the normalized TGA curves at 1°C/min of the support in each step of the coating. The black curve belongs to calcined SiO_2 that loses 1.2% of its weight. This loss is attributed to molecular water in the calcined SiO_2. The blue curve is the SiO_2 after functionalization with APTES. A loss of 8.2% of the total weight is perceived, considering the loss due to molecular water, we can infer there is 7% of the total weight of silane attached to the surface. The red curve is the support after the functionalization with the BPMA-layer. The total loss is around 16%, so the amount of the BPMA-layer is around 8% of the total weight. The yellow curve corresponds to the support after the addition of the IL-organogel and the crosslinking process, the TGA curve from a sample of a typical coating using an IL-polymer containing 5 mol% of benzophenone units

shows around 5% of IL-organogel attached to the support. The green curve is the TGA of a support infiltrated with 5 wt% of free IL.

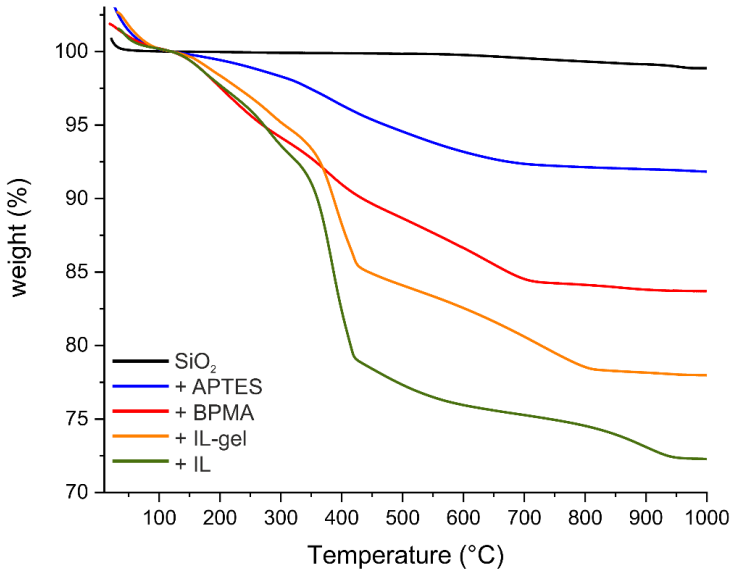

Figure 49. Thermogravimetric analysis of the support in each step of the coating process.

The active ester polymers used for the addition of the BPM-layer in the support and the formation of the IL-gel were synthesized with different amounts of benzophenone units in the polymeric chain to vary the crosslinking density of the polymeric network and observe a potential influence in leaching tests (see experimental, chapter 4). We used 1 mol%, 3 mol% and 5 mol% of benzophenone methacrylate during the polymerization. Using TGA in each step of the process as described before and for the different amount of benzophenone units, we observed that the amount of IL-gel covalently attached to the support depends on the crosslinker content. As shown in Figure 50b, the more crosslinking units there are, the higher the amount of IL-gel covalently attached to the surface.

To verify that the IL-gel is covalently attached to the support we washed all the samples thoroughly with tetrahydrofuran, which was the solvent used in the polymer-analogous reaction to obtain the polymeric IL. In this way, unbound polymers are removed, and remaining polymer coating can be assumed to be covalently bond to the support via crosslinking. Figure 50a shows the TGA analysis of such a washing procedure, using a support fabricated with polymers containing 5 mol% benzophenone. Each curve is the

TGA curve of the support after 1 cycle of washing, there were 4 cycles needed until no further weight loss was detected.

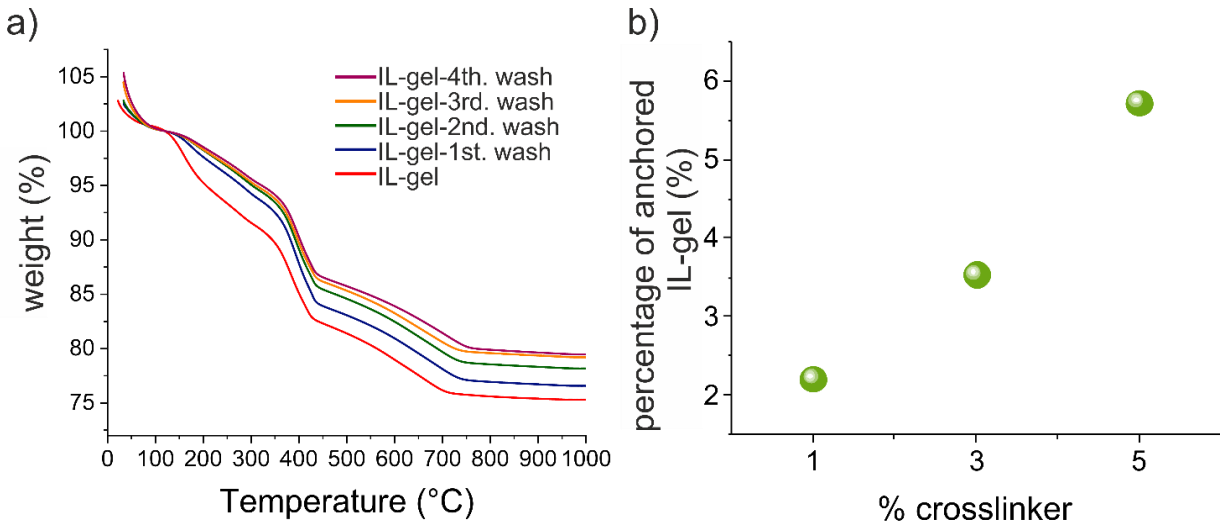

Figure 50. a) TGA curves of the IL-gel support in 4 cycles of washing with tetrahydrofuran b) Percentage of IL-gel in the support as a function of the amount in mol% of the crosslinker (benzophenone).

Additionally, we compared SEM micrographs of the bare porous SiO_2 (Figure 51a) and the SiO_2 coated with the IL-gel (Figure 51b). The porous SiO_2 has characteristic sharp edges and a rough, uneven surface. In contrast, the coated SiO_2 shows a smooth and blunt edges, with a visible increment in electrical conductivity, confirming the polymeric coating. The polymeric film might have a lower porosity than the SiO_2. The access to the crosslinked network is through swelling the film with IL, which stretches the network.

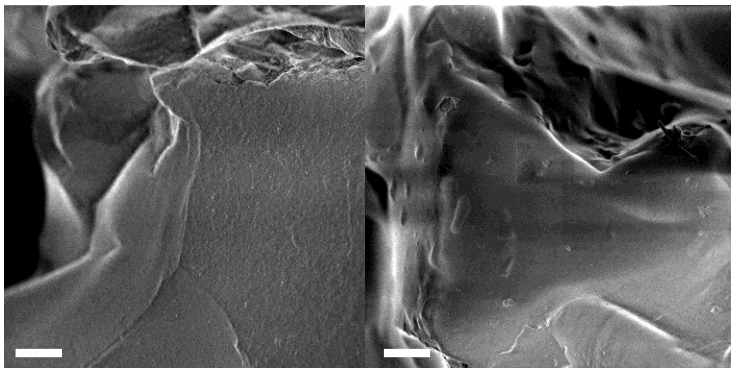

Figure 51. SEM micrographs of porous SiO_2 a) before and b) after coating with the IL-gel. Scale bars= 10 µm

Once the IL-gel support was fully characterized, we investigated the affinity of two ILs with the IL-gel support. By analysing the swelling properties of the IL-gel as a function of the chemical structure of the ILs we confirm which IL is suitable to be confined in the IL-gel. The experiment consisted in the infiltration of the support with the hydrophobic IL, 1-ethyl-3-methylimidazolium bis(trifluoromethylsulfonyl)imide [EMIM][NTf2], which has the same chemical structure as the IL-gel, and in a different experiment, we infiltrated it with the hydrophilic 1-ethyl-3-methyl-imidazolium-ethylsulphate [EMIM][EtOSO3].

For the infiltrations, the different ILs were dissolved in acetone and mixed with a coated support. The mixture was stirred in a rotary evaporator for 1 hour followed by the evaporation of acetone, leaving only IL to infiltrate into the structure. Figure 52a shows the picture of the IL-gel coated support before its infiltration, which behaves as a free-flowing, dry powder. Figure 52b is the picture of the support after infiltration with the hydrophobic [EMIM][NTf2], it is perceived as a dry powder as well, indicating the successful infiltration of the IL inside the polymeric network. Figure 52c shows the IL-gel after the infiltration with [EMIM][EtOSO3], we observe the IL-gel support remains stuck on the walls of the reaction flask, indicating that the powder remained moist, as [EMIM][EtOSO3] was not absorbed inside the polymeric network. With this simple experiment we corroborated the role of matching both cation and anion of the IL with the IL-gel chemical structure. Even though both used ILs have imidazole-base cation as well as the IL-gel, for the [EMIM][EtOSO3] the hydrophilic ethylsulphate anion prevents the IL to interact with the polymeric network.

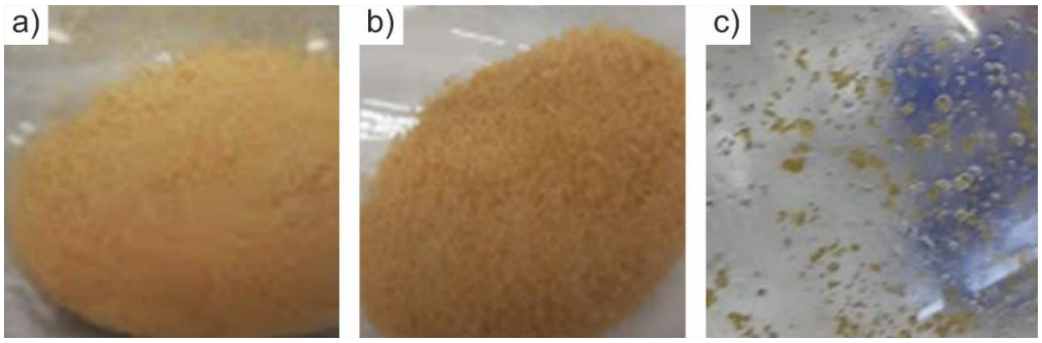

Figure 52. Infiltration of the IL-gel support with two different ionic liquids. a) IL-gel support before infiltration, b) infiltrated with [EMIM][NTf2] and c) IL-gel support infiltrated with [EMIM][EtOSO3]

We infiltrate the IL-gel with different loads of [EMIM][NTf2] to determine the volume of IL that the IL-gel support is able to take up without compromising its dry powder state. We loaded the powder with 100

wt% IL (0.1 g powder containing 0.03 g IL-gel, we add 0.03 g of IL dissolved in 50 mL of acetone) and 200 wt% IL (0.1 g powder containing 0.03 g IL-gel, we add 0.06 g of IL dissolved in 50 mL of acetone) IL. We observed the different samples under the optical microscope after infiltration and once the IL-gel were dried. Figure 53a shows the IL-gel before infiltration. The powder is scattered and present as individual, non-aggregated particles. A similar behaviour is found for the powder after the infiltration with 100 wt% IL (Figure 53b). In contrast, the IL-gel loaded with 200 wt% is agglomerated and a standalone particle cannot be seen, indicating that an excess of IL remained outside of the particles, causing agglomeration via liquid bridges (Figure 53c).

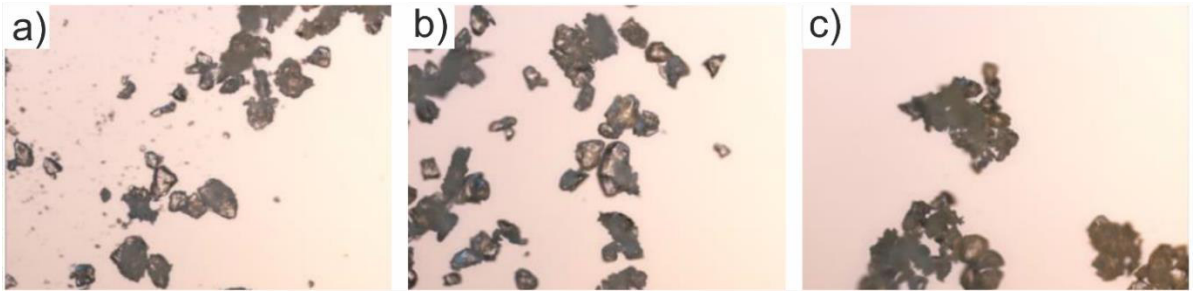

Figure 53. Optical microscope images (x100) of a) IL-gel support before infiltration, b) IL-gel infiltrated with 100 wt% [EMIM][NTf2], and c) IL-gel infiltrated with 200 wt% [EMIM][NTf2].

Conventional SILP supports suffer from depletion of the IL in liquid-phase reactions. [130] As we estimate a stronger confinement of the IL in the IL-gel support we tested the leaching of the IL in presence of different solvents to analyse the potential use of IL-gel in liquid-phase reactions. For these experiments, we mixed 0.1 g of the IL-loaded support particles (100 wt% of [EMIM][NTf2]) with 3 mL of different solvents. We used cyclohexane, n-heptane, 1-butanol, ethanol and acetone as examples of solvents with different polarity. The vials were shaken for 48 hours at room temperature. Afterwards the IL-gel was filtrated, and the solvent was concentrated and analysed using quantitative nuclear magnetic resonance of ^{19}F to calculate the amount of [EMIM][NTf2] leached into the solvent. We used trifluorotoluene as a compound of refence and compared the integral of the signals of a known amount of trifluorotoluene, that presents a peak at -63 ppm and the peak of [EMIM][NTf2] at -80 ppm. Figure 54a shows a typical ^{19}F NMR, where the standard and leached [EMIM][NTf2] are detected. Figure 54b shows the calculated leached IL for the IL-gel and standard SiO_2 in different solvents. For cyclohexane and n-heptane, no leaching of IL was detected in the IL-gel support and nor in the reference SiO_2 powder. In polar solvents, the leaching

decreased substantially using the IL-gels. In presence of ethanol the standard support leached 10 times more IL than in the IL-gel support.

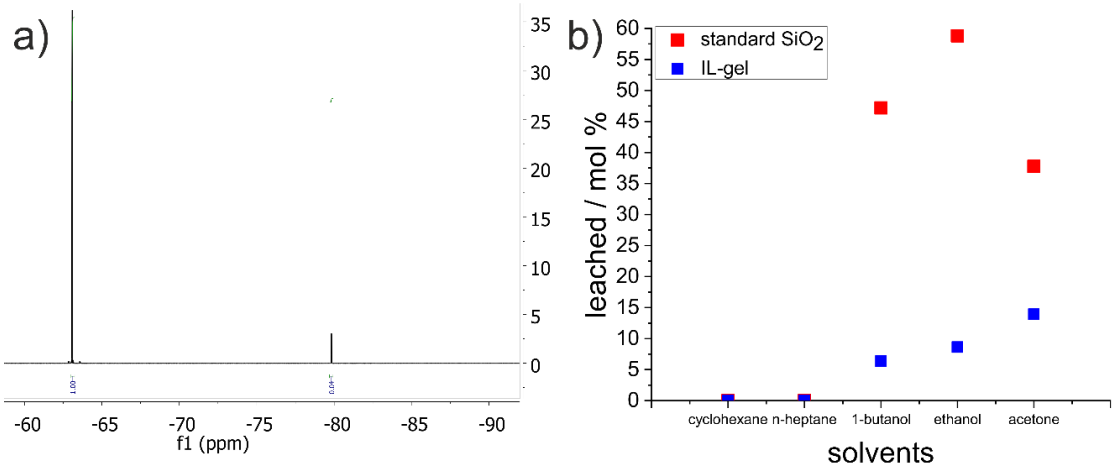

Figure 54.Leaching test of the IL in the IL-gel support using solvents with different polarity. a) a typical quantitative 19F NMR spectrum for the calculation of ionic liquid leached in a solvent using trifluoro toluene as standard compound (standard SiO_2 in acetone), b) IL leached from IL-gel supports and standard SiO_2 in presence of solvents of different polarity after shaking them for 48 h at room temperature.

In chapter 2.4 we have described the SILP catalysis and pointed out that the task of the IL is to dissolve catalytic compounds, the catalyst and ligand. For a SILP support to be effective it needs to retain not just the IL but also the catalyst and ligand. Building on the promising results of the decreased leaching of ILs infused in the polymer-coated particles, we next included a homogeneous catalyst into the IL, to mimic the composition of a realistic SILP system. We used dicarbonyl (2,4-pentanedionato) rhodium(I) (Rh(acac)(CO)2), bis(pentafluorophenyl)-phenylphosphine (bpfpp) as ligand, and the IL [EMIM][NTf2]. In addition, we changed the reaction conditions to elevated temperatures, which are likely to occur in a SILP catalysis[201] and used a Soxhlet extraction column to test IL extraction.. The samples were prepared with ratios typically used in SILP catalysis[202]: 1 wt% IL in the support with 2:1 IL-catalyst ratio and 2:1 mol ratio ligand-catalyst. The Soxhlet column was fill with 0.5 g of loaded IL-gel support and 100 mL of n-heptane were refluxed for 72 hours in a 120°C oil bath. The polymeric supports were analysed before and after the leaching test using inductively coupled plasma - optical emission spectrometry (ICP-OES) to detect Rh and P. Rh as indicator of the catalyst and P as indicator for the ligand (Figure 55).

Figure 55a shows the percentage of Rh leached for each sample. We observed that the amount of Rh leached in the IL-gel supports is significantly reduced compared with the reference SiO_2 powder without

the polymeric coating. We also observed a difference between IL-gel coatings with different crosslinking densities. The sample with 1% BPMA showed the lowest leaching of catalyst and retained 3 times more Rh than the standard support. In contrast, the leaching of P in the different IL-gels is similar to the standard support. We attribute the leaching of ligand to a non-successful formation of the complex during the infiltration of the three components since the Rh is retained but not the P.

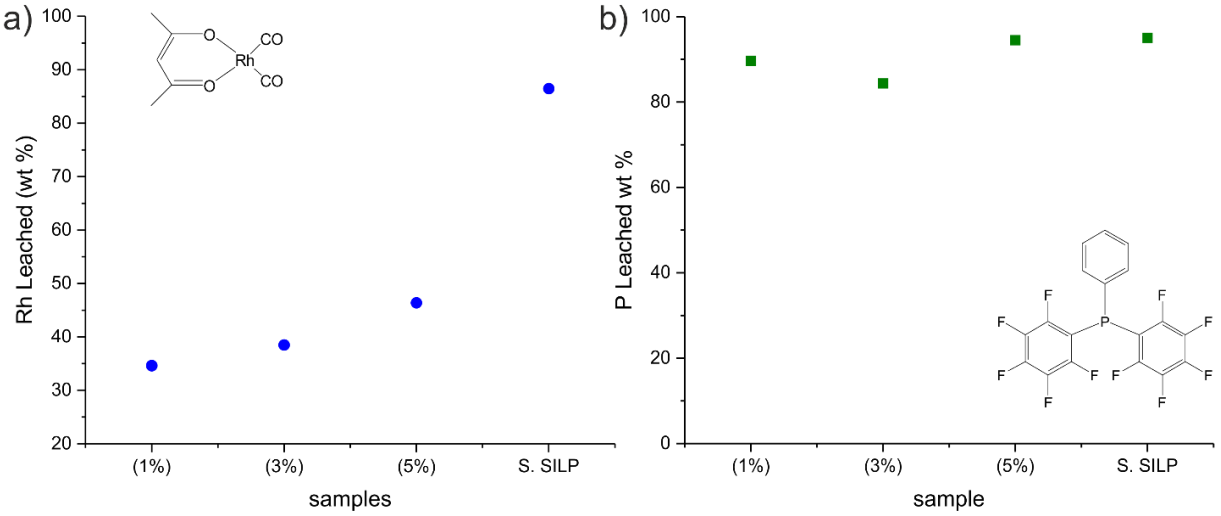

Figure 55. Leaching test results using ICP-OES. a) Amount of Rh leached in the samples and chemical structure of the catalyst Rh(acac)(CO)2, and b) amount of P leached in the different IL-gel supports and the standard SiO_2 and chemical structure of the ligand bpfpp.

Considering the promising results obtained in the leaching test with different solvents and the leaching test of Rh, we believe that using different ligands would make a fully successful catalytic system with enhanced retention of the IL and catalytic species.

5.4.3 Conclusions

In this chapter we made use of polymerized ILs to fabricate a customized polymeric support for the SILP catalysis. We transferred the concept of organogels to enhance the retention of ILs in the design of repellent surface coatings to the SILP catalytic process.

We coated a porous SiO_2 that is typically used as support in conventional SILP catalyst with a polymeric IL-gel. In the first step we silanized the SiO_2 with APTES, in the second step we anchored benzophenone units to the SiO_2 by means of active ester chemistry, we then coated the SiO_2 with a copolymer containing both benzophenone units and the IL as a functional group. Once the support was coated, we crosslinked it via UV radiation to covalently attached the polymerized IL.

The characterization of the IL-gel support in each step of the process was carried out with different techniques including XPS, FTIR, SEM and TGA.

The IL-gel-functionalized supports were successfully infiltrated with [EMIM][NTf2] as a model IL. In a leaching test the IL-gel supports showed superior retention of the IL compared to the non-functionalized silica powder used as reference. Then, in a further leaching experiment with catalyst and ligand, we observed a substantial improvement in the retention of the Rh-catalyst, whereas for the chosen P-ligand the leaching was the same as in the standard SILP support.

As further work in this direction, we would suggest using a bidentate ligand to increase the probability of the formation of coordination complex.

6. Summary and Outlook

In this PhD thesis, we investigated the conditions for the successful confinement of ILs to solid surfaces. We transferred the technology developed in lubricant-infused repellent surfaces to solve the case of partial immobilization of ILs in solid supports.

We confirmed the feasibility to attach ILs to solid surfaces while keeping their liquid-like mobility in the confines of a solid surface. This attachment is possible by increasing the capillary effects on the surface and minimizing the interfacial energy between the IL and the solid surface.

To minimize the interfacial energy, we added functional groups to solid surfaces resembling the diverse functional groups present in imidazole-based ILs. We analysed the wetting behaviour of these ILs as a function of the surface chemistry applied. For the analysis of the surface chemistry, we used water as a standard compound and observed a maximal wetting contrast between the ILs and water when the surface was functionalized with a mixture of self-assembled monolayers i.e. when the solid surface holds more than one functional group present in the IL chemical structure.

We made use of the optical properties of inverse opals to collect more evidence on the wetting behaviour of the ILs as a function of the surface chemistry. By observing a change in the structural colour of the inverse opal, we tracked which surface chemistry configuration allows the ILs to infiltrate successfully the pores of the inverse opal. And more importantly, we observed the surface chemistry that holds up stable retention of the ILs in presence of a contaminating liquid, using water as an example.

We selected an imidazole-containing silane and two silanes with different lengths of hydrocarbon chains to imitate the chemical structure of the ILs, which were also selected with a hydrocarbon-substituted imidazole ring as cation. The structural colour of the inverse opal indicated a stable retention only when the inverse opal was treated with the combination of silanes, making a monolayer of imidazole and hydrocarbon chains the optimal surface chemistry.

With these experiments, we found out that to minimize the interfacial energy of the ILs and a solid surface and confine the ILs in the surface it is necessary to tailor the surface chemistry of the solid support based on the chemical structure of the IL.

We used the Layer-by-Layer technique to add topography and increase the capillary effects for the retention of ILs in solid surfaces. We tackled the limitations of the complex geometry of porous materials during the process of coating LbL. We modified the coating process addressing the diffusive transport limitations by adding convective flows in the addition of nanoparticles in micro-scale porous materials. In materials with nanoscale pores, we additionally screened electrostatic repulsion effects of the coating dispersion by the addition of salt.

Overcoming the limitations of using the LbL technique in coating porous materials resulted in the formation of materials with hierarchical topography for superior retention of IL. As proof of principle, we coated porous SiC monoliths with Al_2O_3 nanoparticles, as a combination of setups used in the catalytic water-gas shift reaction. We tested the retention of an IL, [BMIM][Cl], in coated SiC monoliths and compare it with a non-coated. The leaching of [BMIM][Cl] in coated monolith decreased by a factor of 6.

Then, in the light of the role of tailoring the surface chemistry to maximize the affinity of the IL to the surface, we developed organogels, which entirely match the functional groups to the IL. Using polymeric networks to retain ILs entails higher retention as a result of the larger IL-polymer pairs compared with a monolayer of surface functionality.

We used active ester chemistry for the development of highly functionalized polymer networks. The versatility of active esters allowed us to tailor in detail the chemical structure of the polymer chains so it exactly resembles the chemical structure of the IL we want to confine. We synthesized amine-containing ILs to be introduced in the polymer backbone. Additionally, we co-polymerized benzophenone units to form the crosslinked networks.

As proof of principle, we formed IL organogels with two different IL species. We anchored 1-amonipropyl-3-methyl imidazolium bis(trifluoromethylsulfonyl)imide [APMIM][NTf2] to a polymer chain. And, in another experiment, we anchored aminopropyl tributylphosphonium

bis(trifluoromethylsulfonyl)imide [APTBP][NTf2]. And confirmed the successful functionalization by different spectroscopic techniques.

We used the hydrophobic [APTBP][NTf2]-based organogel to form robust repellent films, by anchoring it covalently to a substrate using a benzophenone functionality and irradiating with UV the film. The anchored organogel was infiltrated with [MTBP][NTf2]. The result was a slippery IL-infused surface with remarkable repellent properties, outperforming existing systems in long-term stability, keeping the contact a low angle hysteresis even after 150 days at 85°C.

Lastly, we extend the applicability of the formed organogels films to coat supports to be used in the SILP catalysis. We used [APMIM][NTf2]-based organogels to coat porous SiO_2 using silanes, active esters and photoactive benzophenone units. Once the coating was completely characterized, we infiltrated the supports with [EMIM][NTf2] and carried out a leaching test, where we observed superior retention. In a further leaching experiment, we infiltrated the organogel-coated supports with IL, a catalyst and ligand and compered it with non-coated SiO_2. The coated support retained 3 times more the catalytic compound but there was no apparent difference in the leaching of the ligand. We attribute the leaching of the ligand to an unsatisfactory formation of the catalytic complex during the infiltration of these three components.

The analysis of the wettability of ILs in solid supports as a function of the surface chemistry of a solid is just the start of a deeper understanding of the behaviour of ILs at the interface. Such understanding has the potential to lead to a detailed control of the interactions of the ILs and the limitless applications that can be developed as consequence. For instance, in catalysis, the precise control of the catalyst position would be extremely beneficial for allowing the direct investigation of the catalytic activity, and such control is possible with the design of the topography and chemical environment of the support.

What is more, enabling the attachment of ILs in solid surfaces while keeping their liquid-like mobility wides the spectrum of applications that can benefit from the properties of ILs.

7. List of Abbreviations

arom	aromatics
AIBN	azobisisobutyronnitrile
APTES	(3-aminopropyl)triethoxysilane
Al_2O_3	aluminium oxide
bpfpp	bis(pentafluorophenyl)-phenylphosphine
BPMA	benzophenylmethacrylate
br	broad signal
But	butyl(chloro)dimethylsilane
CDCl3	deuterated chloroform
CSB	4-(3'Chlorodimethylsilyl)propoxybenzophenone
Cr_2O_3	chromium(III) oxide
DCM	dichloromethane
dd	doublet of doublets
DMSO-d6	deuterated dimethyl sulfoxide
Dod	trichloro-dodecylsilane
FTIR	Fourier-transform infrared spectroscopy
GPC	Gel permeation chromatography
g	gravity
H	liquid depth
HCl	hydrochloric acid
ICP-OES	Inductively couple plasma Optical emission spectrometry
IL(s)	Ionic liquid(s)
Imi	N-(3-triethoxysilylpropyl)-4,5-dihydroimidazole
KOH	potassium hydroxide
LbL	Layer-by-Layer

Li[NTf2]	lithium bis(trifluoromethanesulfonyl)imide
$MgSO_4$	magnesium sulfate
NaCl	sodium chloride
NMR	Nuclear magnetic resonance
OH	hydroxy group
OCH3	methoxy group
OCH_2CH_3	ethoxy group
PDADMAC	poly(diallyldimethylammonium) chloride
PDMS	polydimethylsiloxane
PFPA	pentaflurophenylaacrylate
poly([APMIM][NTf2]A-co-BPMA)	poly(aminopropylmethylimidazolium-bis(trifluoromethylsulfonyl) imide-co-benzophenone methacrylate)
poly([APTBP][NTf2]A-co-BPMA)	poly(aminoaminopropyl tributylposphosponium - bis(trifluoromethylsulfonyl) imide-co-benzophenone methacrylate)
poly(PFPA-co-BPMA)	poly (pentafluoro phenyl acrylate-co-benzophenone methacrylate)
PSS	poly(sodium 4-styrenesulfonate)
R_1 , R_2	radii of an arbitrary curvature
R	roughness factor
r	radius of a capillary tube
Rh(acac)(CO)2	dicarbonyl (2,4-pentanedionato) rhodium(I)
s	singlet
SAMs	self-assembled monolayers
SEM	scanning electron microscopy
SiC	silicon carbide
SiOH	silanol groups
SILP	supported ionic liquid phase
SnO_2	tin(IV) oxide

SLIPs	slippery liquid infused porous surfaces
SiO_2	silicon dioxide
t	triplet
TEOS	tetraethyl ortosilicate
TGA	Thermogravimetric analysis
THF	tetrahydrofuran
TiO_2	titanium dioxide
UV	ultraviolet
WGS	water-gas shift
XPS	X-ray photoelectron spectroscopy
γ_{gl}, γ	surface tension
γ_{sg}	surface free energy
γ_{sl}	interfacial tension
δ/ppm	chemical shift/parts per million
ΔP	Laplace pressure
θ	contact angle
θ_{rough}	contact angle on a textured surface
θ_{flat}	apparent contact angle
ρ	density
[APMIM][Cl]	aminopropylmethylimidazolium chloride
[APMIM][NTf2]	aminopropylmethylimidazolium bis(trifluoromethylsulfonyl)imide
[APTBP][NTf2]	aminopropyl tributylposphosponium bis(trifluoromethylsulfonyl)imide
[BMMIM][Cl]	1-butyl-2,3-dimethylimidazolium chloride
[BMIM][PF_6]	1-butyl-3-methylimidazolium hexafluorophosphate
[EMIM][EtOSO3]	1-ethyl-3-methyl-imidazolium-ethylsulphate
[EMIM][NTf2]	1-ethyl-3-methylimidazolium bis(trifluoromethylsulfonyl)imide
[MEIM][NTf2]	1-methyl-3-ethylimidazolium bis(trifluoromethylsulfonyl)imide

[MPIM][NTf2]	1-methyl-3-propylimidazolium bis(trifluoromethylsulfonyl)imide
[MTBP][Ntf2]	methyltributylphosphonium bis(trifluoromethylsulfonyl)imide

8. Acknowledgments

I want to express my sincere gratitude to Nicolas Vogel, for his generosity with the time he dedicates to his students, for his willingness to listen to us and above all for his kind way of containing and correcting us. Thank you for making me part of your group and giving me the opportunity to grow in many directions. Thank you for offering us a safe and trusting space. You are an example to follow.

I want to thank Ramón Zárraga for his support and trust in me. For offering me his guidance and for his availability. Thank you for making my doctorate possible. And thank you for listening to me whenever I needed it throughout these years. You are another example to follow.

I am grateful to Jorge Cervantes for his guidance during my doctorate, for the support he offered me during these years, for his reviews that I always appreciate very much. I feel very privileged to belong to his academic group. Jorge Cervantes is an inspiration and a great example to follow.

I have not run out of words, believe me when I say that my three mentors are great role models and I treasure very much their mentorship.

I am very grateful to all the people who made the development of the PhD project possible, most closely to Johannes Bauernfeind and Tobias Salbaum and to the CRT team Marco Haumann and Markus Schörner.

I thank Rosario Galindo for her support and reviewing my work and the always fruitful scientific discussions. I also thank Marco García-Revilla for his support to me from the coordination of the graduate program back at the time and for helping me in the process of the cotutelle agreement. Thanks to dr. Elena Zeißler and Aideé Flores for making the cotutelle agreement possible. I thank Eulalia Ramírez and Antonio Villegas for organizing and for valuable contributions through the group seminars. Special thanks to the silicon team Antonio Guerra, Gilberto and Miguel.

Thanks to all the members of the Vogel group for all the group meetings, coffees, beers, barbecues and celebrations. Specially to Umair, Salva, Herbert, Maria Nefeli, Johannes Harrer and Giulia. Cheers for all the shared moments. I treasure the interactions I have had with each of you.

I have no words to express the gratitude and love I feel for the people who have walked with me very close. Frédéric, infinite thanks for your company and support, your friendship is invaluable to me. Octavio,

thank you for all the conversations and company at the distance, for inspiring me so much. Mariana and Abraham, how enjoyable life looks with you.

I feel extremely lucky to have found treasures other than science in Germany. People who have been fundamental for me these years, Junwei, Eric, Reza and Teresa, I owe you a debt of friendship that I will gladly repay forever. Thank you from the bottom of my heart!

Magali, Jesús, Fabiola, Ale Borja, Liliana, Ibrahim thank you very much for being with me for so long and so close, I love you very much.

To my mom and dad, there is no way to express the gratitude and love towards you, but fortunately it is not necessary to express it either because it is there, latent, it cannot be hidden. Infinite thanks.

I also thank my sisters and brothers, who are always there.

I am grateful to the University of Guanajuato, my cradle and home, and to the Friedrich-Alexander University, my second home. To the Mexican Council of Science and Technology for the multiple supports granted, as well as the support received from the Friedrich-Alexander-University and the state of Bavaria.

9. References

(1) de Gennes, P.-G.; Brochard-Wyart, F.; Quéré, D. *Capillarity and Wetting Phenomena*; Springer New York: New York, NY, 2004. https://doi.org/10.1007/978-0-387-21656-0.

(2) Butt, H.; Graf, K.; Kappl, M. *Physics and Chemistry of Interfaces*; Wiley-VCH Verlag GmbH & Co. KGaA, 2003.

(3) Werner, S.; Haumann, M.; Wasserscheid, P. Ionic Liquids in Chemical Engineering. *Annu. Rev. Chem. Biomol. Eng.* **2010**, *1* (1), 203–230. https://doi.org/10.1146/annurev-chembioeng-073009-100915.

(4) Wasserscheid, P.; Keim, W. Ionic Liquids - New Solutions for Transition Metal Catalysis. *Angew. Chemie* **2000**, *39*, 3772–3789.

(5) Wasserscheid, P.; Welton, T. *Ionic Liquids in Synthesis*, First Edit.; Wiley-VCH Verlag GmbH & Co. KGaA, 2002; Vol. 7.

(6) Armand, M.; Endres, F.; MacFarlane, D. R.; Ohno, H.; Scrosati, B. Ionic-Liquid Materials for the Electrochemical Challenges of the Future. *Nat. Mater.* **2009**, *8* (8), 621–629. https://doi.org/10.1038/nmat2448.

(7) Dupont, J. From Molten Salts to Ionic Liquids: A “Nano” Journey. *Acc. Chem. Res.* **2011**, *44* (11), 1223–1231. https://doi.org/10.1021/ar2000937.

(8) Wilkes, J. S.; Wasserscheid, P.; Welton, T. Ionic Liquids in Synthesis. In *Ionic Liquids in Synthesis*; Wiley-VCH Verlag GmbH & Co. KGaA: Weinheim, Germany, 2008; pp 1–6. https://doi.org/10.1002/9783527621194.ch1.

(9) Zhou, F.; Liang, Y.; Liu, W. Ionic Liquid Lubricants: Designed Chemistry for Engineering Applications. *Chem. Soc. Rev.* **2009**, *38* (9), 2590. https://doi.org/10.1039/b817899m.

(10) Lee, S. G. Functionalized Imidazolium Salts for Task-Specific Ionic Liquids and Their Applications. *Chem. Commun.* **2006**, No. 10, 1049–1063. https://doi.org/10.1039/b514140k.

(11) Ohno, H. Functional Design of Ionic Liquids. *Bull. Chem. Soc. Jpn.* **2006**, *79* (11), 1665–1680. https://doi.org/10.1246/bcsj.79.1665.

(12) Rooney, D.; Jacquemin, J.; Gardas, R. Thermophysical Properties of Ionic Liquids; 2009; pp 185–212. https://doi.org/10.1007/128_2008_32.

(13) Vioux, A.; Viau, L.; Volland, S.; Le, J. Use of Ionic Liquids in Sol-Gel ; Ionogels and Applications. **2010**, *13*, 242–255. https://doi.org/10.1016/j.crci.2009.07.002.

(14) Cvjetko Bubalo, M.; Radošević, K.; Radojčić Redovniković, I.; Halambek, J.; Gaurina Srček, V. A Brief Overview of the Potential Environmental Hazards of Ionic Liquids. *Ecotoxicol. Environ. Saf.* **2014**, *99*, 1–12. https://doi.org/10.1016/j.ecoenv.2013.10.019.

(15) Werner, S.; Haumann, M.; Wasserscheid, P. Ionic Liquids in Chemical Engineering. *Annu. Rev. Chem. Biomol. Eng.* **2010**, *1* (1), 203–230. https://doi.org/10.1146/annurev-chembioeng-073009-100915.

(16) Steinrück, H.-P.; Wasserscheid, P. Ionic Liquids in Catalysis. **2015**, 380–397. https://doi.org/10.1007/s10562-014-1435-x.

(17) Wasserscheid, P.; Keim, W. Ionic LiquidsÐNew ªSolutionsº for Transition Metal Catalysis.

(18) Yadav, J. S.; Reddy, B. V. S.; Reddy, M. S.; Niranjan, N.; Prasad, A. R. Lewis Acidic Chloroaluminate Ionic Liquids: Novel Reaction Media for the Synthesis of 4-Chloropyrans. *European J. Org. Chem.* **2003**, No. 9, 1779–1783. https://doi.org/10.1002/ejoc.200210638.

(19) Wong, T.-S.; Kang, S. H.; Tang, S. K. Y.; Smythe, E. J.; Hatton, B. D.; Grinthal, A.; Aizenberg, J. Bioinspired Self-Repairing Slippery Surfaces with Pressure-Stable Omniphobicity. *Nature* **2011**, *477* (7365), 443–447. https://doi.org/10.1038/nature10447.

(20) Maccallum, N.; Howell, C.; Kim, P.; Sun, D.; Friedlander, R.; Ranisau, J.; Ahanotu, O.; Lin, J. J.; Vena, A.; Hatton, B.; Wong, T. S.; Aizenberg, J. Liquid-Infused Silicone As a Biofouling-Free Medical Material. *ACS Biomater. Sci. Eng.* **2015**, *1* (1), 43–51. https://doi.org/10.1021/ab5000578.

(21) Wong, T. S.; Kang, S. H.; Tang, S. K. Y.; Smythe, E. J.; Hatton, B. D.; Grinthal, A.; Aizenberg, J. Bioinspired Self-Repairing Slippery Surfaces with Pressure-Stable Omniphobicity. *Nature* **2011**, *477* (7365), 443–447. https://doi.org/10.1038/nature10447.

(22) Preston, D. J.; Song, Y.; Lu, Z.; Antao, D. S.; Wang, E. N. Design of Lubricant Infused Surfaces. *ACS Appl. Mater. Interfaces* **2017**, *9* (48), 42383–42392. https://doi.org/10.1021/acsami.7b14311.

(23) Smith, J. D.; Dhiman, R.; Anand, S.; Reza-Garduno, E.; Cohen, R. E.; McKinley, G. H.; Varanasi, K. K. Droplet Mobility on Lubricant-Impregnated Surfaces. *Soft Matter* **2013**, *9* (6), 1772–1780. https://doi.org/10.1039/c2sm27032c.

(24) Keiser, A.; Baumli, P.; Vollmer, D.; Quéré, D. Universality of Friction Laws on Liquid-Infused Materials. *Phys. Rev. Fluids* **2020**, *5* (1), 1–12. https://doi.org/10.1103/physrevfluids.5.014005.

(25) Li, J.; Ueda, E.; Paulssen, D.; Levkin, P. A. Slippery Lubricant-Infused Surfaces: Properties and Emerging Applications. *Adv. Funct. Mater.* **2019**, *29* (4), 1802317. https://doi.org/10.1002/adfm.201802317.

(26) Wong, T.-S.; Kang, S. H.; Tang, S. K. Y.; Smythe, E. J.; Hatton, B. D.; Grinthal, A.; Aizenberg, J. Bioinspired Self-Repairing Slippery Surfaces with Pressure-Stable Omniphobicity. *Nature* **2011**, *477* (7365), 443–447. https://doi.org/10.1038/nature10447.

(27) Lafuma, A.; Quéré, D. Slippery Pre-Suffused Surfaces. *Epl* **2011**, *96* (5), 1–5. https://doi.org/10.1209/0295-5075/96/56001.

(28) Young, T. An Essay on the Cohesion of Fluids. *Philos. Trans. R. Soc. London* **1805**, *95* (0), 65–87. https://doi.org/10.1098/rstl.1805.0005.

(29) Vericat, C.; Vela, M. E.; Benitez, G.; Carro, P.; Salvarezza, R. C. Self-Assembled Monolayers of Thiols and Dithiols on Gold: New Challenges for a Well-Known System. *Chem. Soc. Rev.* **2010**, *39* (5), 1805–1834. https://doi.org/10.1039/b907301a.

(30) Silberzan, P.; Leger, L.; Ausserre, D.; Benattar, J. J.; Silberzan, P. Léger, L. Ausserré, D. Benattar, J. J. Silanation of Silica Surfaces. A New Method of Constructing Pure or Mixed Monolayers. *Langmuir* **1991**, *7* (8), 1647–1651. https://doi.org/10.1021/la00056a017.

(31) Baumgärte, T.; von Borczyskowski, C.; Graaf, H. Selective Surface Modification of Lithographic Silicon Oxide Nanostructures by Organofunctional Silanes. *Beilstein J. Nanotechnol.* **2013**, *4* (1), 218–226. https://doi.org/10.3762/bjnano.4.22.

(32) Cras, J. J.; Rowe-Taitt, C. A.; Nivens, D. A.; Ligler, F. S. Comparison of Chemical Cleaning Methods of Glass in Preparation for Silanization. *Biosens. Bioelectron.* **1999**, *14* (8–9), 683–688. https://doi.org/10.1016/S0956-5663(99)00043-3.

(33) Pujari, S. P.; Scheres, L.; Marcelis, A. T. M.; Zuilhof, H. Covalent Surface Modification of Oxide

Surfaces. *Angew. Chemie - Int. Ed.* **2014**, *53* (25), 6322–6356. https://doi.org/10.1002/anie.201306709.

(34) Thissen, P.; Valtiner, M.; Grundmeier, G. Stability of Phosphonic Acid Self-Assembled Monolayers on Amorphous and Single-Crystalline Aluminum Oxide Surfaces in Aqueous Solution. *Langmuir* **2010**, *26* (1), 156–164. https://doi.org/10.1021/la900935s.

(35) Ye, Q.; Zhou, F.; Liu, W. Bioinspired Catecholic Chemistry for Surface Modification. *Chem. Soc. Rev.* **2011**, *40* (7), 4244–4258. https://doi.org/10.1039/c1cs15026j.

(36) Kim, B. H.; Lee, D. H.; Kim, J. Y.; Shin, D. O.; Jeong, H. Y.; Hong, S.; Yun, J. M.; Koo, C. M.; Lee, H.; Kim, S. O. Mussel-Inspired Block Copolymer Lithography for Low Surface Energy Materials of Teflon, Graphene, and Gold. *Adv. Mater.* **2011**, *23* (47), 5618–5622. https://doi.org/10.1002/adma.201103650.

(37) Wang, C. X.; Braendle, A.; Menyo, M. S.; Pester, C. W.; Perl, E. E.; Arias, I.; Hawker, C. J.; Klinger, D. Catechol-Based Layer-by-Layer Assembly of Composite Coatings: A Versatile Platform to Hierarchical Nano-Materials. *Soft Matter* **2015**, *11* (31), 6173–6178. https://doi.org/10.1039/c5sm01374g.

(38) Rosso, M.; Giesbers, M.; Schroen, K.; Zuilhof, H. Controlled Oxidation, Biofunctionalization, and Patterning of Alkyl Monolayers on Silicon and Silicon Nitride Surfaces Using Plasma Treatment. *Langmuir* **2010**, *26* (2), 866–872. https://doi.org/10.1021/la9023103.

(39) Friedlander, R. S.; Vogel, N.; Aizenberg, J. Role of Flagella in Adhesion of Escherichia Coli to Abiotic Surfaces. *Langmuir* **2015**, *31* (22), 6137–6144. https://doi.org/10.1021/acs.langmuir.5b00815.

(40) Israelachvili, J. *Intermolecular and Surface Forces*, Third.; Academic Press, 2010.

(41) Kim, P.; Kreder, M. J.; Alvarenga, J.; Aizenberg, J. Hierarchical or Not? Effect of the Length Scale and Hierarchy of the Surface Roughness on Omniphobicity of Lubricant-Infused Substrates. *Nano Lett.* **2013**, *13* (4), 1793–1799. https://doi.org/10.1021/nl4003969.

(42) Wong, W. S. Y.; Hegner, K. I.; Donadei, V.; Hauer, L.; Naga, A.; Vollmer, D. Capillary Balancing: Designing Frost-Resistant Lubricant-Infused Surfaces. *Nano Lett.* **2020**, *20* (12), 8508–8515. https://doi.org/10.1021/acs.nanolett.0c02956.

(43) Baumli, P.; D'Acunzi, M.; Hegner, K. I.; Naga, A.; Wong, W. S. Y.; Butt, H.-J.; Vollmer, D. The Challenge of Lubricant-Replenishment on Lubricant-Impregnated Surfaces. *Adv. Colloid Interface Sci.* **2020**, 102329. https://doi.org/10.1016/j.cis.2020.102329.

(44) Wenzel, R. N. Resistance of Solid Surfaces to Wetting by Water. *J. Ind. Eng. Chem. (Washington, D. C.)* **1936**, *28*, 988–994. https://doi.org/10.1021/ie50320a024.

(45) Sunny, S.; Vogel, N.; Howell, C.; Vu, T. L.; Aizenberg, J. Lubricant-Infused Nanoparticulate Coatings Assembled by Layer-by-Layer Deposition. *Adv. Funct. Mater.* **2014**, *24* (42), 6658–6667. https://doi.org/10.1002/adfm.201401289 S1 - 10 M4 - Citavi.

(46) Utech, S.; Bley, K.; Aizenberg, J.; Vogel, N. Tailoring Re-Entrant Geometry in Inverse Colloidal Monolayers to Control Surface Wettability. *J. Mater. Chem. A Mater. energy Sustain.* **2015**, *00*, 1–7. https://doi.org/10.1039/C5TA08992A.

(47) Nguyen, V.-H.; Nguyen, B. D.; Pham, H. T.; Lam, S. S.; Vo, D.-V. N.; Shokouhimehr, M.; Vu, T. H. H.; Nguyen, T.-B.; Kim, S. Y.; Le, Q. Van. Anti-Icing Performance on Aluminum Surfaces and Proposed Model for Freezing Time Calculation. *Sci. Rep.* **2021**, *11* (1), 3641. https://doi.org/10.1038/s41598-020-80886-x.

(48) Doll, K.; Fadeeva, E.; Schaeske, J.; Ehmke, T.; Winkel, A.; Heisterkamp, A.; Chichkov, B. N.; Stiesch, M.; Stumpp, N. S. Development of Laser-Structured Liquid-Infused Titanium with Strong Biofilm-Repellent Properties. *ACS Appl. Mater. Interfaces* **2017**, *9* (11), 9359–9368. https://doi.org/10.1021/acsami.6b16159.

(49) Xiao, L.; Li, J.; Mieszkin, S.; Di Fino, A.; Clare, A. S.; Callow, M. E.; Callow, J. A.; Grunze, M.; Rosenhahn, A.; Levkin, P. A. Slippery Liquid-Infused Porous Surfaces Showing Marine Antibiofouling Properties. *ACS Appl. Mater. Interfaces* **2013**, *5* (20), 10074–10080. https://doi.org/10.1021/am402635p.

(50) Hatton, B.; Mishchenko, L.; Davis, S.; Sandhage, K. H.; Aizenberg, J. Assembly of Large-Area, Highly Ordered, Crack-Free Inverse Opal Films. *Proc. Natl. Acad. Sci. U. S. A.* **2010**, *107* (23), 10354–10359. https://doi.org/10.1073/pnas.1000954107.

(51) Stein, A.; Wilson, B. E.; Rudisill, S. G. Design and Functionality of Colloidal–Crystal–Templated Materials—Chemical Applications of Inverse Opals. *Chem. Soc. Rev.* **2013**, *42* (7), 2763–2803. https://doi.org/10.1039/c2cs35317b.

(52) Burgess, I. B.; Koay, N.; Raymond, K. P.; Kolle, M.; Lončar, M.; Aizenberg, J. Wetting in Color: Colorimetric Differentiation of Organic Liquids with High Selectivity. *ACS Nano* **2012**, *6* (2), 1427–1437. https://doi.org/10.1021/nn204220c.

(53) Schroden, R. C.; Al-Daous, M.; Blanford, C. F.; Stein, A. Optical Properties of Inverse Opal Photonic Crystals. *Chem. Mater.* **2002**, *14* (8), 3305–3315. https://doi.org/10.1021/cm020100z.

(54) Decher, G. Fuzzy Nanoassemblies: Toward Layered Polymeric Multicomposites. *Science (80-.).* **1997**, *277* (5330), 1232–1237. https://doi.org/10.1126/science.277.5330.1232.

(55) Decher, G.; Hong, J. D. Buildup of Ultrathin Multilayer Films by a Self-Assembly Process .1. Consecutive Adsorption of Anionic and Cationic Bipolar Amphiphiles on Charged Surfaces. *Makromol. Chemie-Macromolecular Symp.* **1991**, *46*, 321–327. https://doi.org/10.1002/masy.19910460145.

(56) Muller, W.; Ringsdorf, H.; Rump, E.; Wildburg, G.; Zhang, X.; Angermaier, L.; Knoll, W.; Liley, M.; Spinke, J. Attempts to Mimic Docking Processes of the Immune System: Recognition-Induced Formation of Protein Multilayers. *Science (80-.).* **1993**, *262* (5140), 1706–1708. https://doi.org/10.1126/science.8259513.

(57) Mansouri, S.; Merhi, Y.; Winnik, F. M.; Tabrizian, M. Investigation of Layer-by-Layer Assembly of Polyelectrolytes on Fully Functional Human Red Blood Cells in Suspension for Attenuated Immune Response. *Biomacromolecules* **2011**, *12* (3), 585–592. https://doi.org/10.1021/bm101200c.

(58) Hammond, P. T. Building Biomedical Materials Layer-by-Layer. *Mater. Today* **2012**, *15* (5), 196–206. https://doi.org/10.1016/S1369-7021(12)70090-1.

(59) Sunny, S.; Vogel, N.; Howell, C.; Vu, T. L.; Aizenberg, J. Lubricant-Infused Nanoparticulate Coatings Assembled by Layer-by-Layer Deposition. *Adv. Funct. Mater.* **2014**, *24* (42), 6658–6667. https://doi.org/10.1002/adfm.201401289.

(60) Bravo, J.; Zhai, L.; Wu, Z.; Cohen, R. E.; Rubner, M. F. Transparent Superhydrophobic Films Based on Silica Nanoparticles. *Langmuir* **2007**, *23* (13), 7293–7298. https://doi.org/10.1021/la070159q.

(61) Flory, P. J. *Principles of Polymer Chemistry*; Cornell University Press, 1953.

(62) Meléndez-Zamudio, M.; Villegas, A.; González-Calderón, J. A.; Meléndrez, R.; Meléndez-Lira, M.;

Cervantes, J. Study of a Polydimethylsiloxane (PDMS) Elastomer Generated by γ Irradiation: Correlation Between Properties (Thermal and Mechanical) and Structure (Crosslink Density Value). *J. Inorg. Organomet. Polym. Mater.* **2017**, *27* (3), 622–632. https://doi.org/10.1007/s10904-017-0503-2.

(63) Wooh, S.; Butt, H. J. A Photocatalytically Active Lubricant-Impregnated Surface. *Angew. Chemie - Int. Ed.* **2017**, *56* (18), 4965–4969. https://doi.org/10.1002/anie.201611277.

(64) Lee, J. N.; Park, C.; Whitesides, G. M. Solvent Compatibility of Poly(Dimethylsiloxane)-Based Microfluidic Devices. *Anal. Chem.* **2003**, *75* (23), 6544–6554. https://doi.org/10.1021/ac0346712.

(65) Rumens, C. V.; Ziai, M. A.; Belsey, K. E.; Batchelor, J. C.; Holder, S. J. Swelling of PDMS Networks in Solvent Vapours; Applications for Passive RFID Wireless Sensors. *J. Mater. Chem. C* **2015**, *3* (39), 10091–10098. https://doi.org/10.1039/c5tc01927c.

(66) Cui, J.; Daniel, D.; Grinthal, A.; Lin, K.; Aizenberg, J. Dynamic Polymer Systems with Self-Regulated Secretion for the Control of Surface Properties and Material Healing. *Nat. Mater.* **2015**, *14* (8), 790–795. https://doi.org/10.1038/nmat4325.

(67) Urata, C.; Dunderdale, G. J.; England, M. W.; Hozumi, A. Self-Lubricating Organogels (SLUGs) with Exceptional Syneresis-Induced Anti-Sticking Properties against Viscous Emulsions and Ices. *J. Mater. Chem. A* **2015**, *3* (24), 12626–12630. https://doi.org/10.1039/c5ta02690c.

(68) Howell, C.; Vu, T. L.; Lin, J. J.; Kolle, S.; Juthani, N.; Watson, E.; Weaver, J. C.; Alvarenga, J.; Aizenberg, J. Self-Replenishing Vascularized Fouling-Release Surfaces. **2014**.

(69) Das, A.; Theato, P. Activated Ester Containing Polymers : Opportunities and Challenges for the Design of Functional Macromolecules. **2016**. https://doi.org/10.1021/acs.chemrev.5b00291.

(70) Eberhardt, M.; Mruk, R.; Zentel, R.; Théato, P. Synthesis of Pentafluorophenyl(Meth)Acrylate Polymers: New Precursor Polymers for the Synthesis of Multifunctional Materials. *Eur. Polym. J.* **2005**, *41* (7), 1569–1575. https://doi.org/10.1016/j.eurpolymj.2005.01.025.

(71) Günay, K. A.; Theato, P.; Klok, H. A. Standing on the Shoulders of Hermann Staudinger: Post-Polymerization Modification from Past to Present. *J. Polym. Sci. Part A Polym. Chem.* **2013**, *51* (1), 1–28. https://doi.org/10.1002/pola.26333.

(72) Graisuwan, W.; Zhao, H.; Kiatkamjornwong, S.; Theato, P.; Hoven, V. P. Formation of Thermo-

Sensitive and Cross-Linkable Micelles by Self-Assembly of Poly (Pentafluorophenyl Acrylate) - Containing Block Copolymer. **2015**, 1103–1113. https://doi.org/10.1002/pola.27541.

(73) Jochum, F. D.; Theato, P. Temperature- and Light-Responsive Polyacrylamides Prepared by a Double Polymer Analogous Reaction of Activated Ester Polymers. **2009**, 5941–5945. https://doi.org/10.1021/ma900945s.

(74) Kakuchi, R.; Zamfi, M.; Lutz, J.; Theato, P. Controlled Positioning of Activated Ester Moieties on Well-Defi Ned Linear Polymer Chains. **2012**, 54–60.

(75) Nilles, K.; Theato, P. POLYMER Synthesis and Polymerization of Active Ester Monomers Based on 4-Vinylbenzoic Acid. **2007**, *43*, 2901–2912. https://doi.org/10.1016/j.eurpolymj.2007.04.038.

(76) Tahir, M. N.; Eberhardt, M.; Theato, P.; Faiß, S.; Janshoff, A.; Gorelik, T.; Kolb, U.; Tremel, W. Reactive Polymers: A Versatile Toolbox for the Immobilization of Functional Molecules on TiO 2 Nanoparticles**. **2006**, 908–912. https://doi.org/10.1002/anie.200502517.

(77) Cline, G. W.; Hanna, S. B. The Aminolysis of N-Hydroxysuccinimide Esters. A Structure-Reactivity Study. *J. Am. Chem. Soc.* **1987**, No. 8, 3087–3091. https://doi.org/10.1021/ja00244a035.

(78) Batz, H.; H., R. Model Reactions for Synthesis of Pharmacologically Active Polymers. *Angew. Chem. Int. Ed. Engl.* **1972**, No. 70, 1103–1104.

(79) Ferruti, P.; Bettelli, A.; Fere, A. High Polymers of Acrylic and Methacrylic Esters of N-Hydroxysuccinimide as Polyacrylamide and Polymethacrylamide Precursors. **1972**, *13*, 462–464.

(80) Das, A.; Theato, P. Activated Ester Containing Polymers. *Chem. Rev.* **2016**, *116* (3), 1434–1495. https://doi.org/10.1021/acs.chemrev.5b00291 T4 - Opportunities and Challenges for the Design of Functional Macromolecules PM - 26305991 S1 - 62 M4 - Citavi.

(81) Theato, P.; Kim, J.; Lee, J. Controlled Radical Polymerization of Active Ester Monomers: Precursor Polymers for Highly Functionalized Materials. *Macromolecules* **2004**, *37* (15). https://doi.org/10.1021/ma035876f.

(82) Nilles, K.; Theato, P. Sequential Conversion of Orthogonally Functionalized Diblock Copolymers Based on Pentafluorophenyl Esters. **2010**, *48* (May), 3683–3692. https://doi.org/10.1002/POLA.

(83) Theato, P. Synthesis of Well-Defined Polymeric Activated Esters. **2008**, *46*, 6677–6687. https://doi.org/10.1002/pola.

(84) Vogel, N.; The, P. Controlled Synthesis of Reactive Polymeric Architectures Using 5-Norbornene-2-Carboxylic Acid Pentafluorophenyl Ester. **2007**, 383–391. https://doi.org/10.1002/masy.200750408.

(85) Eberhardt, M.; Mruk, R.; Zentel, R.; Théato, P. Synthesis of Pentafluorophenyl(Meth)Acrylate Polymers: New Precursor Polymers for the Synthesis of Multifunctional Materials. *Eur. Polym. J.* **2005**, *41* (7), 1569–1575. https://doi.org/10.1016/j.eurpolymj.2005.01.025.

(86) Blazejewski, J. C.; Hofstraat, J. W.; Lequesne, C.; Wakselman, C.; Wiersum, U. E. Halogenoaryl Acrylates: Preparation, Polymerization and Optical Properties. *J. Fluor. Chem.* **1999**, *97* (1–2), 191–199. https://doi.org/10.1016/S0022-1139(99)00048-2.

(87) Moad, G.; Solomon, D. H. *The Chemistry of Radical Polymerization*; Elsevier Science, 2005.

(88) Riscoe, A. R.; Wrasman, C. J.; Herzing, A. A.; Hoffman, A. S.; Menon, A.; Boubnov, A.; Vargas, M.; Bare, S. R.; Cargnello, M. Transition State and Product Diffusion Control by Polymer–Nanocrystal Hybrid Catalysts. *Nat. Catal.* **2019**. https://doi.org/10.1038/s41929-019-0322-7.

(89) Anac, I.; Aulasevich, A.; Junk, M. J. N.; Jakubowicz, P.; Roskamp, R. F.; Menges, B.; Jonas, U.; Knoll, W. Optical Characterization of Co-Nonsolvency Effects in Thin Responsive PNIPAAm-Based Gel Layers Exposed to Ethanol / Water Mixtures. 1018–1025. https://doi.org/10.1002/macp.200900533.

(90) Beines, P. W.; Klosterkamp, I.; Menges, B.; Jonas, U.; Knoll, W. Responsive Thin Hydrogel Layers from Photo-Cross-Linkable. **2007**, No. 7, 2231–2238.

(91) Gianneli, M.; Anac, I.; Rostkamp, R.; Menges, B.; Loppinet, B.; Jonas, U.; Knoll, W.; Fytas, G. Dynamic Response of Anchored Poly (N - Benzophenone Methacrylate) Terpolymer Hydrogel Layers to Physicochemical Stimuli. **2015**, 277–286.

(92) Jonas, U.; Junk, M. J. N. Atomic Force Spectroscopy of Thermoresponsive Photo-Cross-Linked Hydrogel Films. **2010**, *45* (28), 7262–7269. https://doi.org/10.1021/la903396v.

(93) Toma, M.; Jonas, U.; Mateescu, A.; Knoll, W.; Dostalek, J. Active Control of SPR by Thermoresponsive Hydrogels for Biosensor Applications. **2013**.

(94) Mateescu, A.; Wang, Y.; Dostalek, J.; Jonas, U. Thin Hydrogel Films for Optical Biosensor Applications. **2012**, 40–69. https://doi.org/10.3390/membranes2010040.

(95) Rydzek, G.; Schaaf, P.; Voegel, J. C.; Jierry, L.; Boulmedais, F. Strategies for Covalently Reticulated Polymer Multilayers. *Soft Matter* **2012**, *8* (38), 9738–9755. https://doi.org/10.1039/c2sm25719j.

(96) Van Den Brom, C. R.; Anac, I.; Roskamp, R. F.; Retsch, M.; Jonas, U.; Menges, B.; Preece, J. A. The Swelling Behaviour of Thermoresponsive Hydrogel/Silica Nanoparticle Composites. *J. Mater. Chem.* **2010**, *20* (23), 4827–4839. https://doi.org/10.1039/b927314j.

(97) Yue, C.; Su, D.; Zhang, X.; Wu, W.; Xiao, L. Amino-Functional Imidazolium Ionic Liquids for CO 2 Activation and Conversion to Form Cyclic Carbonate. *Catal. Letters* **2014**, *144* (7), 1313–1321. https://doi.org/10.1007/s10562-014-1241-5.

(98) Barthlott, W.; Neinhuis, C. Purity of the Sacred Lotus, or Escape from Contamination in Biological Surfaces. *Planta* **1997**, *202* (1), 1–8. https://doi.org/10.1007/s004250050096.

(99) Ma, M.; Hill, R. M. Superhydrophobic Surfaces. *Curr. Opin. Colloid Interface Sci.* **2006**, *11* (4), 193–202. https://doi.org/10.1016/j.cocis.2006.06.002.

(100) Quéré, D. Non-Sticking Drops. *Reports Prog. Phys.* **2005**, *68* (11), 2495–2532. https://doi.org/10.1088/0034-4885/68/11/R01.

(101) Cassie, A. B. D.; Baxter, S. Wettability of Porous Surfaces. *Trans. Faraday Soc.* **1944**, *40*, 546. https://doi.org/10.1039/tf9444000546.

(102) Quéré, D. Wetting and Roughness. *Annu. Rev. Mater. Res.* **2008**, *38* (1), 71–99. https://doi.org/doi:10.1146/annurev.matsci.38.060407.132434.

(103) Cheng, Q.; Li, M.; Zheng, Y.; Su, B.; Wang, S.; Jiang, L. Janus Interface Materials: Superhydrophobic Air/Solid Interface and Superoleophobic Water/Solid Interface Inspired by a Lotus Leaf. *Soft Matter* **2011**, *7* (13), 5948–5951. https://doi.org/10.1039/c1sm05452j.

(104) Tuteja, A.; Choi, W.; Ma, M.; Mabry, J. M.; Mazzella, S. a; Rutledge, G. C.; McKinley, G. H.; Cohen, R. E. Designing Superoleophobic Surfaces. *Science* **2007**, *318* (5856), 1618–1622. https://doi.org/10.1126/science.1148326.

(105) Deng, X.; Mammen, L.; Butt, H.-J.; Vollmer, D. Candle Soot as a Template for a Transparent Robust Superamphiphobic Coating. *Science (80-.).* **2012**, *335* (6064), 67–70. https://doi.org/10.1126/science.1207115.

(106) Mishchenko, L.; Hatton, B.; Bahadur, V.; Taylor, J. A.; Krupenkin, T.; Aizenberg, J. Design of Ice-

Free Nanostructured Surfaces Based on Repulsion of Impacting Water Droplets. *ACS Nano* **2010**, *4* (12), 7699–7707. https://doi.org/10.1021/nn102557p.

(107) Epstein, A. K.; Wong, T. S.; Belisle, R. A.; Boggs, E. M.; Aizenberg, J. Liquid-Infused Structured Surfaces with Exceptional Anti-Biofouling Performance. *Proc. Natl. Acad. Sci. U. S. A.* **2012**, *109* (33), 13182–13187. https://doi.org/10.1073/pnas.1201973109.

(108) Wang, J.; Kato, K.; Blois, A. P.; Wong, T.-S. Bioinspired Omniphobic Coatings with a Thermal Self-Repair Function on Industrial Materials. *ACS Appl. Mater. Interfaces* **2016**, *8* (12), 8265–8271. https://doi.org/10.1021/acsami.6b00194.

(109) Scholz, I.; Bückins, M.; Dolge, L.; Erlinghagen, T.; Weth, a; Hischen, F.; Mayer, J.; Hoffmann, S.; Riederer, M.; Riedel, M.; Baumgartner, W. Slippery Surfaces of Pitcher Plants: Nepenthes Wax Crystals Minimize Insect Attachment via Microscopic Surface Roughness. *J. Exp. Biol.* **2010**, *213* (Pt 7), 1115–1125. https://doi.org/10.1242/jeb.035618.

(110) Bauer, U.; Federle, W. The Insect-Trapping Rim of Nepenthes Pitchers. *Plant Signal. Behav.* **2009**, *4* (11), 1019–1023. https://doi.org/10.4161/psb.4.11.9664.

(111) Chen, H.; Zhang, P.; Zhang, L.; Liu, H.; Jiang, Y.; Zhang, D.; Han, Z.; Jiang, L. Continuous Directional Water Transport on the Peristome Surface of Nepenthes Alata. *Nature* **2016**, *532* (7597), 85–89. https://doi.org/10.1038/nature17189.

(112) Lafuma, A.; Quéré, D. Slippery Pre-Suffused Surfaces. *EPL (Europhysics Lett.* **2011**, *96* (5), 56001. https://doi.org/10.1209/0295-5075/96/56001.

(113) Smith, J. D.; Dhiman, R.; Anand, S.; Reza-Garduno, E.; Cohen, R. E.; McKinley, G. H.; Varanasi, K. K. Droplet Mobility on Lubricant-Impregnated Surfaces. *Soft Matter* **2013**, *9* (6), 1772–1780. https://doi.org/10.1039/c2sm27032c.

(114) Lv, J.; Yao, X.; Zheng, Y.; Wang, J.; Jiang, L. Antiadhesion Organogel Materials: From Liquid to Solid. *Adv. Mater.* **2017**, *29* (45), 1–8. https://doi.org/10.1002/adma.201703032.

(115) Rykaczewski, K.; Anand, S.; Subramanyam, S. B.; Varanasi, K. K. Mechanism of Frost Formation on Lubricant-Impregnated Surfaces. *Langmuir* **2013**, *29* (17), 5230–5238. https://doi.org/10.1021/la400801s.

(116) Adera, S.; Alvarenga, J.; Shneidman, A. V.; Zhang, C. T.; Davitt, A.; Aizenberg, J. Depletion of

Lubricant from Nanostructured Oil-Infused Surfaces by Pendant Condensate Droplets. *ACS Nano* **2020**, *14* (7), 8024–8035. https://doi.org/10.1021/acsnano.9b10184.

(117) Kim, P.; Kreder, M. J.; Alvarenga, J.; Aizenberg, J. Hierarchical or Not? Effect of the Length Scale and Hierarchy of the Surface Roughness on Omniphobicity of Lubricant-Infused Substrates. *Nano Lett.* **2013**, *13* (4), 1793–1799. https://doi.org/10.1021/nl4003969.

(118) Amini, S.; Kolle, S.; Petrone, L.; Ahanotu, O.; Sunny, S.; Sutanto, C. N.; Hoon, S.; Cohen, L.; Weaver, J. C.; Aizenberg, J.; Vogel, N.; Miserez, A. Preventing Mussel Adhesion Using Lubricant-Infused Materials. *Science* **2017**, *357* (6352), 668–673. https://doi.org/10.1126/science.aai8977 PM - 28818939 S1 - 7 M4 - Citavi.

(119) Li, J.; Kleintschek, T.; Rieder, A.; Cheng, Y.; Baumbach, T.; Obst, U.; Schwartz, T.; Levkin, P. A. Hydrophobic Liquid-Infused Porous Polymer Surfaces for Antibacterial Applications. *ACS Appl. Mater. Interfaces* **2013**, *5* (14), 6704–6711. https://doi.org/10.1021/am401532z.

(120) Cao, M.; Guo, D.; Yu, C.; Li, K.; Liu, M.; Jiang, L. Water-Repellent Properties of Superhydrophobic and Lubricant-Infused "Slippery" Surfaces: A Brief Study on the Functions and Applications. *ACS Appl. Mater. Interfaces* **2016**, *8* (6), 3615–3623. https://doi.org/10.1021/acsami.5b07881.

(121) Kreder, M. J.; Alvarenga, J.; Kim, P.; Aizenberg, J. Design of Anti-Icing Surfaces: Smooth, Textured or Slippery? *Nat. Rev. Mater.* **2016**, *1* (1). https://doi.org/10.1038/natrevmats.2015.3.

(122) Sunny, S.; Cheng, G.; Daniel, D.; Lo, P.; Ochoa, S.; Howell, C.; Vogel, N. Transparent Antifouling Material for Improved Operative Field Visibility in Endoscopy. **2016**, 2–7. https://doi.org/10.1073/pnas.1605272113.

(123) Kim, P.; Wong, T.-S.; Alvarenga, J.; Kreder, M. J.; Adorno-martinez, W. E.; Aizenberg, J.; Al, K. I. M. E. T. Liquid-Infused Nanostructured Surfaces with Extreme Anti-Ice and Anti-Frost Performance. *ACS Nano* **2012**, *6* (8), 6569–6577. https://doi.org/10.1021/nn302310q.

(124) Tesler, A. B.; Kim, P.; Kolle, S.; Howell, C.; Ahanotu, O.; Aizenberg, J. Extremely Durable Biofouling-Resistant Metallic Surfaces Based on Electrodeposited Nanoporous Tungstite Films on Steel. *Nat. Commun.* **2015**, *6*. https://doi.org/10.1038/ncomms9649.

(125) Riisager, A.; Fehrmann, R.; Haumann, M.; Wasserscheid, P. Supported Ionic Liquids: Versatile Reaction and Separation Media. *Top. Catal.* **2006**, *40* (1–4), 91–102.

https://doi.org/10.1007/s11244-006-0111-9.

(126) Riisager, A.; Eriksen, K. M.; Wasserscheid, P.; Fehrmann, R. Propene and 1-Octene Hydroformylation with Silica-Supported , Ionic Liquid-Phase (SILP) Rh-Phosphine Catalysts in Continuous Fixed-Bed Mode. **2003**, *90* (October), 149–153.

(127) Riisager, A.; Fehrmann, R.; Flicker, S.; Hal, R. Van; Haumann, M.; Wasserscheid, P. Very Stable and Highly Regioselective Supported Ionic-Liquid-Phase (SILP) Catalysis: Continuous- Flow Fixed-Bed Hydroformylation of Propene**. **2005**, 815–819. https://doi.org/10.1002/anie.200461534.

(128) Riisager, A.; Jørgensen, B.; Fehrmann, R. First Application of Supported Ionic Liquid Phase (SILP) Catalysis for Continuous Methanol Carbonylation {. **2006**, 994–996. https://doi.org/10.1039/b516314e.

(129) Wolf, P.; Logemann, M.; Schörner, M.; Keller, L.; Haumann, M.; Wessling, M. Multi-Walled Carbon Nanotube-Based Composite Materials as Catalyst Support for Water-Gas Shift and Hydroformylation Reactions. *RSC Adv.* **2019**, *9* (47), 27732–27742. https://doi.org/10.1039/c9ra04830h.

(130) Riisager, A.; Fehrmann, R.; Haumann, M.; Wasserscheid, P. Supported Ionic Liquid Phase (SILP) Catalysis : An Innovative Concept for Homogeneous Catalysis in Continuous Fixed-Bed Reactors Anders Riisager ,* [a] Rasmus Fehrmann , [a] Marco Haumann ,* [b] and Peter Wasserscheid [B]. **2006**, 695–706. https://doi.org/10.1002/ejic.200500872.

(131) Valkenberg, M. H.; deCastro, C.; Hölderich, W. F. Immobilisation of Ionic Liquids on Solid Supports. *Green Chem.* **2001**, *4* (2), 88–93. https://doi.org/10.1039/b107946h.

(132) Vogel, N.; Belisle, R. a; Hatton, B.; Wong, T.-S.; Aizenberg, J. Transparency and Damage Tolerance of Patternable Omniphobic Lubricated Surfaces Based on Inverse Colloidal Monolayers. *Nat. Commun.* **2013**, *4*, 2167. https://doi.org/10.1038/ncomms3176.

(133) Eberhardt, M.; Mruk, R.; Zentel, R.; Théato, P. Synthesis of Pentafluorophenyl(Meth)Acrylate Polymers. *Eur. Polym. J.* **2005**, *41* (7), 1569–1575. https://doi.org/10.1016/j.eurpolymj.2005.01.025 T4 - New precursor polymers for the synthesis of multifunctional materials M4 - Citavi.

(134) Huang, J.; Cusick, B.; Pietrasik, J.; Wang, L.; Kowalewski, T.; Lin, Q.; Matyjaszewski, K. Synthesis

and in Situ Atomic Force Microscopy Characterization of Temperature-Responsive Hydrogels Based on Poly(2-(Dimethylamino)Ethyl Methacrylate) Prepared by Atom Transfer Radical Polymerization. *Langmuir* **2007**, *23* (1), 241–249. https://doi.org/10.1021/la061683k PM - 17190510 S1 - 9 M4 - Citavi.

(135) Oswald Prucker Jürgen Rühe, Wolfgang Knoll, Curtis W. Frank, C. A. N. Photochemical Attachment of Polymer Films to Solid Surfaces via Monolayers of Benzophenone Derivatives. *Am. Chem. Soc.* **1999**. https://doi.org/10.1021/ja990962 S1 - 5 M4 - Citavi.

(136) Galvan, Y.; Phillips, K. R.; Haumann, M.; Wasserscheid, P.; Zarraga, R.; Vogel, N. Ionic-Liquid-Infused Nanostructures as Repellent Surfaces. *Langmuir* **2018**, *34* (23), 6894–6902. https://doi.org/10.1021/acs.langmuir.7b03993.

(137) Hatton, B.; Mishchenko, L.; Norwood, R.; Davis, S.; Sandhage, K.; Aizenberg, J. An Evaporative Co-Assembly Method for Highly Ordered Inverse Opal Films. *Proc. SPIE* **2009**, *7205*, 72050F-72050F – 5. https://doi.org/10.1117/12.809656.

(138) Aguirre, C. I.; Reguera, E.; Stein, A. Tunable Colors in Opals and Inverse Opal Photonic Crystals. *Adv. Funct. Mater.* **2010**, *20* (16), 2565–2578. https://doi.org/10.1002/adfm.201000143.

(139) Huddleston, J. G.; Visser, A. E.; Reichert, W. M.; Willauer, H. D.; Broker, G. A.; Rogers, R. D.; April, R. Characterization and Comparison of Hydrophilic and Hydrophobic Room Temperature Ionic Liquids Incorporating the Imidazolium Cation Green Context. **2001**. https://doi.org/10.1039/b103275p.

(140) Bhargava, G.; Ramanarayanan, T. A.; Bernasek, S. L. Imidazole-Fe Interaction in an Aqueous Chloride Medium: Effect of Cathodic Reduction of the Native Oxide. *Langmuir* **2010**, *26* (1), 215–219. https://doi.org/10.1021/la9020355.

(141) Decher, G. Fuzzy Nanoassemblies: Toward Layered Polymeric Multicomposites. *Science (80-.).* **1997**, *277* (5330), 1232–1237. https://doi.org/10.1126/science.277.5330.1232.

(142) Escobar, A.; Muzzio, N.; Moya, S. E. Antibacterial Layer-by-Layer Coatings for Medical Implants. *Pharmaceutics* **2020**, *13* (1), 16. https://doi.org/10.3390/pharmaceutics13010016.

(143) Motay, M.; Martel, D.; Vileno, B.; Soraru, C.; Ploux, L.; Méndez-Medrano, M. G.; Colbeau-Justin, C.; Decher, G.; Keller, N. Virtually Transparent TiO2/Polyelectrolyte Thin Multilayer Films as High-

Efficiency Nanoporous Photocatalytic Coatings for Breaking down Formic Acid and for Escherichia Coli Removal. *ACS Appl. Mater. Interfaces* **2020**, *12* (50), 55766–55781. https://doi.org/10.1021/acsami.0c13545.

(144) Szweda, R.; Tschopp, M.; Felix, O.; Decher, G.; Lutz, J. F. Sequences of Sequences: Spatial Organization of Coded Matter through Layer-by-Layer Assembly of Digital Polymers. *Angew. Chemie - Int. Ed.* **2018**, *57* (48), 15817–15821. https://doi.org/10.1002/anie.201810559.

(145) Öchsner, E.; Schneider, M. J.; Meyer, C.; Haumann, M.; Wasserscheid, P. Challenging the Scope of Continuous, Gas-Phase Reactions with Supported Ionic Liquid Phase (SILP) Catalysts - Asymmetric Hydrogenation of Methyl Acetoacetate. *Appl. Catal. A Gen.* **2011**, *399* (1–2), 35–41. https://doi.org/10.1016/j.apcata.2011.03.038.

(146) Ruta, M.; Yuranov, I.; Dyson, P. J.; Laurenczy, G.; Kiwi-Minsker, L. Structured Fiber Supports for Ionic Liquid-Phase Catalysis Used in Gas-Phase Continuous Hydrogenation. *J. Catal.* **2007**, *247* (2), 269–276. https://doi.org/10.1016/j.jcat.2007.02.012.

(147) Wolf, P.; Aubermann, M.; Wolf, M.; Bauer, T.; Blaumeiser, D.; Stepic, R.; Wick, C. R.; Smith, D. M.; Smith, A. S.; Wasserscheid, P.; Libuda, J.; Haumann, M. Improving the Performance of Supported Ionic Liquid Phase (SILP) Catalysts for the Ultra-Low-Temperature Water-Gas Shift Reaction Using Metal Salt Additives. *Green Chem.* **2019**, *21* (18), 5008–5018. https://doi.org/10.1039/c9gc02153a.

(148) Lazzara, T. D.; Lau, Ḱ. K. H. A.; Abou-kandil, A. I.; Caminade, A.; Majoral, P.; Knoll, W. Polyelectrolyte Layer-by-Layer. **2010**, *4* (7), 3909–3920.

(149) Roy, C. J.; Dupont-Gillain, C.; Demoustier-Champagne, S.; Jonas, A. M.; Landoulsi, J. Growth Mechanism of Confined Polyelectrolyte Multilayers in Nanoporous Templates. *Langmuir* **2010**, *26* (5), 3350–3355. https://doi.org/10.1021/la903121e.

(150) Ali, M.; Yameen, B.; Cervera, J.; Ramírez, P.; Neumann, R.; Ensinger, W.; Knoll, W.; Azzaroni, O. Layer-by-Layer Assembly of Polyelectrolytes into Ionic Current Rectifying Solid-State Nanopores: Insights from Theory and Experiment. *J. Am. Chem. Soc.* **2010**, *132* (24), 8338–8348. https://doi.org/10.1021/ja101014y.

(151) Derocher, J. P.; Mao, P.; Kim, J. Y.; Han, J.; Rubner, M. F.; Cohen, R. E. Layer-by-Layer Deposition of All-Nanoparticle Multilayers in Confined Geometries. *ACS Appl. Mater. Interfaces* **2012**, *4* (1),

391–396. https://doi.org/10.1021/am2014647.

(152) Kim, J. Y.; DeRocher, J. P.; Mao, P.; Han, J.; Cohen, R. E.; Rubner, M. F. Formation of Nanoparticle-Containing Multilayers in Nanochannels via Layer-by-Layer Assembly. *Chem. Mater.* **2010**, *22* (23), 6409–6415. https://doi.org/10.1021/cm1025816.

(153) Dotzauer, D. M.; Bhattacharjee, S.; Wen, Y.; Bruening, M. L. Nanoparticle-Containing Membranes for the Catalytic Reduction of Nitroaromatic Compounds. *Langmuir* **2009**, *25* (3), 1865–1871. https://doi.org/10.1021/la803220z.

(154) Xiao, F. Layer-by-Layer Self-Assembly Construction of Highly Ordered Metal-TiO 2 Nanotube Arrays Heterostructures (M/TNTs, M = Au, Ag, Pt) with Tunable Catalytic Activities. *J. Phys. Chem. C* **2012**, *116* (31), 16487–16498. https://doi.org/10.1021/jp3034984.

(155) Dotzauer, D. M.; Dai, J.; Sun, L.; Bruening, M. L. Catalytic Membranes Prepared Using Layer-by-Layer Adsorption of Polyelectrolyte/Metal Nanoparticle Films in Porous Supports. *Nano Lett.* **2006**, *6* (10), 2268–2272. https://doi.org/10.1021/nl061700q.

(156) Ouyang, L.; Dotzauer, D. M.; Hogg, S. R.; MacAnás, J.; Lahitte, J. F.; Bruening, M. L. Catalytic Hollow Fiber Membranes Prepared Using Layer-by-Layer Adsorption of Polyelectrolytes and Metal Nanoparticles. *Catal. Today* **2010**, *156* (3–4), 100–106. https://doi.org/10.1016/j.cattod.2010.02.040.

(157) Kanungo, S.; Paunovic, V.; Schouten, J. C.; Neira D'Angelo, M. F. Facile Synthesis of Catalytic AuPd Nanoparticles within Capillary Microreactors Using Polyelectrolyte Multilayers for the Direct Synthesis of H2O2. *Nano Lett.* **2017**, *17* (10), 6481–6486. https://doi.org/10.1021/acs.nanolett.7b03589.

(158) Alem, H.; Blondeau, F.; Glinel, K.; Demoustier-Champagne, S.; Jonas, A. M. Layer-by-Layer Assembly of Polyelectrolytes in Nanopores. *Macromolecules* **2007**, *40* (9), 3366–3372. https://doi.org/10.1021/ma0703251.

(159) Derocher, J. P.; Mao, P.; Han, J.; Rubner, M. F.; Cohen, R. E. Layer-by-Layer Assembly of Polyelectrolytes in Nanofluidic Devices. *Macromolecules* **2010**, *43* (5), 2430–2437. https://doi.org/10.1021/ma902451s.

(160) Marinkovic, J. M.; Benders, S.; Garcia-Suarez, E. J.; Weiß, A.; Gundlach, C.; Haumann, M.;

Küppers, M.; Blümich, B.; Fehrmann, R.; Riisager, A. Elucidating the Ionic Liquid Distribution in Monolithic SILP Hydroformylation Catalysts by Magnetic Resonance Imaging. *RSC Adv.* **2020**, *10* (31), 18487–18495. https://doi.org/10.1039/c9ra09515b.

(161) Logemann, M.; Wolf, P.; Loipersböck, J.; Schrade, A.; Wessling, M.; Haumann, M. Ultra-Low Temperature Water–Gas Shift Reaction Catalyzed by Homogeneous Ru-Complexes in a Membrane Reactor – Membrane Development and Proof of Concept. *Catal. Sci. Technol.* **2021**. https://doi.org/10.1039/d0cy02111c.

(162) Phillips, K. R.; England, G. T.; Sunny, S.; Shirman, E.; Shirman, T.; Vogel, N.; Aizenberg, J. A Colloidoscope of Colloid-Based Porous Materials and Their Uses. *Chem. Soc. Rev.* **2016**, *45* (2), 281–322. https://doi.org/10.1039/c5cs00533g.

(163) Taketa, T. B.; Rocha Neto, J. B. M.; Dos Santos, D. M.; Fiamingo, A.; Beppu, M. M.; Campana-Filho, S. P.; Cohen, R. E.; Rubner, M. F. Tracking Sulfonated Polystyrene Diffusion in a Chitosan/Carboxymethyl Cellulose Layer-by-Layer Film: Exploring the Internal Architecture of Nanocoatings. *Langmuir* **2020**, *36* (18), 4985–4994. https://doi.org/10.1021/acs.langmuir.0c00544.

(164) Giraudet, C.; Knoll, M. S. G.; Galvan, Y.; Süß, S.; Segets, D.; Vogel, N.; Rausch, M. H.; Fröba, A. P. Diffusion of Gold Nanoparticles in Inverse Opals Probed by Heterodyne Dynamic Light Scattering. *Transp. Porous Media* **2020**, *131* (2), 723–737. https://doi.org/10.1007/s11242-019-01364-1.

(165) Raccis, R.; Nikoubashman, A.; Retsch, M.; Jonas, U.; Koynov, K.; Butt, H.-J.; Likos, C. N.; Fytas, G. Confined Diffusion in Periodic Porous Nanostructures. *ACS Nano* **2011**, *5* (6), 4607–4616. https://doi.org/10.1021/nn200767x.

(166) Zhang, S.; Vlémincq, C.; Ramirez Wong, D.; Magnin, D.; Glinel, K.; Demoustier-Champagne, S.; Jonas, A. M. Nanopapers of Layer-by-Layer Nanotubes. *J. Mater. Chem. B* **2016**, *4* (47), 7651–7661. https://doi.org/10.1039/c6tb02737g.

(167) Hunter, R. J. *Zeta Potential in Colloid Science*; Ottewill, R. H., Rowell, R. ., Eds.; Academic Press, 1981. https://doi.org/10.1016/c2013-0-07389-6.

(168) Werner, S.; Szesni, N.; Bittermann, A.; Schneider, M. J.; Härter, P.; Haumann, M.; Wasserscheid, P. Screening of Supported Ionic Liquid Phase (SILP) Catalysts for the Very Low Temperature Water-Gas-Shift Reaction. *Appl. Catal. A Gen.* **2010**, *377* (1–2), 70–75.

https://doi.org/10.1016/j.apcata.2010.01.019.

(169) Mehnert, C. P. Supported Ionic Liquid Catalysis. *Chem. - A Eur. J.* **2005**, *11* (1), 50–56. https://doi.org/10.1002/chem.200400683.

(170) Bauer, T.; Stepic, R.; Wolf, P.; Kollhoff, F.; Karawacka, W.; Wick, C. R.; Haumann, M.; Wasserscheid, P.; Smith, D. M.; Smith, A. S.; Libuda, J. Dynamic Equilibria in Supported Ionic Liquid Phase (SILP) Catalysis:: In Situ IR Spectroscopy Identifies [Ru(CO)XCly]n Species in Water Gas Shift Catalysis. *Catal. Sci. Technol.* **2018**, *8* (1), 344–357. https://doi.org/10.1039/c7cy02199b.

(171) Salbaum, T.; Galvan, Y.; Haumann, M.; Wasserscheid, P.; Zarraga, R.; Vogel, N. Enduring Liquid Repellency through Slippery Ionic Liquid-Infused Organogels. *J. Mater. Chem. A* **2021**, 31–34. https://doi.org/10.1039/d0ta10237g.

(172) Guo, P.; Wang, Z.; Heng, L.; Zhang, Y.; Wang, X.; Jiang, L. Magnetocontrollable Droplet and Bubble Manipulation on a Stable Amphibious Slippery Gel Surface. *Adv. Funct. Mater.* **2019**, *29* (11), 1–10. https://doi.org/10.1002/adfm.201808717.

(173) Yao, X.; Dunn, S. S.; Kim, P.; Duffy, M.; Alvarenga, J.; Aizenberg, J. Fluorogel Elastomers with Tunable Transparency , Elasticity , Shape- Memory , and Antifouling Properties. *Angew. Commun.* **2014**, 4418–4422. https://doi.org/10.1002/anie.201310385.

(174) Lee, J.; Wooh, S.; Choi, C.-H. Fluorocarbon Lubricant Impregnated Nanoporous Oxide for Omnicorrosion-Resistant Stainless Steel. *J. Colloid Interface Sci.* **2020**, *558*, 301–309. https://doi.org/10.1016/j.jcis.2019.09.117.

(175) Ye, L.; Chen, F.; Liu, J.; Gao, A.; Kircher, G.; Liu, W.; Kappl, M.; Wegner, S.; Butt, H.; Steffen, W. Responsive Ionogel Surface with Renewable Antibiofouling Properties. *Macromol. Rapid Commun.* **2019**, *1900395*, 1900395. https://doi.org/10.1002/marc.201900395.

(176) Eberhardt, M.; The, P. RAFT Polymerization of Pentafluorophenyl Methacrylate : Preparation of Reactive Linear Diblock Copolymers A. **2005**, 1488–1493. https://doi.org/10.1002/marc.200500390.

(177) Zhao, H.; Theato, P. Copolymers Featuring Pentafluorophenyl Ester and Photolabile Amine Units: Synthesis and Application as Reactive Photopatterns. *Polym. Chem.* **2013**, *4* (4), 891–894.

https://doi.org/10.1039/c2py21050a.

(178) Vagias, A.; Sergelen, K.; Koynov, K.; Košovan, P.; Dostalek, J.; Jonas, U.; Knoll, W.; Fytas, G. Diffusion and Permeation of Labeled IgG in Grafted Hydrogels. *Macromolecules* **2017**, *50* (12), 4770–4779. https://doi.org/10.1021/acs.macromol.7b00514.

(179) Melzak, K. A.; Mateescu, A.; Toca-Herrera, J. L.; Jonas, U. Simultaneous Measurement of Mechanical and Surface Properties in Thermoresponsive, Anchored Hydrogel Films. *Langmuir* **2012**, *28* (35), 12871–12878. https://doi.org/10.1021/la3019666.

(180) Pirani, F.; Sharma, N.; Moreno-Cencerrado, A.; Fossati, S.; Petri, C.; Descrovi, E.; Toca-Herrera, J. L.; Jonas, U.; Dostalek, J. Optical Waveguide-Enhanced Diffraction for Observation of Responsive Hydrogel Nanostructures. *Macromol. Chem. Phys.* **2017**, *218* (6), 1–10. https://doi.org/10.1002/macp.201600400.

(181) Deegan, R. D.; Bakajin, O.; Dupont, T. F.; Huber, G.; Nagel, S. R.; Witten, T. A. Nature1997, Capillary Flowas the Cause of Ring Stains Fromdried Liquid Drops.Pdf. *Nature* **1997**, *389* (23), 827–829.

(182) Mampallil, D.; Eral, H. B. A Review on Suppression and Utilization of the Coffee-Ring Effect. *Adv. Colloid Interface Sci.* **2018**, *252*, 38–54. https://doi.org/10.1016/j.cis.2017.12.008.

(183) Hu, M.; Butt, H. J.; Landfester, K.; Bannwarth, M. B.; Wooh, S.; Thérien-Aubin, H. Shaping the Assembly of Superparamagnetic Nanoparticles. *ACS Nano* **2019**, *13* (3), 3015–3022. https://doi.org/10.1021/acsnano.8b07783.

(184) Wooh, S.; Huesmann, H.; Tahir, M. N.; Paven, M.; Wichmann, K.; Vollmer, D.; Tremel, W.; Papadopoulos, P.; Butt, H. J. Synthesis of Mesoporous Supraparticles on Superamphiphobic Surfaces. *Adv. Mater.* **2015**, *27* (45), 7338–7343. https://doi.org/10.1002/adma.201503929.

(185) Daniel, D.; Mankin, M. N.; Belisle, R. A.; Wong, T. S.; Aizenberg, J. Lubricant-Infused Micro/Nano-Structured Surfaces with Tunable Dynamic Omniphobicity at High Temperatures. *Appl. Phys. Lett.* **2013**, *102* (23), 2–6. https://doi.org/10.1063/1.4810907.

(186) Wang, T.; Can, I.; Zhang, S.; He, J.; Sun, P.; Liu, F.; Lu, G. Self-Assembly Template Driven 3D Inverse Opal Microspheres Functionalized with Catalyst Nanoparticles Enabling a Highly Efficient Chemical Sensing Platform. *ACS Appl. Mater. Interfaces* **2018**, *10* (6), 5835–5844.

https://doi.org/10.1021/acsami.7b19641.

(187) Haumann, M.; Schönweiz, A.; Breitzke, H.; Buntkowsky, G.; Werner, S.; Szesni, N. Solid-State NMR Investigations of Supported Ionic Liquid Phase Water-Gas Shift Catalysts: Ionic Liquid Film Distribution vs. Catalyst Performance. *Chem. Eng. Technol.* **2012**, *35* (8), 1421–1426. https://doi.org/10.1002/ceat.201200025.

(188) Bai, S.; Da, P.; Li, C.; Wang, Z.; Yuan, Z.; Fu, F.; Kawecki, M.; Liu, X.; Sakai, N.; Wang, J. T. W.; Huettner, S.; Buecheler, S.; Fahlman, M.; Gao, F.; Snaith, H. J. Planar Perovskite Solar Cells with Long-Term Stability Using Ionic Liquid Additives. *Nature* **2019**, *571* (7764), 245–250. https://doi.org/10.1038/s41586-019-1357-2.

(189) Lau, G. P. S.; Decoppet, J. D.; Moehl, T.; Zakeeruddin, S. M.; Gratzel, M.; Dyson, P. J. Robust High-Performance Dye-Sensitized Solar Cells Based on Ionic Liquid-Sulfolane Composite Electrolytes. *Sci. Rep.* **2015**, *5* (July), 1–8. https://doi.org/10.1038/srep18158.

(190) Wang, P.; Zakeeruddin, S. M.; Exnar, I.; Grätzel, M. High Efficiency Dye-Sensitized Nanocrystalline Solar Cells Based on Ionic Liquid Polymer Gel Electrolyte. *Chem. Commun.* **2002**, *8* (24), 2972–2973. https://doi.org/10.1039/b209322g.

(191) Francis, C. F. J.; Kyratzis, I. L.; Best, A. S. Lithium-Ion Battery Separators for Ionic-Liquid Electrolytes: A Review. *Adv. Mater.* **2020**, *32* (18), 1–22. https://doi.org/10.1002/adma.201904205.

(192) Susan, M. A. B. H.; Kaneko, T.; Noda, A.; Watanabe, M. Ion Gels Prepared by in Situ Radical Polymerization of Vinyl Monomers in an Ionic Liquid and Their Characterization as Polymer Electrolytes. *J. Am. Chem. Soc.* **2005**, *127* (13), 4976–4983. https://doi.org/10.1021/ja045155b.

(193) Fuller, J.; Breda, A. C.; Carlin, R. T. Ionic Liquid-Polymer Gel Electrolytes from Hydrophilic and Hydrophobic Ionic Liquids. *J. Electroanal. Chem.* **1998**, *459* (1), 29–34. https://doi.org/10.1016/S0022-0728(98)00285-X.

(194) Shi, F.; Zhang, Q.; Li, D.; Deng, Y. Silica-Gel-Confined Ionic Liquids: A New Attempt for the Development of Supported Nanoliquid Catalysis. *Chem. - A Eur. J.* **2005**, *11* (18), 5279–5288. https://doi.org/10.1002/chem.200500107.

(195) Carlin, R. T.; Fuller, J. Ionic Liquid-Polymer Gel Catalytic Membrane. *Chem. Commun.* **1997**, No.

15, 1345–1346. https://doi.org/10.1039/a702195j.

(196) Eftekhari, A.; Saito, T. Synthesis and Properties of Polymerized Ionic Liquids. *Eur. Polym. J.* **2017**, *90* (March), 245–272. https://doi.org/10.1016/j.eurpolymj.2017.03.033.

(197) Steinrück, H. P. Recent Developments in the Study of Ionic Liquid Interfaces Using X-Ray Photoelectron Spectroscopy and Potential Future Directions. *Phys. Chem. Chem. Phys.* **2012**, *14* (15), 5010–5029. https://doi.org/10.1039/c2cp24087d.

(198) Maiti, R.; Midya, A.; Narayana, C.; Ray, S. K. Tunable Optical Properties of Graphene Oxide by Tailoring the Oxygen Functionalities Using Infrared Irradiation. *Nanotechnology* **2014**, *25* (49). https://doi.org/10.1088/0957-4484/25/49/495704.

(199) Kolbeck, C.; Killian, M.; Maier, F.; Paape, N.; Wasserscheid, P.; Steinrück, H. P. Surface Characterization of Functionalized Imidazolium-Based Ionic Liquids. *Langmuir* **2008**, *24* (17), 9500–9507. https://doi.org/10.1021/la801261h.

(200) Kerber, S. J.; Bruckner, J. J.; Wozniak, K.; Seal, S.; Hardcastle, S.; Barr, T. L. The Nature of Hydrogen in X-ray Photoelectron Spectroscopy: General Patterns from Hydroxides to Hydrogen Bonding. *J. Vac. Sci. Technol. A Vacuum, Surfaces, Film.* **1996**, *14* (3), 1314–1320. https://doi.org/10.1116/1.579947.

(201) Haumann, M.; Jakuttis, M.; Franke, R.; Schönweiz, A.; Wasserscheid, P. Continuous Gas-Phase Hydroformylation of a Highly Diluted Technical C4 Feed Using Supported Ionic Liquid Phase Catalysts. *ChemCatChem* **2011**, *3* (11), 1822–1827. https://doi.org/10.1002/cctc.201100117.

(202) Marinkovic, J. M.; Riisager, A.; Franke, R.; Wasserscheid, P.; Haumann, M. Fifteen Years of Supported Ionic Liquid Phase-Catalyzed Hydroformylation: Material and Process Developments. *Ind. Eng. Chem. Res.* **2019**, *58* (7), 2409–2420. https://doi.org/10.1021/acs.iecr.8b04010.